SANDIA REPORT

SAND2003-3313
Unlimited Release
Printed September 2003

Potential Applications of Nanostructured Materials in Nuclear Waste Management

Yifeng Wang, Charles Bryan, Huizhen Gao, Phillip I. Phol, C. Jeffrey Brinker, Kui Yu, Huifang Xu, Yi Yang, Paul S. Braterman, and Zhiping Xu

Prepared by
Sandia National Laboratories
Albuquerque, New Mexico 87185 and Livermore, California 94550

Sandia is a multiprogram laboratory operated by Sandia Corporation,
a Lockheed Martin Company, for the United States Department of Energy's
National Nuclear Security Administration under Contract DE-AC04-94AL85000.

Issued by Sandia National Laboratories, operated for the United States Department of Energy by Sandia Corporation.

Available to DOE and DOE contractors from
U.S. Department of Energy
Office of Scientific and Technical Information
P.O. Box 62
Oak Ridge, TN 37831

Telephone: (865)576-8401
Facsimile: (865)576-5728
E-Mail: reports@adonis.osti.gov
Online ordering: http://www.doe.gov/bridge

Available to the public from
U.S. Department of Commerce
National Technical Information Service
5285 Port Royal Rd
Springfield, VA 22161

Telephone: (800)553-6847
Facsimile: (703)605-6900
E-Mail: orders@ntis.fedworld.gov
Online order: http://www.ntis.gov/help/ordermethods.asp?loc=7-4-0#online

SAND2003-3313
Unlimited Release
Printed September 2003

Potential Applications of Nanostructured Materials in Nuclear Waste Management

Yifeng Wang and Charles Bryan,
Subsystems Performance Assessment Department, Sandia National Laboratories,
Huizhen Gao
Repository Performance Department
Phillip I. Pohl
International Environmental Analysis Department
C. Jeffrey Brinker and Kui Yu
Advanced Materials Laboratory
Sandia National Laboratories
P.O. Box 5800
Albuquerque, NM 87185-0776

Huifang Xu
Department of Earth and Planetary Sciences
Yi Yang
Advanced Materials Laboratory
University of New Mexico
Albuquerque, NM 87106

Paul S. Braterman and Zhiping Xu
Department of Chemistry
The University of North Texas
Denton, TX 76203-5070

Abstract

This report summarizes the results obtained from a Laboratory Directed Research & Development (LDRD) project entitled "Investigation of Potential Applications of Self-Assembled Nanostructured Materials in Nuclear Waste Management". The objectives of this project are to (1) provide a mechanistic understanding of the control of nanometer-scale structures on the ion sorption capability of materials and (2) develop appropriate engineering approaches to improving material properties based on such an understanding.

The project has been focused on two types of nanostructured materials: self-assembled mesoporous materials and layered double hydroxides. The major results are summarized below:

- Acid-base titration experiments were performed on both mesoporous alumina and alumina particles under various ionic strengths. Under the same chemical conditions, the surface charge per mass on mesoporous alumina was as much as 45 times higher than that on alumina particles. This difference cannot be fully explained by the surface area difference between the two materials. The titration data have demonstrated that the nano-scale confinement has a significant effect, most likely via the overlap of the electric double layer (EDL), on ion sorption onto mesopore surfaces. This effect cannot be adequately modeled by existing surface complexation models, which were developed mostly for an unconfined solid-water interface.
- As the pore size is reduced to a few nanometers, the difference between surface acidity constants *(*$\Delta pK = pK_2 - pK_1$) decreases, giving rise to a higher surface charge density on a nanopore surface than that on an unconfined mineral-water interface. The change in surface acidity constants results in a shift of ion sorption edges and enhances ion sorption on nanopore surfaces. Also, the water activity in a nanopore is greatly reduced, thus increasing the tendency for inner sphere complexation and mineral precipitation. All these effects combine to preferentially enrich trace elements in nanopores. This enrichment mechanism has a significant implication to many fundamental geochemical issues such as the irreversibility of ion sorption/desorption and the bioavailability of subsurface contaminants. The discovery of this mechanism provides a scientific basis for engineering high-performance ion adsorbents for nuclear waste management.
- Layered double hydroxides (LDH) have shown a great promise for removing anionic contaminants. The anion sorption coefficients (K_d) have been measured for both activated and non-activated Mg-Al LDH materials. The activated material has a much higher anion sorption coefficient than the non-activated one, indicating that calcination can significantly improve anion sorption capacity of LDH. Sorption isotherms for Re and Se on the activated LDH material roughly follow the Freundlich isotherm, indicating the existence of various sorption sites with different sorption capabilities. Anions tend to first sorb on the external surface sites. As the anion concentration or the ionic strength increases, more anions are forced into the interlayer of LDH, and consequently the sorption becomes dominated by an interlayer ion exchange. The experimental data have indicated that the external surface sites have a very high affinity for anions, especially divalent and trivalent anion.
- To study sorption kinetics, calcined Mg-Al LDH was added to the solution both as a pre-wetted slurry (allowing 24 hours for rehydration), and as a dry powder. Sorption results varied for different anionic complexes. For selenate and perrhenate, an incubation time was required for the dry material to achieve the same K_d value as the pre-wetted material. For arsenate, however, both wetted and dry materials initially had high K_ds, which decreased with time. These behaviors are attributed to the structural reconstruction of the calcined LDH material in solution. Se and Re are not highly sorbed by the phases present in the calcined material, but are incorporated as interlayer anions in the LDH structure upon hydration and reconstruction, while As

may be sorbing onto the dehydration products, and being partially released during rehydration.

- A self-assembled layered double hydroxide-surfactant hybrid nanomaterial was developed. A novel packing mode specific to the cis-unsaturated hydrocarbon chain in this material was proposed. The kink imposed by the cis-double bond in oleate leads to partial overlap between chains on adjacent layers. Incorporation of surfactant into the growing crystallite leads to a reversal of the usual LDH growth habit, and results in crystallite shapes featuring ribbon-like sheets, therefore increasing external surface sites for anion sorption. The thermal decomposition behavior of as-prepared organic/inorganic nanocomposites in air and N_2 was determined. The thermal decomposition of the LDH-surfactant nanomaterial in N_2 leads to the formation of a highly dispersed nanocomposite material of metal oxides and activated-carbon-like compound, which is expected to exhibit a high sorption affinity for both anions and cations.

Contents

Figures

Tables

1. General Introduction

1.1 Purposes

Successful waste and environmental management requires technology innovation to address challenging technical problems. One of the keys to this technology innovation is the development of functional materials that can be used for effective waste treatment, separation, containment, and monitoring. For instance, with an increasing concern with pertechnetate (TcO_4^-) in radioactive wastes and arsenate (AsO_4^{3-}) contamination in groundwater, the development of effective anion getters is particularly of environmental interest (e.g., Balsley et al., 1998). Also, the development of a new generation of chemical sensors for environmental monitoring relies on the discovery of novel sensing materials. The traditional approach to developing new materials is no longer able to meet increasing waste management needs. The major limitation of the traditional approach is the lack of flexibility for engineering material physical/chemical properties.

With the emergence of so-called nanotechnology, now comes the age that we are able to manipulate material structures at nanometer scales, thus opening up unlimited possibilities for new functional material development. This report summarizes the results obtained from a Laboratory Directed Research & Development (LDRD) project entitled "Investigation of Potential Applications of Self-Assembled Nanostructured Materials in Nuclear Waste Management". The objectives of this project are to (1) provide a mechanistic understanding of the control of nanometer-scale structures on the ion sorption capability of materials and (2) develop appropriate engineering approaches to improving material properties based on such an understanding. The project has been focused on two types of nanostructured materials: self-assembled mesoporous materials and layered double hydroxides.

1.2 Nanostructured Materials

Mesoporous materials possess nanometer-scale pore structures and are synthesized using self-assembled supramolecular templating processes (Figure 1-1) (e.g., Brinker et al., 1999; Zhang et al., 2003). Self-assembly is the spontaneous organization of materials through noncovalent interactions. It typically employs molecules of low symmetry that are programmed to organize into well-defined supramolecular assemblies. Most common are amphiphilic surfactant molecules or polymers composed of hydrophobic and hydrophilic parts. Above the critical concentration, surfactants in aqueous solution assemble into micelles, spherical or cylindrical structures that maintain the hydrophilic parts of the surfactant in contact with water while shielding the hydrophobic parts within the micellar interior. Further increases in surfactant concentration result in the self-organization of micelles into periodic hexagonal, cubic, or lamellar mesophases. Inorganic precursors then precipitate on the surfactant structural template. Inorganic mesoporous materials are obtained through removal of surfactants by chemical methods or calcination. Due to very large surface area, controllable pore size, and, in some important cases, high surface charge density, mesoporous can potentially serve as an ion

getter, separation membrane, catalyst, and sensing material with high sorption capacity and chemical selectivity.

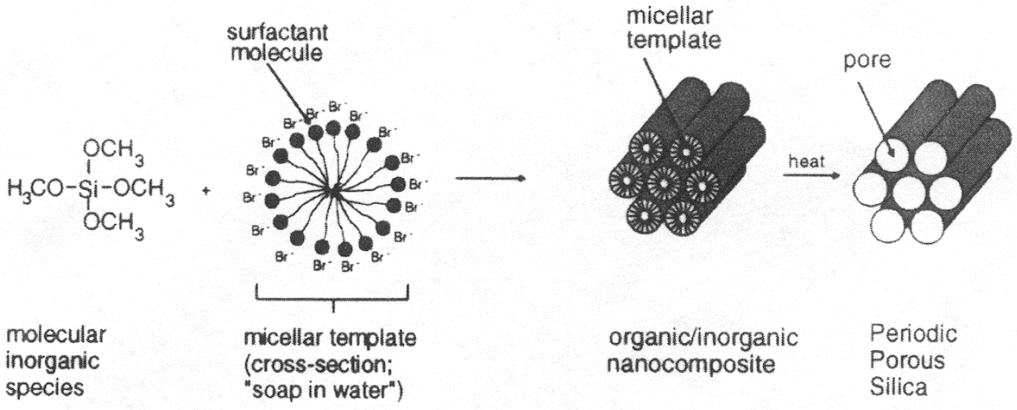

Figure 1-1 Schematic illustration of using surfactant templating approach to prepare mesophase silica with controlled pore structure and pore size

The layered double hydroxides (LDH) consist of positively charged, close-packed, metal hydroxide layers, whose surplus positive charge, arising from the substitution of the trivalent cation M(III) for the divalent cation M(II), is neutralized by the exchangeable anion Y (Figure 1-2) (Rives and Ulibarri, 1999). LDH swell with large anions, but do not exfoliate, presumably because in these materials, unlike normal clays, there is hydrogen bonding between the layers and the interlayer species). Since hydrotalcite, $Mg_6Al_2(OH)_{16}CO_3.4H_2O$, is a member of this family, they are often referred to as hydrotalcite-like compounds. The materials occur in nature but are easily and cheaply synthesized in bulk and some formulations are commercially available. Mineral specimens commonly include Mg, Mn, Fe, Co or Ni as divalent cations, along with Fe(III), Al(III), or occasionally Cr(III), and the exchangeable anion is usually chloride, carbonate, or sulfate. Synthetic analogs can incorporate Cu(II), V(III), and Ga(III) among others, while almost any anion can be incorporated, subject to restrictions on size that have not as yet been fully determined. Among candidate anion getter materials identified so far, layer double hydroxides (LDH) have shown the most promise (Kang et al., 1999).

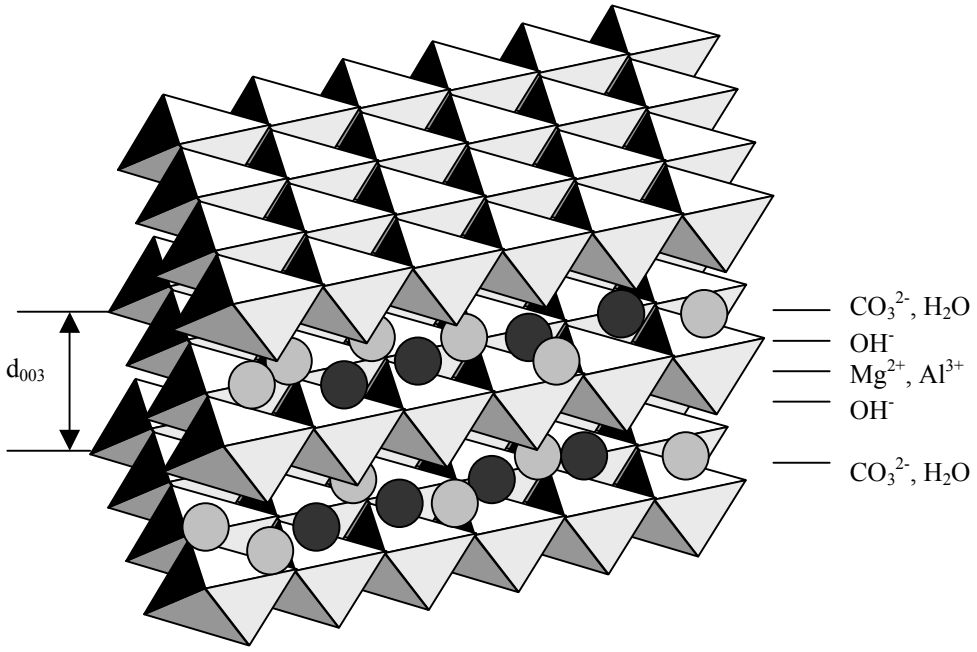

Figure 1-2 Schematic illustration of crystallographic structure of hydrotalcite.

1.3 Organization of Report

This report is assembled from five published or to be published papers with each section relatively self-independent. The report is organized as follows:

- Section 1.0: A general introduction to the background information and the basic concept of nanostructured materials. (Contributor: Wang).
- Section 2.0: Interface chemistry of mesoporous materials in terms of surface protonation and deprotonation. (Contributors: Wang, Bryan, H. Xu, Pohl, Yang, and Brinker).
- Section 3.0: The effect of nanopore confinement on ion sorption and its geochemical implications. (Contributors: Wang, Bryan, H. Xu, and Gao).
- Section 4.0: Equilibrium sorption of anions onto LDH materials. (Contributors: Wang, Bryan, H. Xu, and Braterman).
- Section 5.0: The effect of structure restoration on anion sorption onto LDH materials. (Contributors: Bryan, Wang, H. Xu, Braterman, and Gao).
- Section 6.0: Development of surfactant-LDH nanocomposite materials. (Contributors: Z. Xu, Braterman, Yu, H. Xu , Wang, and Brinker).
- Section 7.0: General conclusions. (Contributor: Wang).

1.4 References

Balsley, S. D., P. V. Brady, J. L. Krumhansl, and H. L. Anderson. 1998. "Anion scavengers for low-level radioactive waste repository backfills," *J. Soil Contamination*. Vol. 7, pp. 125-141.

Brinker, C.J., Y. F. Lu, A. Sellinger and H. Y. Fan. 1999. "Evaporation-induced self-assembly: Nanostructures made easy," *Advanced Materials*. Vol.11, no.7, pp.579-585.

Kang, M. J., K. S. Chun, S. W. Rhee, and Y. Do. 1999. "Comparison of sorption behavior of I- and TcO4- on Mg/Al layered double hydroxide," *Radiochimica Acta*. Vol. 85, no.1-2, pp. 57-63.

Rives, V and M. A. Ulibarri. 1999. "Layered double hydroxides (LDH) intercalated with metal coordination compounds and oxometalates," *Coordination Chemistry Reviews*. Vol. 181, pp.61-120.

Zhang, J., Z.-L. Wang, J. Liu, S. Chen, and G.-Y. Liu. 2003. *Self-Assembled Nanostructures*. New York: Kluwer Academic/Plenum Publishers.

2. Interface Chemistry of Nanostructured Materials: Effect of Nanopore Confinement on Surface Acidity Constants

2.1 Introduction

Functional materials that can effectively remove specific ions from aqueous solutions are of great interest for chemical separation and environmental cleanup applications. Recent progress in the synthesis of nanostructured materials opens a new arena for developing such materials. Mesoporous materials synthesized using supramolecular templating processes (Kresge et al., 1992; McCullen et al., 1995; Tanev and Pinnavaia, 1995; Anderson et al., 1995; Brinker et al., 1999; Selvam et al., 2001) have attracted particular attention, due to their large specific surface area and controllable nano-scale pore size and geometry. Mesoporous silica with a monolayer of thiol (-SH) group grafted on its pore surface displays a high sorption capacity for removing mercury from aqueous solutions (Feng et al., 1997; Chen et al., 1999). Uncalcined mesoporous silicate materials synthesized with hexadecyltrimethylammonium bromide as a template are able to remove significant amounts of trichlorethylene and tetrachloroethylene from water (Zhao et al., 2000), while calcined mesoporous silicates or titanosilicates were found to have a capability for removing copper, lead, and uranyl ions from aqueous solutions (Xu et al., 1999; Shin et al., 1999; Jung et al., 2001). Furthermore, an ordered mesoporous anion-exchange inorganic/organic hybrid resin has been suggested for radionuclide separation (Ju et al., 2000).

Various mesoporous materials have been synthesized using self-assembled supramolecular templating processes (Kresge et al., 1992; McCullen et al., 1995; Tanev and Pinnavaia, 1995; Anderson et al., 1995; Brinker et al., 1999; Selvam et al., 2001). Self-assembly is the spontaneous organization of materials through noncovalent interactions. It typically employs molecules of low symmetry that are programmed to organize into well-defined supramolecular assemblies. Most common are amphiphilic surfactant molecules or polymers composed of hydrophobic and hydrophilic parts. Above the critical concentration, surfactants in aqueous solution assemble into micelles, spherical or cylindrical structures that maintain the hydrophilic parts of the surfactant in contact with water while shielding the hydrophobic parts within the micellar interior. Further increases in surfactant concentration result in the self-organization of micelles into periodic hexagonal, cubic, or lamellar mesophases. Inorganic precursors then precipitate on the surfactant structural template. Inorganic mesoporous materials are obtained through removal of surfactants by chemical methods or calcination. Materials synthesized as such would have controllable nano-scale pore size and pore geometry and therefore provide an ideal system for studying the effect of nano-scale confinement on ion sorption.

The detailed mechanism of ion sorption by mesoporous materials is yet to be understood. It is generally known that a condensed phase could exhibit different physical and chemical properties than its bulk phase as its dimension is reduced to a nanometer scale (Adair et al., 1998; José-Yacamán and Mehl, 1998). For a given mesoporous

material, two factors are expected to control the ion sorption capability of the material: the accessible pore surface area and the effect of nano-scale pore space confinement. The former is determined by the geometry and connectivity of mesopores and, to some degree, can be optimized by controlling the formation of an appropriate mesophase during material synthesis (Brinker et al., 1999; Selvam et al., 2001). A uniform pore structure with well defined channels has been shown to have a great advantage over a disordered pore network in terms of the access of guest species to the binding sites (Mercier and Pinnavaia, 1997). One direct consequence of the nano-scale pore space confinement is the overlap of the electric double layer (EDL) within a mesopore, creating a different surface complexation environment relative to that for an unconfined surface. This overlap certainly affects the overall ion sorption on mesoporous materials. In this section, we present the results of our pH titration and ion sorption experiments with mesoporous alumina and of the related molecular simulations. We want to demonstrate the importance of the nano-scale pore space confinement for the ion uptake by mesoporous materials.

2.2 Experimental Section

Materials: Mesoporous alumina was obtained from Aldrich Chemical Company, Inc. The pore size of this material is reported to be 6.5 nm. Transmission Electron Microscopic (TEM) images show that this material has a "worm-hole-like" meso-structure (Figure 2-1A). Mesopores are irregular and have dimensions of ~ 2 nm x 2 nm x 10 nm. The surface area of the mesoporous alumina was measured to be ~ 284 m^2/g, consistent with reported values (Cabrera et al., 1999). Lattice fringes in Figure 2-1B indicate that the material is composed of amorphous alumina and nano-crystalline particles. These crystallites are identified to be γ-Al_2O_3 from electron diffraction patterns. For a comparison between mesoporous and non-mesoporous materials, 80 - 200 mesh activated alumina particles were purchased from Fisher Chemicals. Our TEM observation indicates that the outer rims of particles consist of an amorphous Al_2O_3 phase and very closely resemble the mesoporous alumina in chemical composition and crystallinity. The surface area of the activated alumina particles is determined to be 118 m^2/g; the large surface area of the material is probably due to the presence of micro-fractures on particle surfaces. The surface areas of both mesoporous alumina and activated alumina particles were determined using a Micrometritics Gemini 2360 surface analyzer.

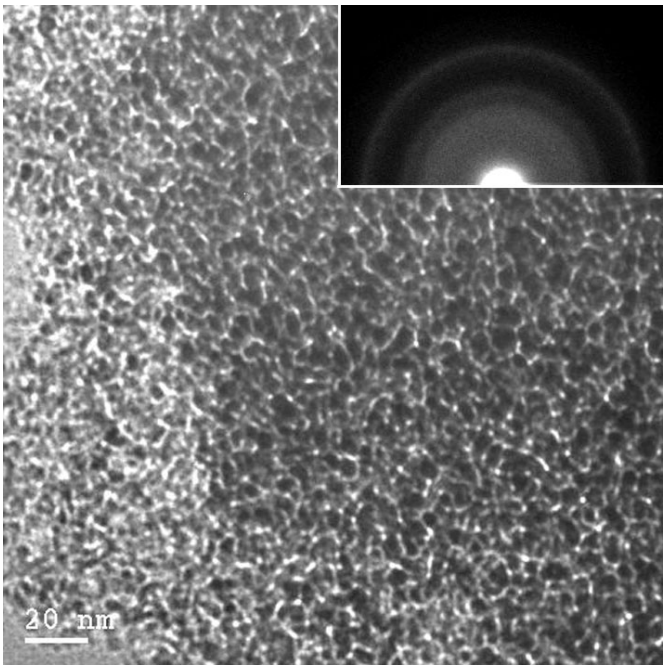

A

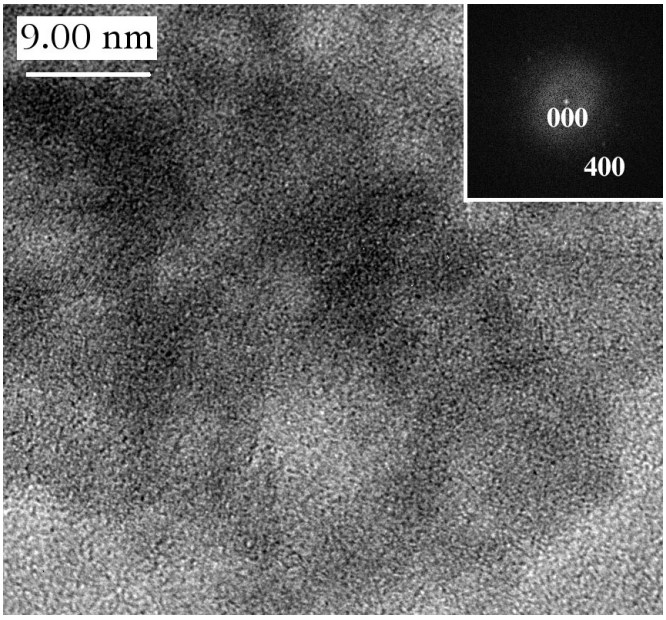

B

Figure 2-1. Transmission Electron Microscopic (TEM) images of mesoporous alumina used in this study. A - The material has a "worm-hole-like" meso-structure. Mesopores are irregular and have dimensions of ~ 2 nm x 2 nm x 10 nm. Inserted is a selected-area electron diffraction (SAED) pattern of the mesoporous alumina. B - Lattice fringes indicate that the material is composed of nano-scale crystalline particles. From electron diffraction patterns, these crystallites are identified to be γ-Al_2O_3. Inserted is a Fast Fourier Transform (FFT) from an area of the HRTEM image showing 2 Å spot corresponding to 400 reflection.

Titration: pH titration experiments were conducted for both mesoporous alumina and 80 - 200 mesh alumina particles using a Mettler DL25 Autotitrator. The titration was performed in three electrolyte solutions: deionized (D.I) water, 0.01 M NaCl, and 0.1 M NaCl. For mesoporous alumina, 0.1 gram of solid was added to 50 mL of electrolyte solution and then titrated with 0.0564 M NaOH. The titration time interval was set to 90 seconds (the maximum time allowed by the instrument) to minimize the possible effect of slow diffusion of ions in mesopores. For alumina particles, 1 gram of solid was mixed with 50 mL of electrolyte solutions. The initial pH of the suspension was then adjusted to an acidic range by adding 2.3 mL of 0.0366 M HCl solution. The suspension was then titrated with 0.0564 M NaOH solution. As pH re-equilibration between each titration step was extremely rapid, the titration time interval was set to 20 seconds. All the titration experiments were performed under CO_2-free conditions.

Kinetic studies: 0.1 gram of mesoporous alumina or 1 gram of 80 - 200 mesh alumina particles was mixed with 50 mL of deionized water and stirred for 5 minutes. A small amount of 0.094 M NaOH was then added to each suspension: 400 μL for mesoporous alumina and 100 μL for alumina particles. The pH of the suspension was then monitored at 10 second intervals using the autotitrator.

pH/sorption edge experiments: Each sample consisted of 20 mL of deionized water and 0.2 g of mesoporous alumina. The pH of each sample was adjusted using HCl or NaOH to obtain a range of pH values from 4 to 9, and then each suspension was spiked with Zn to produce an initial concentration of 10 ppm. The samples were then stirred continuously for 16 – 20 hours, and the liquid was sampled, filtered with a 0.2 μm syringe filter, and analyzed for Zn using an Inductively Coupled Plasma Optical Emission Spectrometer (ICP-OES).

2.3 Experimental Results

Surface charge: The titration results for both mesoporous alumina and alumina particles are shown in Figure 2-2. The effect of ionic strength on pH titration curves follows a similar trend for both materials. All the titration curves cross over a common pH value, corresponding to a so-called point of zero charge (PZC), at which the surface charge becomes neutral and the effect of ionic strength on surface H^+ exchange diminishes. From Figure 2-2, the PZC is estimated to be ~ 9.1 for mesoporous alumina and ~ 8.7 for alumina particles, both within the range reported for alumina oxides (Stumm, 1992), thus indicating that the nano-scale pore space confinement does not have a significant effect on the PZC of pore surfaces. This observation is consistent with a general consideration that the PZC is an intrinsic property of a solid-water interface and mainly determined by the chemical identity and crystallinity of the solid (Stumm, 1992).

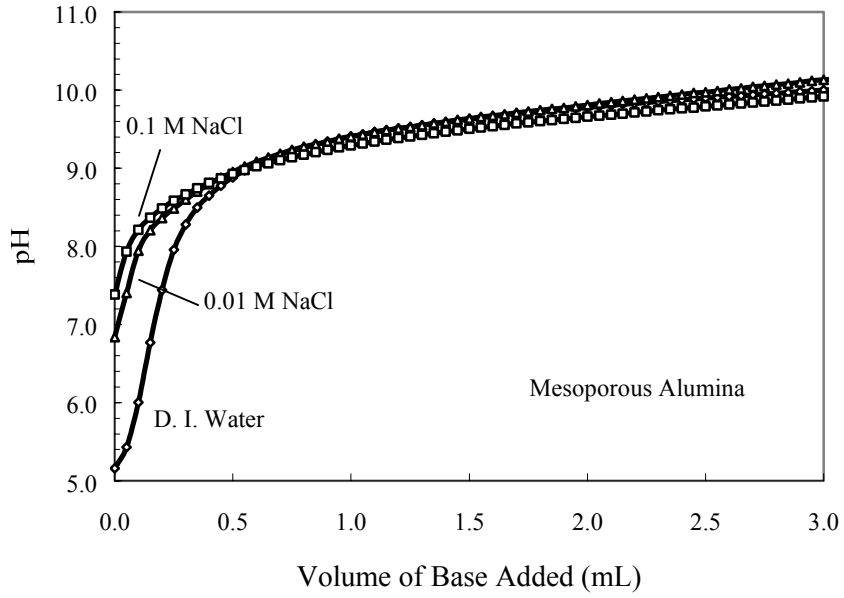

A

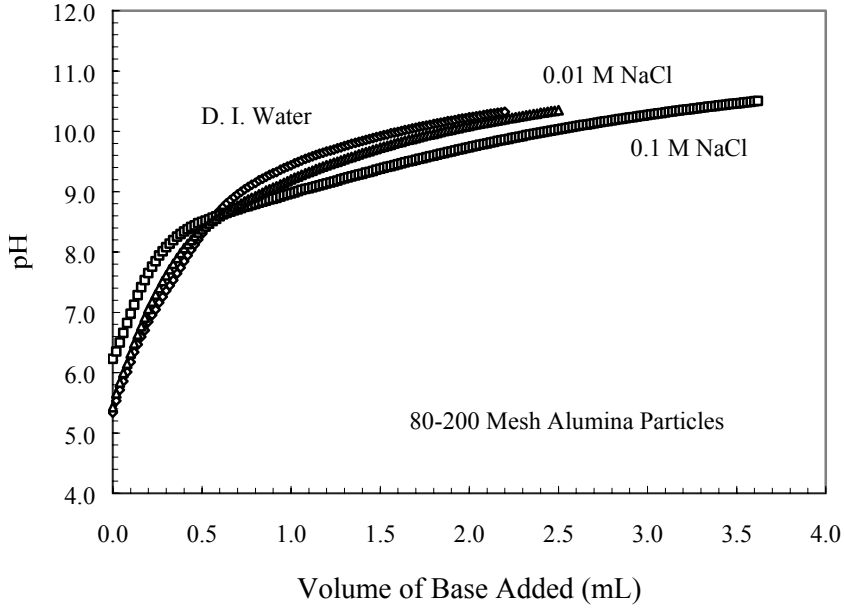

B

Figure 2-2. Results of pH titration experiments. A - 0.1 gram mesoporous alumina in 50 mL electrolytes. B - 1 gram of 80 - 200 mesh alumina particles in 50 mL of solutions. Each solid-liquid suspension was titrated with 0.0564 M NaOH in three electrolyte solutions: deionized (D.I.) water, 0.01 M NaCl, and 0.1 M NaCl. The point of zero charge (PZC) is defined as the pH at which all three titration curves cross.

With the estimated PZC, the moles of surface charge per gram of material (Q) can be calculated by (Stumm, 1992):

$$Q = \frac{c_A - c_B + ([H^+] - [OH^-])V}{M} - Q_c \quad \text{(2-1A)}$$

$$Q_c = \left.\frac{c_A - c_B + ([H^+] - [OH^-])V}{M}\right|_{pH = PZC} \quad \text{(2-1B)}$$

where c_A and c_B are moles of acid and base added; V is the volume (L) of liquid; M is the mass of solid in the sample; Q_c is a correction term for the possible presence of additional acid or base in the initial materials; and [] indicates the concentrations of aqueous species. The concentrations of ions H^+ and OH^- are calculated from the measured pH with a correction for activity coefficients. For the mesoporous material, the correction term (Q_c) is calculated to be negative, indicating the presence of additional acid in the initial material that needs to be taken into account in the surface charge balance calculation. This is confirmed by the observation that adding 0.1 g mesoporous alumina to 50 mL deionized water results in a pH of 5.0. The functional dependence of surface charge on solution (pH – PZC) is shown in Figure 2-3. The figure shows that, for a given (pH – PZC), the surface charge per mass on mesoporous alumina can be as much as 45 times as high as that of the alumina particles, thus demonstrating the excellent ion sorption capability of mesoporous materials. Since the surface charges in mesoporous materials distribute within intra-particle nano-scale pores, in which a differential movement between solution and pore surface is expected to be difficult, the measurement of these charges using an electrokinetic method might not be feasible.

For simplicity, the surface charge calculation in Equation (2-1) ignores a possible contribution of dissolved aluminum species. This approximation is reasonable because the total dissolved aluminum concentrations measured at the end of titration (i.e., at the high pH end) are too low to account for the observed large surface charge difference (Table 2-1). Also, the large variations in the surface charge ratio between the two materials for different ionic strengths cannot be explained by the presence of dissolved aluminum species, because the effect of ionic strength on the activity coefficients of dissolved species are negligible under the relevant experimental conditions. To rule out the effect of a possible formation of a secondary surface layer on the surface charge calculation, a careful TEM observation was performed, which indicates that surface structure and composition of both mesoporous and activated alumina particles remained intact and no surface layer was formed during the titration.

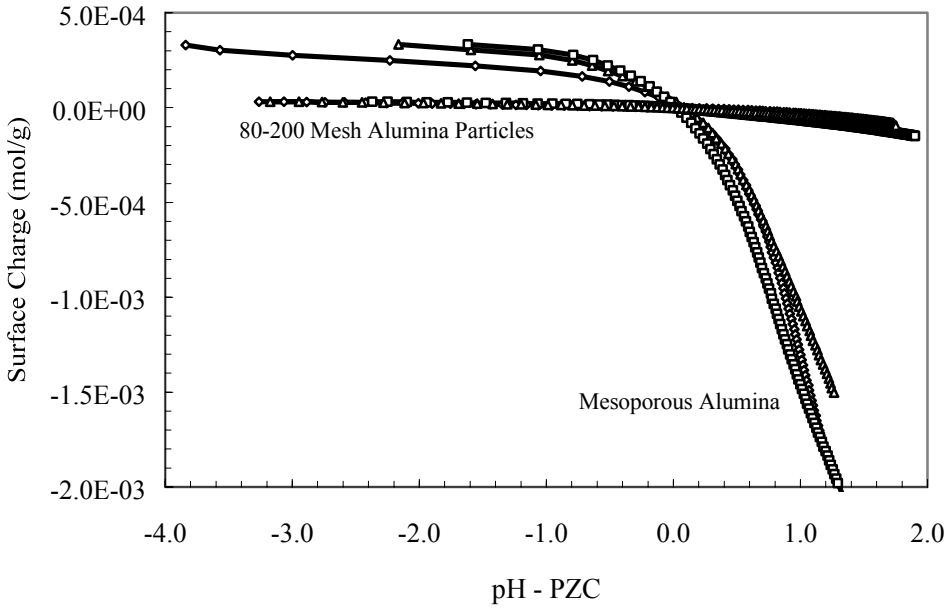

Figure 2-3. Surface charge density as a function of (pH – PZC). For a given (pH – PZC), the surface charge per mass on mesoporous alumina can be as much as 45 times higher than that on alumina particles.

Table 2-1. Comparison of dissolved Al concentrations with surface charges calculated using Equation (2-1). The dissolved Al concentrations were measured at the end of titration experiments (at pH = 10). For pH > 7, $Al(OH)_4^-$ is a dominant species (Drever, 1982). The dissolution of alumina materials follows: $AlO_{2/3} + 3/2H_2O = Al(OH)_3 + OH^- = Al(OH)_4^-$, i.e., one dissolved Al consumes one hydroxyl ion. For an easy comparison, both dissolved Al concentrations and surface charge densities are converted to the same unit (mol/L of solution). The calculated surface charge ratios, whether corrected for dissolved Al or not, are much larger than the surface area ratio between the two materials (= 2.4), indicating the effect of nano-scale pore space confinement.

	Dissolved Al (mol/L)		Surface charge (mol/L)*		Surface charge ratio, mesoporous alumina (mol/g) /alumina particles (mol/g)*	
	Alumina particles	Mesoporous alumina	Alumina particles	Mesoporous alumina	Not corrected for dissolved Al	Corrected for dissolved Al
D.I. water	0.00014	0.00079	0.0011	0.0026	24.1	19.3
0.01 M NaCl	0.00017	0.00065	0.0013	0.0021	15.9	12.7
0.1 M NaCl	0.00020	0.00073	0.0020	0.0029	14.8	12.3

* Negative charge.

** In each titration, either 0.1 g of mesoporous alumina or 1.0 g of alumina particles was added to a 50 mL solution.

Acidity Constants: For pH values far from the PZC, $Q \cong \{SOH_2^+\}$ for pH < PZC and $Q \cong \{SO^-\}$ for pH > PZC, where Q is the surface charge and {} indicates surface concentrations. Acidity constants of the materials used in the experiments can be calculated by:

$$pK_1 = -\log\left(\frac{\{SOH\}[H+]}{\{SOH_2^+\}}\right) \cong -\log\left(\frac{(S_{tot} - Q)[H+]}{Q}\right) \quad \text{(2-2A)}$$

$$pK_2 = -\log\left(\frac{\{SO^-\}[H+]}{\{SOH\}}\right) \cong -\log\left(\frac{Q[H+]}{S_{tot} - Q}\right) \quad \text{(2-2B)}$$

where S_{tot} is the mole of total surface sites per gram of solid and is estimated to be 0.0023 mol/g for the mesoporous alumina and 0.00098 mol/g for the activated alumina particles assuming 5 hydroxyls per nm^2 (Stumm, 1992). The calculated acidity constants for mesoporous alumina are shown in Figure 4A. Linear extrapolation of *pK*s to zero surface charge gives intrinsic acidity constants: $pK_{1,intr}$ = 9.0 and $pK_{2,intr.}$ = 10.3. For the approximations in Equation (2-2) to be valid, the extrapolation only uses the data with pH values far from the PZC (Figure 2-4A). It should be pointed out that the mesoporous material used in the experiments also includes a certain number of external (unconfined) surface sites. Here, however, we have no intention to differentiate these sites from the sites on mesopore surface, because the latter is dominant. The acidity constants obtained above mainly reflects the chemistry of mesopore surface. Similarly, the intrinsic acidity constants for activated alumina particles are estimated to be $pK_{1,intr}$ = 7.7 and $pK_{2,intr.}$ = 11.0 (Figure 2-4B). Using the relationship of $PZC = (pK_1 + pK_2)/2$, we can estimate the PZC of 9.65 for mesoporous alumina and 9.35 for activated alumina particles. Both values, though slightly higher than those estimated directly from Figure 2-2 (probably due to uncertainties associated with the linear extrapolation in Figures 2-4A and B), are close to each other, again indicating little effect of nano-scale pore space confinement on the PZC of mesopore surfaces.

Interestingly enough, however, the pore space confinement does have a significant effect on the acidity constants of the materials. As shown in Figure 2-4C, the separation between the two acidity constants, ΔpK (= pK_2 - pK_1), becomes significantly narrowed for the mesoporous alumina as compared to that for the alumina particles. As a result, within mesopores, neutral surface species SOH become depleted, and the pore surface tends to be either positively or negatively charged. This is one of the reasons why a mesoporous material has a much higher surface charge density than the corresponding non-mesoporous material. This result is consistent with the molecular modeling simulations presented below.

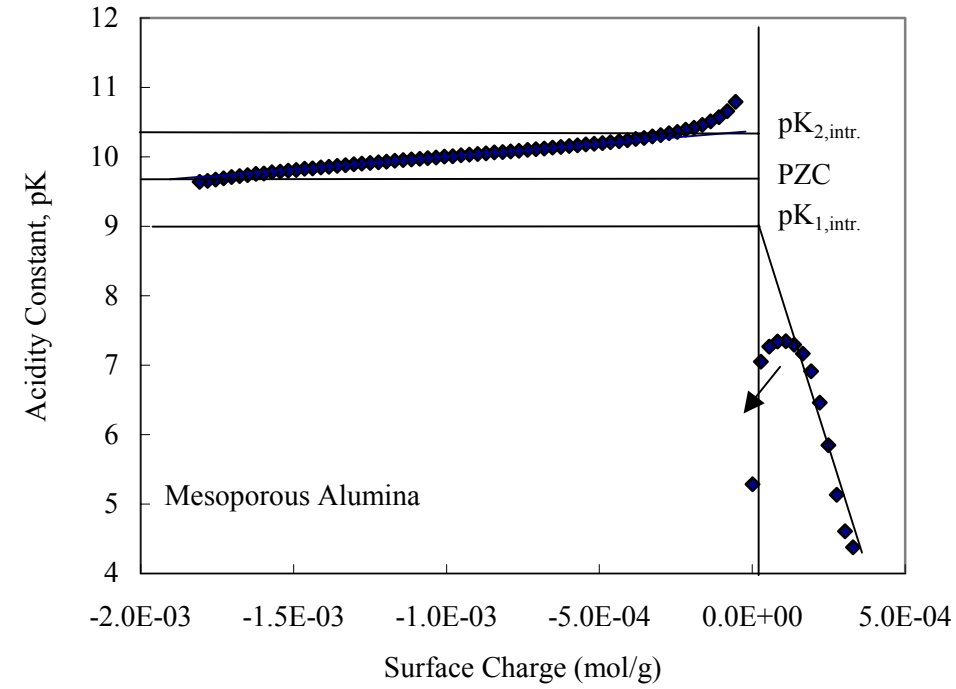
12
11
10
9
8
7
6
5
4
Acidity Constant, pK
pK2,intr.
PZC
pK1,intr.
Mesoporous Alumina
-2.0E-03
-1.5E-03
-1.0E-03
-5.0E-04
0.0E+00
5.0E-04
Surface Charge (mol/g)

A

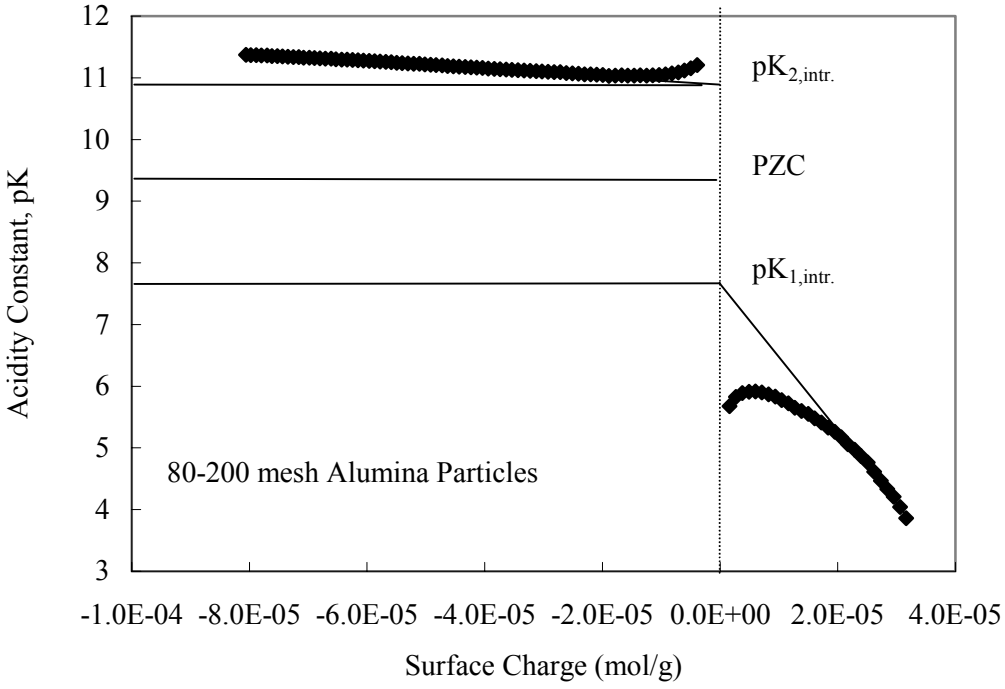
12
11
10
9
8
7
6
5
4
3
Acidity Constant, pK
pK2,intr.
PZC
pK1,intr.
80-200 mesh Alumina Particles
-1.0E-04
-8.0E-05
-6.0E-05
-4.0E-05
-2.0E-05
0.0E+00
2.0E-05
4.0E-05
Surface Charge (mol/g)

B

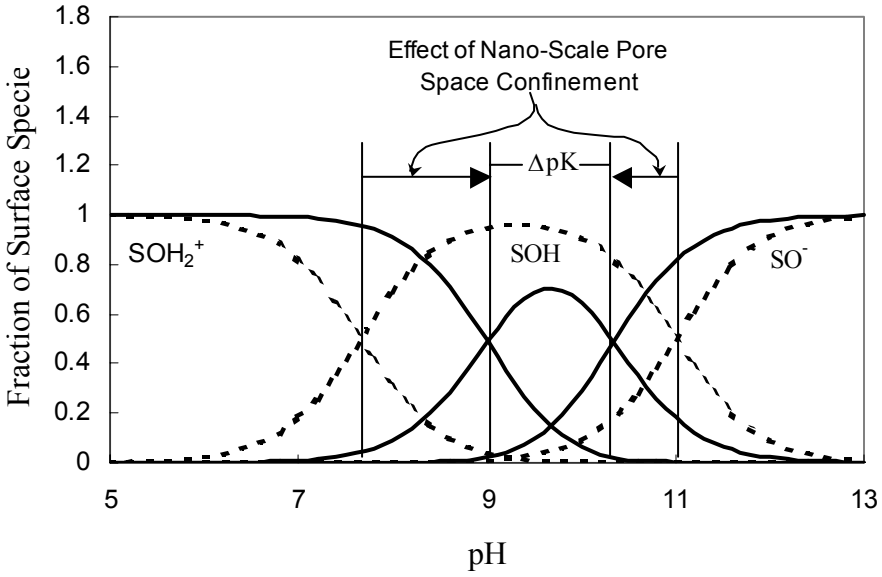

C

Figure 2-4. Acidity constants for mesoporous alumina (A) and activated alumina particles (B) calculated from the titration data in Figure 2-3 using Equation (2). The calculation only includes the data points for the titration in D. I. water and far from the PZC. Linear extrapolation of pK to zero surface charge gives the intrinsic acidity constants $pK_{1,intr.}$ and $pK_{2,intr.}$ C – Surface speciation on mesoporous alumina (solid lines) and activated alumina particles (dashed lines). The separation between the two acidity constants, ΔpK (= pK_2 - pK_1), becomes significantly narrowed for the mesoporous alumina as compared to that for the alumina particles.

Effect of EDL overlap: Two factors could contribute to the observed high surface charge density per mass of mesoporous materials: the large accessible pore surface area per mass and the effect of nano-scale pore space confinement. Since the surface area ratio of the mesoporous alumina to the activated alumina particles is only about 2.4:1, the surface area alone is not sufficient to account for the observed large surface charge difference between the two materials. In Figure 2-5, the surface charges on the mesoporous material are plotted against those on the non-mesoporous material (alumina particles) for the corresponding (pH – PZC) values and ionic strength. If the surface area were the only controlling factor, the resulting curves should fall on a single straight line with its slope defined by the ratio of the measured surface areas. As shown in Figure 2-5, this is not the case, indicating that the nano-scale pore space confinement significantly contributes to the surface charge development on mesoporous materials. For the systems we studied, this contribution is even more important than that from the surface area difference (Figure 2-5). The effect of the pore space confinement must arise from the change in the electric double layer structure (e.g., the overlap of EDL) within mesopores, because it strongly depends on ionic strength.

At a room temperature, the thickness of an electric double layer developed at a planar solid-water interface (L) can be calculated by (Stumm, 1992):

$$L = \frac{1}{3.29 I^{1/2}} \quad [\text{nm}] \qquad (2\text{-}3)$$

where I is the ionic strength of the solution (M). The thickness of EDL for the ionic strength of 0.01 and 0.1 M NaCl are estimated to be 1 and 3 nm respectively. As shown in Figure 2-1A, the shortest dimension of the mesopores in mesoporous alumina is about 2 nm, and a significant overlap of EDL within the mesopores is thus expected.

Most existing surface complexation models have been developed for unconfined solid-water interfaces, for which the overlap of EDL is not a concern (Stumm, 1992; Davis and Kent, 1990; Dzombak and Morel, 1990). The results shown in Figure 2-5 demonstrate that such models are not adequate for predicting the ion sorption onto mesoporous materials if the effect of nano-scale pore space confinement is not explicitly taken into account. Zhmud and his colleagues have attempted to develop a charge regulation model for the surface of porous matrices (Zhmud and Golub, 1995; Zhumd, 1996; Zhumd et al., 1997). In their model, a pore is represented by a cylindrical cavity, and the overlap of EDL is taken into account by diminishing the radius of the cylinder. Their model predicts a decrease in surface charge density with decreasing pore size. This prediction seems inconsistent with the titration data we obtained (Figure 2-5). It should be pointed out that the terminology “electric double layer (EDL)” used here only loosely refers to the electric charge distribution at mesopore surfaces, which does not necessarily resembles the EDL conceptualized for an unconfined interface. A generalization of the existing EDL concept to a nano-scale confined system is warranted.

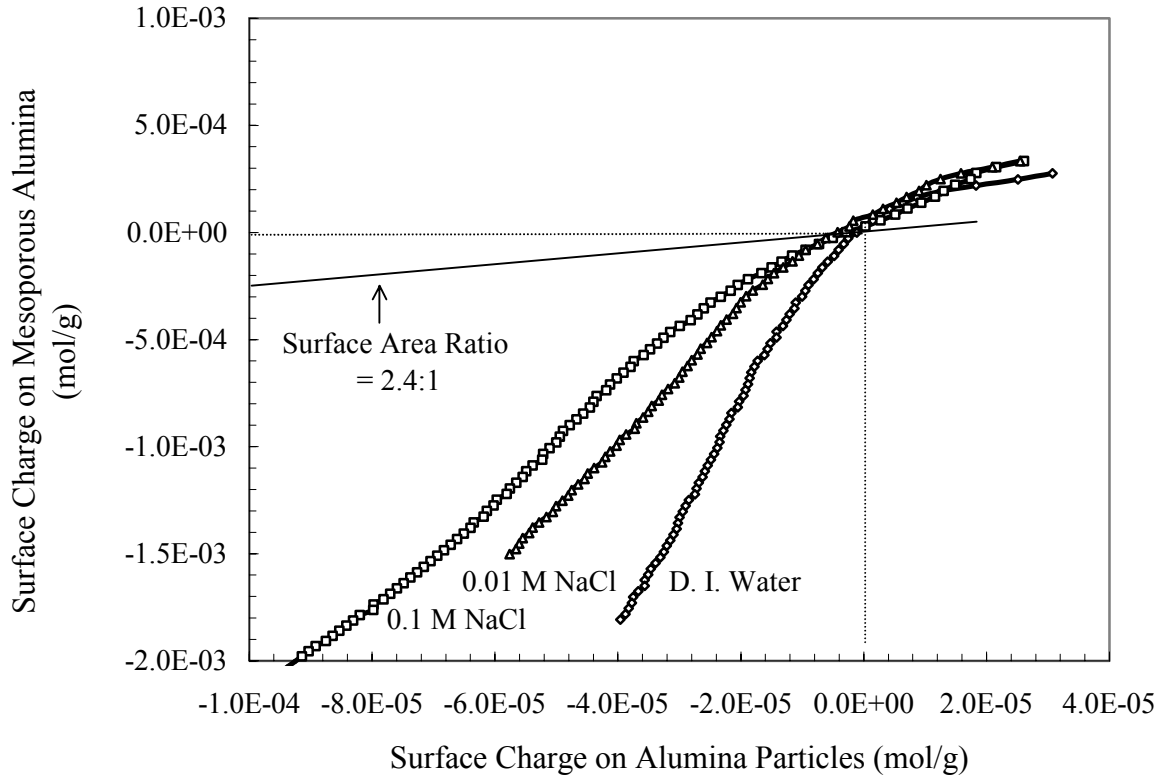

Figure 2-5. Surface charge on mesoporous alumina vs. surface charge on alumina particles for corresponding (pH – PZC) values and ionic strengths. For each ionic strength, the surface charges on both materials at various (pH – PZC) values are read from Figure 3, and then the charges on one material are plotted against the charges on the other material for the same pH – PZC values. If the difference in surface charge between the two materials were controlled only by the surface area difference, the obtained surface charge vs. surface charge curves would fall on a single straight line with its slope defined by the ratio of the measured surface areas (= ~ 2.4:1). The deviation from the straight line is attributed to the effect of nano-scale pore space confinement, probably via the overlap of the electric double layer.

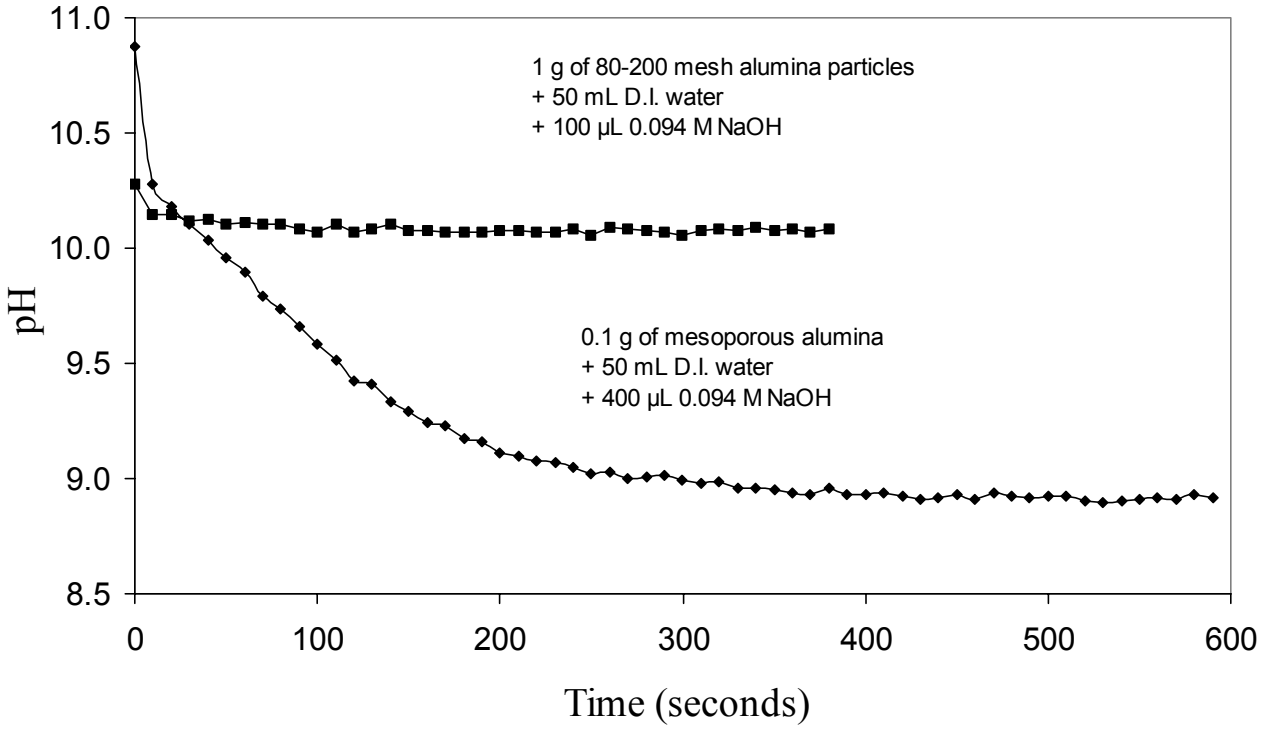

Figure 2-6. Rates of ion uptake by mesoporous alumina and alumina particles. The rate for the mesoporous material is relatively slow, and it could take as long as 4 - 5 minutes for ion sorption to completely reach equilibrium.

Kinetics of ion sorption on mesoporous alumina: The ion uptake rates for both mesoporous alumina and alumina particles are shown in Figure 2-6. Clearly, the rate for the mesoporous material is relatively slow, and it could take as long as 4 - 5 minutes for ion sorption to completely reach equilibrium. The slow rate is due to ion diffusion in small pores. The surface area of mesoporous alumina might not be totally accessible during our titration experiments, because the maximum titration interval allowed by the instrument is 90 seconds. However, this kinetic effect is negligible to our surface charge balance calculations, because at a linear concentration scale, ion sorption can still reach more than 90% of completion over the 90 second time interval.

Zinc sorption on mesoporous alumina: The pH/sorption edge for Zn sorption on mesoporous alumina is shown in Figure 2-7. The sorption coefficient for mesoporous alumina is generally about two orders of magnitude higher than that reported for alumina particles (Tao et al., 2000), which seems consistent with the molecular modeling results summarized below. As a result, the sorption edge for a mesoporous material generally shifts to a lower pH and become sharper relative to that for a non-mesoporous material.

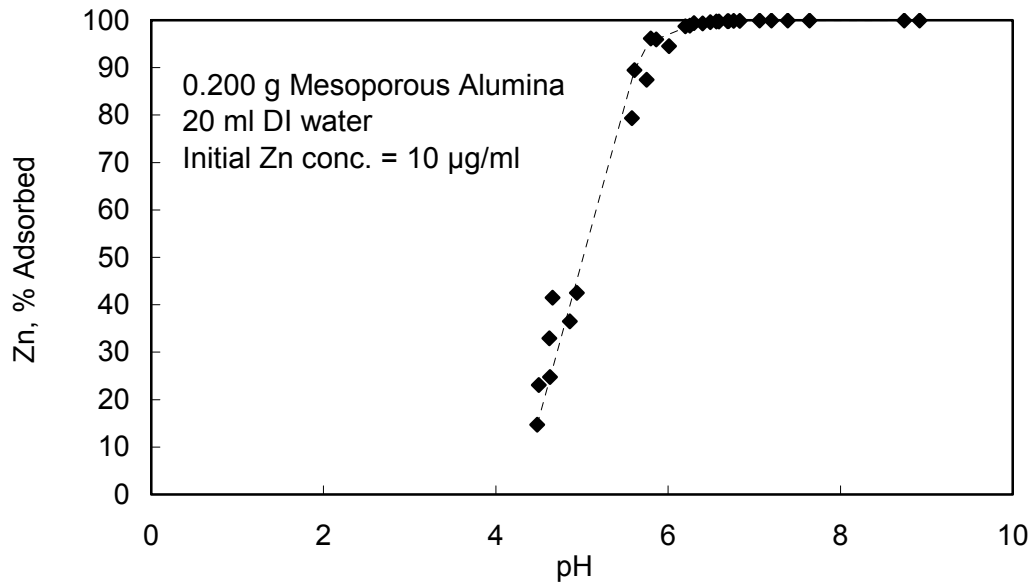

A

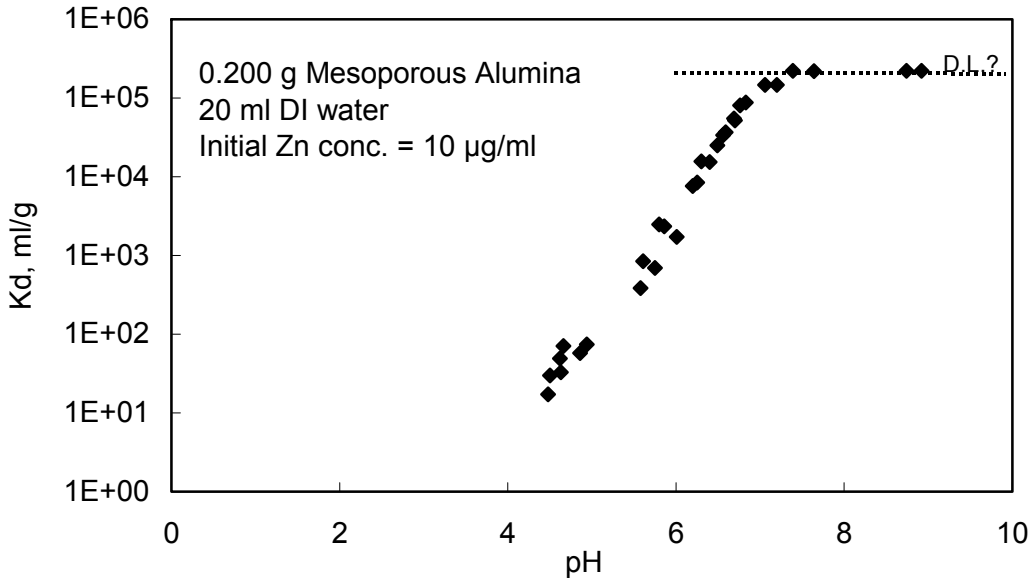

B

Figure 2-7. Zn sorption on mesoporous alumina. The sorption edge is around the pH of 5. A – percentage of Zn adsorbed vs. pH; B – K_d vs pH. The values shown above pH 7 are minimum values, based upon the detection limit for Zn.

2.4 Molecular Modeling

To further clarify the effect of nano-scale pore space confinement, a molecular modeling simulation was performed for ion sorption between two parallel oxide surfaces. Modeling took place at two different scales of length. At the lowest level, a quantum mechanic calculation was conducted for determining the size and charge distribution of adsorbates. The program DMol3 from MSI was used to carry out this geometry optimization modeling (Molecular Simulations, Inc., 1997). The final simulations were performed using the density functional theory (DFT) described by Frink and Van Swol (Frink and Van Swol, 1994, 1997, 1998). In these simulations, the molecular detail is removed and only the component's density is determined based on the equilibrium of the system.

The DFT simulations were performed separately for two types of idealized oxide surfaces arranged in a parallel slit pore: a surface covered with hydroxyls and with a surface charge of 0.17 per hydroxyl, and a surface with all hydroxyls removed and with a surface charge of -0.54 per oxygen atom. These values were determined using a charge equilibration method (Rappe and Goddard, 1991). The effect of pore space confinement was simulated by varying the separation between the two oxide surfaces while maintaining the same chemical potential for each chemical species as that in the bulk solution. The sorption coefficient of an ion was then calculated as the ratio of the ion concentration integrated over the mesopore to the concentration in the bulk solution. Figure 2-8 shows the effect of pore size and surface chemistry on the adsorption coefficient. Note that the adsorption coefficients in the figure are normalized to the values corresponding to an unconfined system, i.e., to an infinite separation between the two parallel oxide surfaces in our modeling system, and therefore any deviation from 1 in these coefficients directly indicates the effect of nano-scale confinement on ion sorption. As expected, the surface charge has a significant effect on ion sorption. And more interestingly, this effect is greatly amplified as the pore space decreases down to nanometer scales. This effect could become even more significant for ion sorption in a spherical or cylindrical confined environment. It is shown in Figure 2-8 that for a divalent ion a mesoporous material with a pore size of 2 nm could have an adsorption coefficient two orders of magnitude higher or lower than the corresponding non-mesoporous material. The typical scale for the confinement effect to become significant is less than 10 nm. The modeling results are generally consistent with the experimental data summarized above.

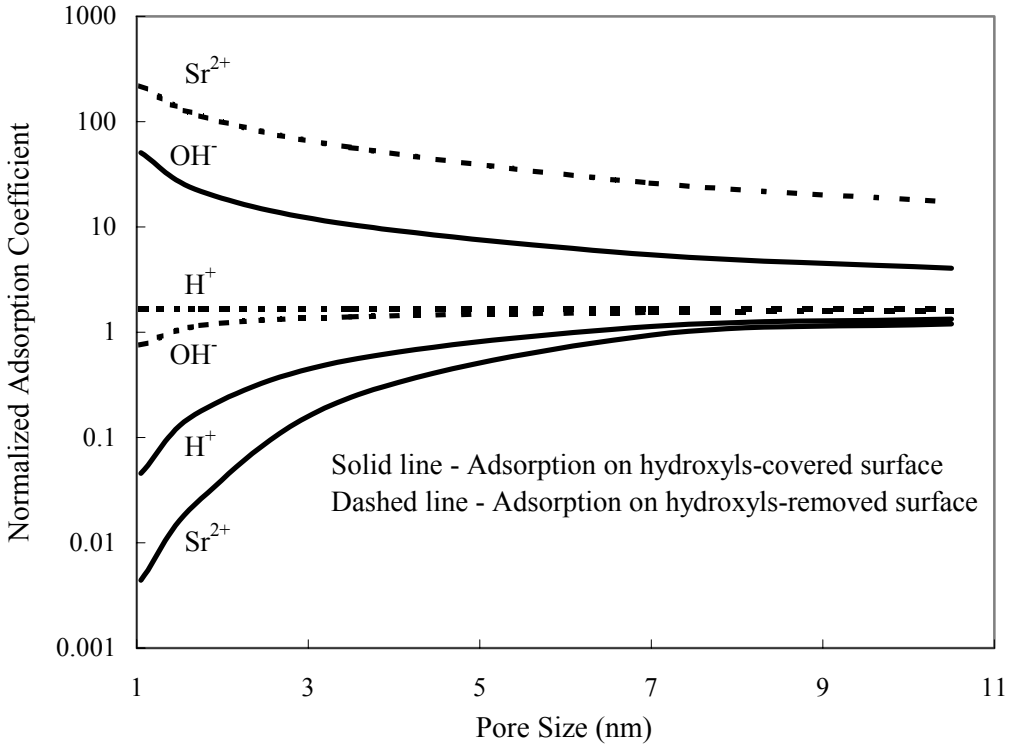

Figure 2-8. Normalized adsorption coefficients calculated as a function of pore size. The adsorption coefficients are normalized to the values corresponding to an infinite separation between the two parallel oxide surfaces.

2.5 Conclusions

Acid-base titration experiments were performed on both mesoporous alumina and alumina particles under various ionic strengths in order to clarify the control of mesopore structures on the surface chemistry of materials. The point of zero charge (PZC) for mesoporous alumina was measured to be 9.1, similar to that for non-mesoporous alumina particles, indicating that the nano-scale pore space confinement does not have a significant effect on the PZC of pore surfaces. However, for a given pH deviation from the PZC, (pH – PZC), the surface charge on mesoporous alumina was as much as 45 times higher than that on alumina particles. This difference cannot be fully explained by the surface area difference between the two materials. Our titration data have demonstrated that the nano-scale pore space confinement has a significant effect, most likely via the overlap of the electric double layer (EDL), on ion sorption on mesopore surface. This effect cannot be adequately modeled by the existing surface complexation models, which were developed mostly for unconfined solid-water interfaces. Our titration data have also indicated that the rate of ion uptake by mesoporous alumina is relatively slow, probably due to ion diffusion into mesopores, and complete equilibration for sorption could take 4 - 5 minutes. To further clarify the effect of nano-scale confinement on ion sorption, a molecular modeling calculation was performed using the density functional theory. The calculation has shown that as the pore size is reduced to nano-scales (< 10 nm), the adsorption coefficients of ions can vary by more than two orders of magnitude relative to those on unconfined interfaces. The prediction is supported by our experimental data on Zn sorption on mesoporous alumina. Owing to their unique surface chemistry, mesoporous materials can be potentially used as effective ion adsorbents for separation processes and environmental cleanup.

2.6 References

Adair, J. H., T. Li, T. Kido, K. Havey, J. Moon, J. Mecholsky, A. Morrone, D. R. Talham, M. H. Ludwig, and L. Wang. 1998. "Recent developments in the preparation and properties of nanometer-size spherical and platelet-shaped particles and composite particles," *Mater. Sci. Eng.* Vol. 23, pp. 139-242.

Anderson, M. T., J. E. Martin, J. Odinek, P. Newcomer. 1995. "Synthesis of surfactant-templated mesoporous materials from homogeneous solution," in: T. J. Pinnavaia & M. F. Thorpe (eds.), *Access in Nanoporous Materials*. New York: Plenum Press. pp. 29-37.

Brinker, C.J., Y. F. Lu, A. Sellinger and H. Y. Fan. 1999. "Evaporation-induced self-assembly: Nanostructures made easy," *Advanced Materials*. Vol.11, no.7, pp.579-585.

Cabrera, S. J. E. Haskouri, J. Alamo, A. Beltrán, D. Beltrán, S. Mendioroz, M. D. Marcos, and P. Amorós. 1999. "Surfactant-assisted synthesis of mesoporous alumina showing continuously adjustable pore sizes," *Adv. Mater.* Vol. 11, pp. 379-381.

Chen, X., X. Feng, J. Liu, G. E. Fryxell, and M. Gong. 1999. "Mercury separation and immobilization using self-assembled monolayers on mesoporous supports (SAMMS)," *Separation Sci. Technol.* Vol. 34, pp. 1121-1131.

Davis, J. A. and D. B. Kent. 1990. "Surface complexation modeling in aqueous geochemistry," in: M. F. Hochella Jr. & A. F. White (eds.), *Mineral-Water Interface Geochemistry*. Mineralogical Society of America. pp. 177-260.

Drever, J. I. 1982. *The Geochemistry of Natural Waters*. Prentice-Hall. 388pp.

Dzombak, D. A. and F. M. M. Morel. 1990. *Surface Complexation Modeling: Hydrous Ferric Oxide*. Wiley-Interscience.

Feng, X., G. E. Fryxell, L. Q. Wang, A. Y. Kim, J. Liu, and K. M. Kemner. 1997. "Functionalized monolayers on ordered mesoporous supports," *Science*. Vol. 276, pp. 923-926.

Frink, L. J. D. and F. Van Swol. 1997. "A molecular theory for surface forces adhesion measurements," *J. Chem. Physics*. Vol. 106(9), pp. 3782-3791.

Frink, L. J. D. and F. Van Swol. 1994. "Solvation forces and colloidal stability - a combined monte-carlo and density-functional theory approach," *J. Chem. Physics*. Vol. 100(12), pp. 9106-9116.

Frink, L. J. D. and F. Van Swol. 1998. "Solvation forces between rough surfaces," *J. Chem. Physics.* Vol. 108(13), pp. 5588-5598.

José-Yacamán, M. and R. F. Mehl. 1998. "The role of nanosized particles. A frontier in modern materials science, from nanoelectronics to environmental problems," *Metallurgical and Materials Transactions A*. Vol. 29A, no. 3, pp. 713-725.

Ju, Y. H., O. F. Webb, S. Dai, J. S. Lin, and C. E. Barnes. 2000. "Synthesis and characterization of ordered mesoporous anion-exchange inorganic/organic hybrid resins for radionuclide separation," *Ind. Eng. Chem. Res.* Vol. 39, pp. 550-553.

Jung, J., J. A. Kim, J. K. Suh, J. M. Lee, and S. K. Ryu,. 2001. "Microscopic and macroscopic approaches of Cu(II) removal by FSM-16," *Water Research*. Vol. 35, pp. 937-942.

Kresge, C. T., M. E. Leonowicz, W. J. Roth, J. C. Vartuli, and J. S. Beck. 1992. "Ordered mesoporous molecular-sieves synthesized by a liquid-crystal template mechanism," Nature. Vol. 359, pp. 710-712.

McCullen, S. B., J. C. Vartuli, C. T. Kresge, W. J. Roth, J. S. Beck, K. D. Schmitt, M. E. Leonowicz, J. L. Schlenker, S. S. Shih, and J. D. Lutner. 1995. "A new family of mesoporous molecular sieves," in: T. J. Pinnavaia & M. F. Thorpe (eds.), *Access in Nanoporous Materials*. New York: Plenum Press. pp. 1-11.

Mercier, L. and T. J. Pinnavaia. 1997. "Access in mesoporous materials: Advantages of a uniform pore structure in the design of a heavy metal ion adsorbent for environmental remediation," *Adv. Mater.* Vol. 9, pp. 500-503.

Molecular Simulations, Inc. 1997. *Cerius2 User Guide*. San Diego.

Rappe, A. K. and W. A. Goddard. 1991. "Charge equilibration for molecular-dynamics simulations," *J. Phys. Chem.* Vol. 95(8), pp. 3358-3363.

Selvam, P., S. K. Bhatia, and C. G. Sonwane. 2001. "Recent advances in processing and characterization of periodic mesoporous MCM-41 silicate molecular sieves," *Ind. Eng. Chem. Res.* Vol. 40, pp. 3237-3261.

Shin, Y. S., M. C. Burleigh, S. Dai, C. E. Barnes, and Z. L. Xue. 1999. "Investigation of uranyl adsorption on mesoporous titanium-based sorbents," *Radiochimica Acta*. Vol. 84, pp. 37-42.

Stumm, W. 1992. *Chemistry of the Solid-Water Interface*. John Wiley & Son. 428 pp.

Tanev, P. T. and T. J. Pinnavaia. 1995. "Recent advances in synthesis and catalytic applications of mesoporous molecular sieves," in: T. J. Pinnavaia & M. F. Thorpe (eds.), *Access in Nanoporous Materials*. New York: Plenum Press, pp. 13-27.

Tao, Z., T. Chu, J. Du, X. Dai, and Y. Gu. 2000. "Effect of fulvic acids on sorption of U(VI), Zn, Yb, I and Se(IV) onto oxides of aluminum, iron and silicon," *Applied Geochemistry*. Vol. 15, pp. 133-139.

Xu, Y.-M., R.-S. Wang, and F. Wu. 1999. "Surface characterization and adsorption behavior of Pb(II) onto a mesoporous titanosilicate molecular sieve," *Journal of Colloid and Interface Science*. Vol. 209, pp. 380-385.

Zhao, H., K. L. Nagy, J. S. Waples, and G. F. Vance. 2000. "Surfactant-templated mesoporous silicate materials as sorbents for organic pollutants in water," *Environmental Science and Technology*. Vol. 34, pp. 4822-4827.

Zhmud, B. V. 1996. "Charge regulation at the surface of porous solids: A comparison between the results obtained using different potential-to-charge relations," *J. Colloid Interface Sci.* Vol. 183, pp. 111-117.

Zhmud, B. V. and A. A. Golub. 1995. "Thermodynamic and kinetic study on protolytic reactions at the surface of porous matrices," *Colloids & Surfaces – A*. Vol. 105, pp. 173-180.

Zhmud, B. V., J. Sonnefeld, W. A. House. 1997. "Role of ion hydration in the charge regulation at the surface of porous silica gel," *J. Chem. Soc., Faraday Trans.* Vol. 93, 3129-3136.

3. Nanogeochemistry: Geochemical Reactions and Mass Transfers in Nanopores

3.1 Introduction

The emergence of nanotechnology has not only made it possible to purposefully manipulate material structures at nanometer scales but has also greatly advanced our understanding of how nanometer-scale structures give rise to novel physical and chemical properties of materials (e.g., Hummer et al., 2001; Klabunde, 2001). Nanometer-scale bimetallic particles have been shown to have an enhanced capability for the reduction of chlorinated hydrocarbons in the environment (Wang and Zhang, 1997). Mesoporous materials modified with specific surface functional groups are found to have high sorption capacities for removing mercury (Feng et al., 1997), chlorinated organic compounds (Zhao et al., 2000), copper, lead, and uranyl ions (Xu et al., 1999; Shin et al., 1999; Jung et al., 2001) from aqueous solutions. The study of nanometer-scale mineral-water interface phenomena is a necessary step to bridge the existing gap between the molecular level understanding of a geochemical process and the macro-scale laboratory and field observations (Hochella, 2002). In this section, we report that the space confinement within nanopores – pores of nanometer scale – can significantly modify geochemical reactions in porous geologic media and can lead to a preferential enrichment of trace elements in nanopores. This effect has a wide range of implications for many fundamental geochemical issues.

3.2 Nanopores In Geologic Media

Nanopores are ubiquitous in porous geologic media and constitute an integral part of total porosity of rocks. A listing of typical examples, illustrated in Figure 3-1, follows.

Diatomaceous Materials. Transmission electron microscopic (TEM) observations reveal that diatomaceous materials display both micrometer-scale and nanometer-scale pore structures. The nanopores are regularly distributed with a pore size of ~ 3 nm (Figure 3-1A). The nanopore structure may have been formed by organic molecules (probably a specific protein) in template fashion (Ollver et al., 1995; Lobel et al., 1996; Wang et al., 2002a), similar to a process used by material scientists to synthesize mesoporous materials (Kresge et al., 1992).

Mesoporous Iron Oxyhydroxides. Nanopores are commonly associated with Fe-oxyhydroxides in soils (Figure 3-1B).

Grain Boundaries. Figure 3-1C shows nanometer-scale channels at a grain boundary. It has been postulated that these nanometer-scale channels provide necessary passages for mass transport during mineral reactions, such as polysomatic reactions, and could possibly limit overall geochemical processes (Veblen, 1991). A quantitative evaluation of mass transport in these channels requires a mechanistic understanding of fluid movement and chemical diffusion within nanopores.

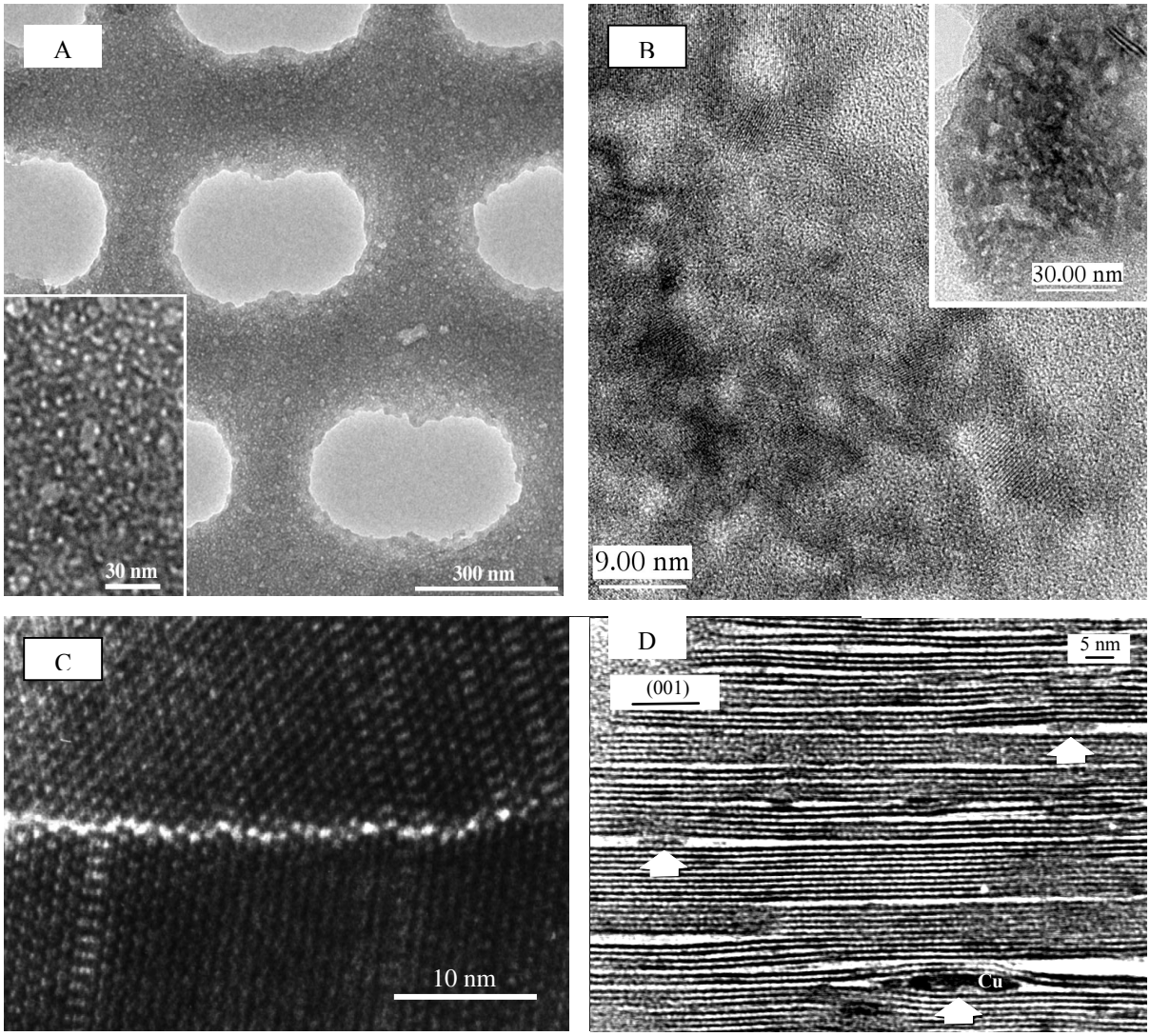

Figure 3-1. TEM images of mesoporous structures in geologic materials. A: Diatomaceous material displaying both micrometer-scale and nanometer-scale pore structures (with a pore size of ~ 3 nm) (see the inserted image). B: Mesoporous Fe-oxyhydroxide from a paleosol with inserted low-magnification TEM image showing nanometer-scale pores. C: Nanometer-scale channels (large white "dots" on the image) along a grain boundary between two amphibole crystals. D: Partially weathered illite containing nanometer-scale elemental copper inclusions (modified from Ahn et al., 1997), indicating preferential enrichment of heavy metal in nanometer-scale pores.

Nanometer-Scale Inclusions. Figure 3-1D shows the presence of nanometer-scale copper inclusions in partially weathered illite (Ahn et al., 1997), pointing to the control of nanostructures on geochemical reactions. Similarly, our TEM studies on samples from Changken cataclastic gold ore deposit in southern China indicate that gold is mainly present as nanoparticles with microfractures of quartz crystals or along quartz-illite grain boundaries, indicating that the nanopore confinement may have enhanced gold enrichment.

Surface-Area Effects. Existing data indicate that the contribution of nanopores to the total surface area in geologic materials can be very significant. In B-horizon soils, the pores with diameters smaller than 100 nm account for 10 - 40% of the total porosity (Görres et al., 2000). The porosity of a Georgia kaolinite was dominated by pores smaller than 10 nm (Tardy and Nahon, 1985). Because the specific surface area for a given pore volume is inversely proportional to the pore diameter, the contribution of nanopores to the total surface area in those materials is very high, probably >90%. This estimate is consistent with our TEM observations (Figure 3-1) and other literature data (Tachi et al., 1998; Trivedi and Axe, 2001).

3.3 Experiments

To isolate the effect of nanopore confinement, in this study, we chose to use synthetic mesoporous materials, which can be synthesized using a process involving a self-assembled supramolecular template (Kresge et al., 1992). The material we used was the synthetic mesoporous alumina purchased from Aldrich Chemical Company, Inc. This material has an irregular pore structure with a pore size of ~ 2 nm x 2 nm x 10 nm and a surface area of ~ 284 m^2/g. For a comparison with a nonmesoporous material, 80 - 200 mesh activated alumina particles from Fisher Chemicals were also used. The activated alumina particles have a surface area of 118 m^2/g. The large surface area in this material is due to the presence of microfractures on particle surfaces. The surface areas of both materials were measured with a N_2 BET method using Micrometritics Gemini 2360 surface analyzer. Our TEM observation indicates that the outer rims of the particles consist of an amorphous Al_2O_3 phase and very closely resemble the mesoporous alumina in chemical composition and crystallinity. Acid-base titration and Zn and As sorption experiments were conducted on both materials with procedures developed by Wang et al. (2002).

3.4 Results

From the pH titration data, the points of zero charge (PZC), corresponding to the cross points of titration curves for different ionic strengths (Stumm, 1992), are determined to be 9.1 for mesoporous alumina and 8.7 for activated alumina particles; both are close to each other and within the range reported for alumina oxides (Stumm, 1992), thus indicating that the nanopore confinement has little effect on the PZC of pore surfaces. Also from pH titration data, we calculated surface charges as a function of ΔpH (= pH – PZC). In Figure 3-2, the surface charge per unit of surface area on the

mesoporous alumina is plotted against that on the activated alumina particles for given ΔpH values. If the surface-charge difference between the two materials were controlled only by the surface area difference, all the experimental data points in the plot would fall on a 1:1 straight line. Apparently this is not the case; the surface charge density on mesoporous alumina is much higher than that on alumina particles. We thus postulate that this high surface charge density is likely caused by the nanopore confinement. Figure 3-2 also indicates that, for a given ΔpH, the surface charge density on a nanopore surface is less sensitive to ionic strength changes than that on an unconfined surface.

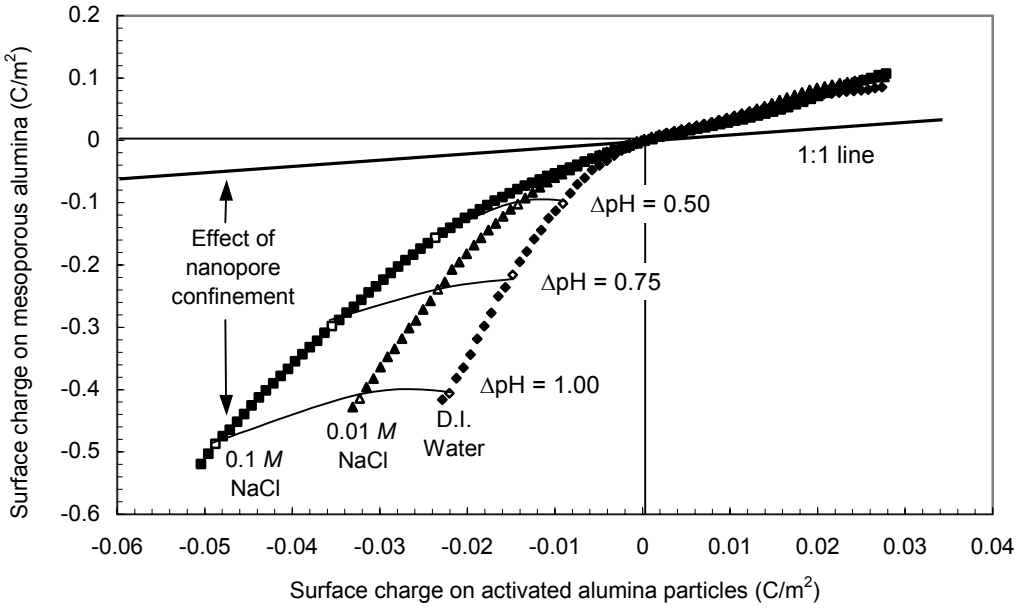

Figure 3-2. Surface charge on mesoporous alumina vs. surface charge on alumina particles for corresponding (pH – PZC) values and ionic strengths. If surface-charge difference between the two materials were controlled only by the surface-area difference, all the data points would fall on 1:1 straight line. Deviation from the straight line is due to the effect of nanopore confinement.

The attainment of a high surface charge density by a mesoporous material is attributed to the modification of surface acidity constants by the nanospore confinement. If five sorption sites per square nanometer of alumina surface (Stumm, 1992) are assumed, the acidity constants for both materials, which characterize the ability for surface protonation and deprotonation, are calculated to be: $pK_1 = 9.0$, $pK_2 = 10.3$ for mesoporous alumina and $pK_1 = 7.7$, $pK_2 = 11.0$ for activated alumina particles (Wang et al., 2002b). (A slight difference between the PZC values determined from the crossing point of titration curves and those calculated from the relationship $PZC= (pK_1 + pK_2)/2$

may be due to the uncertainty associated with a linear extrapolation of acidity constants from a highly charged surface to a neutral environment.) Thus, owing to the nanopore confinement, the separation between the two acidity constants, ΔpK (= pK_2 - pK_1), becomes significantly narrowed for the mesoporous alumina ($\Delta pK = 1.3$) as compared to that for the alumina particles ($\Delta pK = 3.3$). As a result, within nanopores, neutral-surface species become depleted, and the pore surface tends to be either positively or negatively charged, giving rise to a high surface charge density on mesoporous materials (Figure 2-4). The resulting change in surface acidity constants is expected to shift ion adsorption edges and consequently enhance both cation and anion sorption on nanopore surfaces.

We measured the sorption coefficients (K_d) of Zn and Ason both mesoporous alumina and activated alumina particles as a function of pH (Fig.3-3). In these experiments, we added 0.1 g of mesoporous alumina or 0.25 g of activated alumina particles to 20 ml deionized (D. I.) water in each sample, resulting in the same ratio of solid surface area to liquid volume in both systems. The equilibrated pH of each sample was adjusted by adding a concentrated HCl or NaOH solution. It is interesting to note that, at a given pH value, the sorption coefficient (K_d) for mesoporous alumina was ~10 to 100-fold higher than that for activated alumina particles (Figure 3). To our knowledge, this is the first set of data that convincingly demonstrates the effect of nanopore confinement on ion sorption on nanopore surfaces. Two factors may contribute the observed high sorption capability of nanopore surfaces. First, as already mentioned, the confinement-induced change in ΔpK shifts sorption edges to a lower pH range for cation and a higher pH range for anion, and therefore enhances both cation and anion sorption. The increase in K_d for Zn seems comparable in magnitude with the shift in surface acidity constants. Second, as subsequently demonstrated, the low water activity in nanopores reduces ion hydration and thus increases the possibility for inner-sphere complexation. As a result of the pore space confinement, trace elements in natural environments tend to be enriched in nanopores.

This enrichment is further enhanced by water activity (a_w) changes in nanopores. The nanopore confinement modifies water properties (Denoyel and Pellenq, 2002). The behavior of confined water is similar to that of supercooled water at lower (~ 30 K) temperatures (Teixeira et al., 1997), implying a low water activity in nanopores. According to Kelvin's equation (e.g., Hiemenz, 1986), $\ln(a_w)$ in a pore of radius r is roughly proportional to $-r^{-1}$. Therefore, the water activity in nanopores can be much lower than that of bulk water (Tardy and Nahon, 1985). The reduction in water activity has two fundamental impacts on ion sorption and mineral precipitation. First, it reduces the hydration of aqueous species and therefore increases the possibility for inner-sphere complexation on nanopore surfaces. Second, it forces solutes to precipitate out from solutions and therefore results in preferential precipitation of minerals in nanopores (e.g., $H_4SiO_4(aq) \rightarrow SiO_2(s) + H_2O$). A similar mechanism has been proposed for nonelectrical exclusion of ions in thin water films (Zilberbrand, 1997).

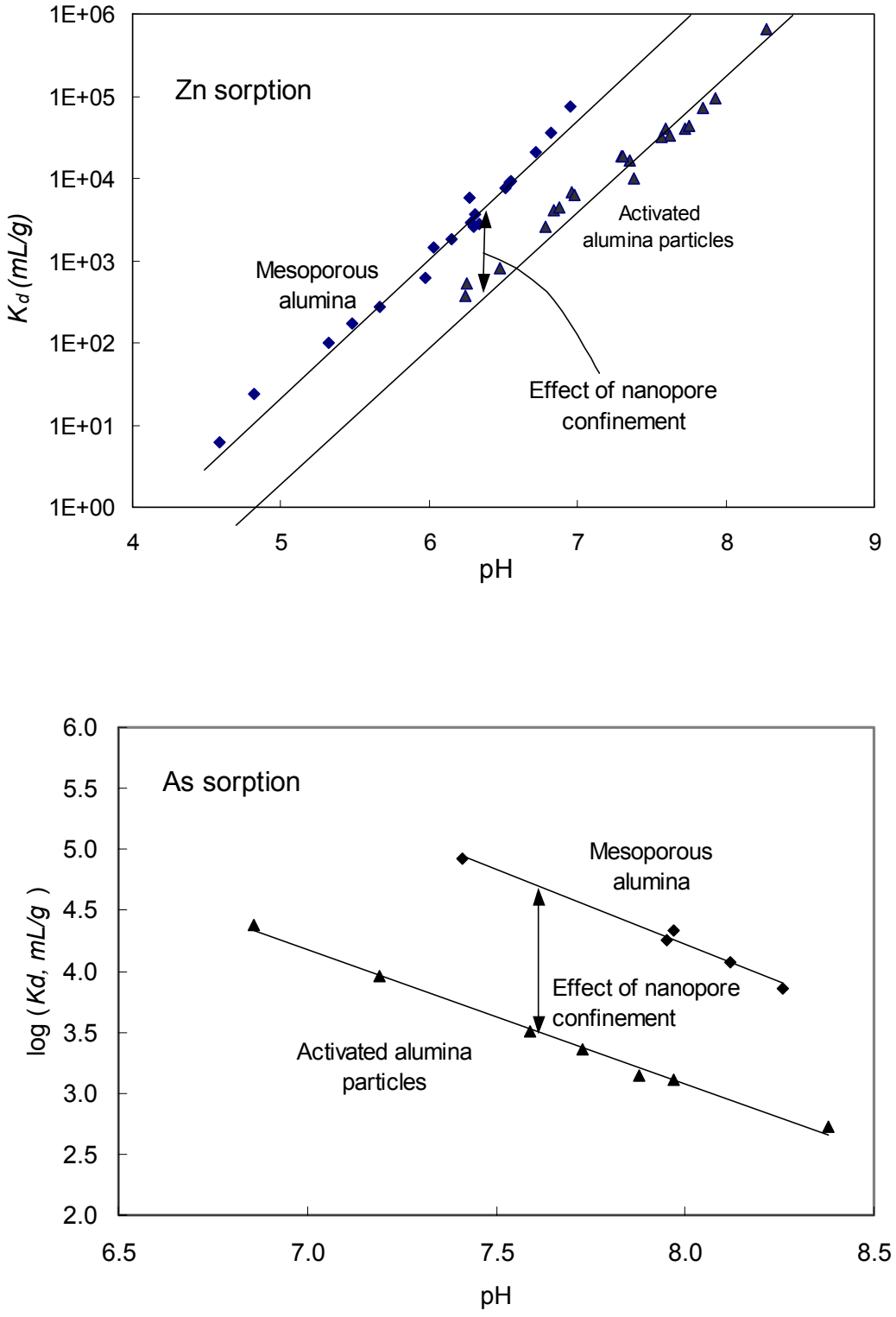

Figure 3-3. Sorption coefficients (K_d) of Zn and As on both mesoporous alumina and activated alumina particles, measured as a function of pH.

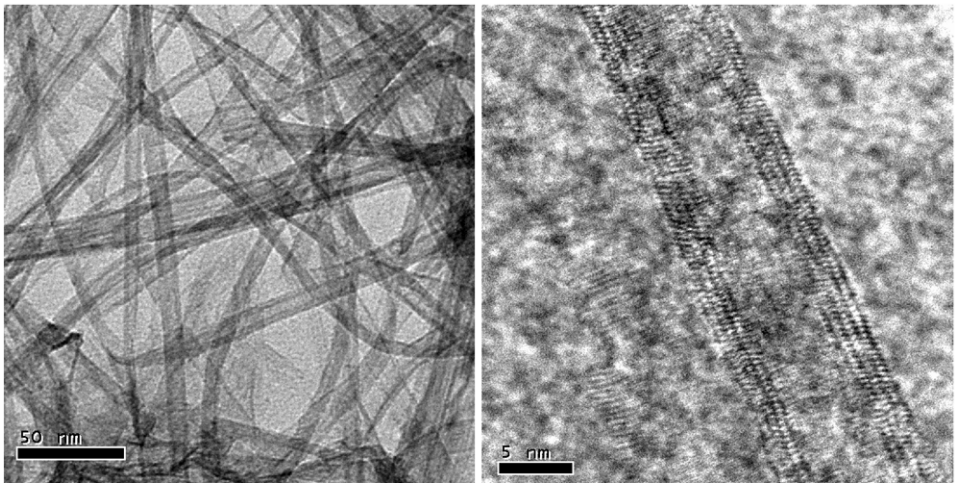

Figure 3-4: Bright-field TEM (left) and high-resolution TEM (right) images of the titanium oxide nanotubes synthesized using the method we developed.

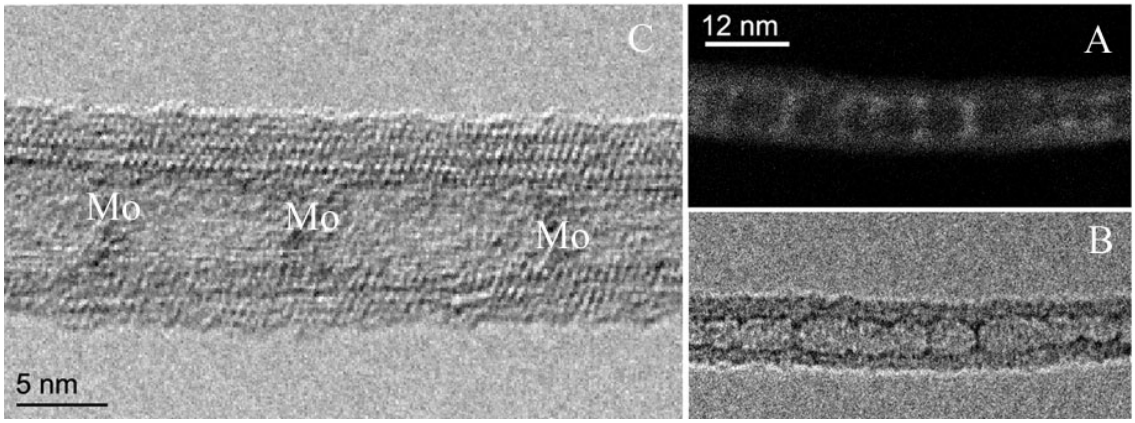

Figure 3-5: High-angle annular dark-field (Z-contrast) image (A), birght-field TEM image (B) and HRTEM image of titanium oxide nanotubes showing enrichment of Mo inside the nanotubes. HRTEM image shows clean outer surface of the nanotube and pillar-like Mo clusters inside the nanotube (labeled by "Mo"), indicating the difference in chemical environment between outer (not confined) and inner (confined) surfaces.

To further confirm the observed phenomenon, we developed a method to synthesize TiO_2 nanotubes. These nanotubes provide an ideal system for studying the effect of nanopore confinement, because both the inner surface (the confined surface) and the outer surface (the confined surface) have identical chemical compositions and crystal structures (Figure 3-4). We first suspended the nanotubes in an aqueous solution spiked with MoO_4^{2-} and then imaged the nanotubes, both chemically and structurally, using a high resolution transmission electron microscope (HRTEM). The TEM images show a clean outer surface of the nanotube and the formation of pillar-like Mo clusters inside the nanotube (Figure 3-5), clearly indicating the preferential enrichment of trace metal in the confined pore space.

3.5 Discussion

The work reported here sheds new light on our understanding of the irreversibility of ion sorption and desorption and the bioavailability of contaminants in natural environments. Typically, metal ion desorption from geologic materials occurs in two phases. One fraction desorbs rapidly, whereas the rest desorbs only slowly, and the proportion of slowly desorbing metal ions increases with sorption time (e.g., McLaren et al., 1998; Glover et al., 2002). Figure 3-6 shows the desorption behavior of uranyl from a synthetic goethite material, which contains a large number of intra- and inter-grain nanopores as revealed by our TEM observation. Note that intraparticle diffusion could be a rate-limiting process in the sorption of metal ions to amorphous iron oxyhydroxides (Axe and Trivedi, 2002). We postulate that the slow-release phase may result from preferential metal sorption and precipitation in nanopores, whereas the initial-release phase is related to the metal desorption from outer surfaces of the material. The dependence of desorption kinetics on sorption times may arise from the slow migration of uranyl from large pores (and outer surfaces) to nanopores owing to a chemical potential gradient created by the pore-space confinement. Such a mechanism can greatly reduce the bioavailability of contaminants in natural environments, because nanopores are generally too small to be accessible by microorganisms.

Our work suggests that the ion-sorption measurements on disaggregated geologic materials may not represent chemical conditions in actual systems, because they may not be able to capture the effect of nanopore confinement. This possibility is consistent with the measurement of apparent distribution coefficients of radionuclides in saturated bentonite as a function of compaction density (Conca and Wright, 1992). It was found that physical compaction could change retardation behaviors of radionuclides and even enhance retardation capability. Such behaviors can be readily explained by the nanopore-confinement effect we observed. Because of this effect, the surface sites on the same mineral surface can exhibit different sorption affinities in porous geologic media, and the sorbed ions in nanopores are more strongly bound than those outside the nanopores.

Our pH titration results suggest that the existing surface-complexation models (e.g., Davis and Kent, 1990; Dzombak and Morel, 1990), which have been developed mostly for unconfined surfaces, might not be adequate for modeling ion sorption on nanopore surfaces without taking into account the effect of pore-space confinement. Zhmud and his

colleagues have attempted to develop a charge-regulation model for the surface of porous matrices (Zhmud et al., 1997), in which a pore is represented by a cylindrical cavity and the overlap of the electrical double layer is taken into account by diminishing the radius of the cylinder. The model predicts a decrease in surface charge density with decreasing pore size, which seems inconsistent with our experimental results.

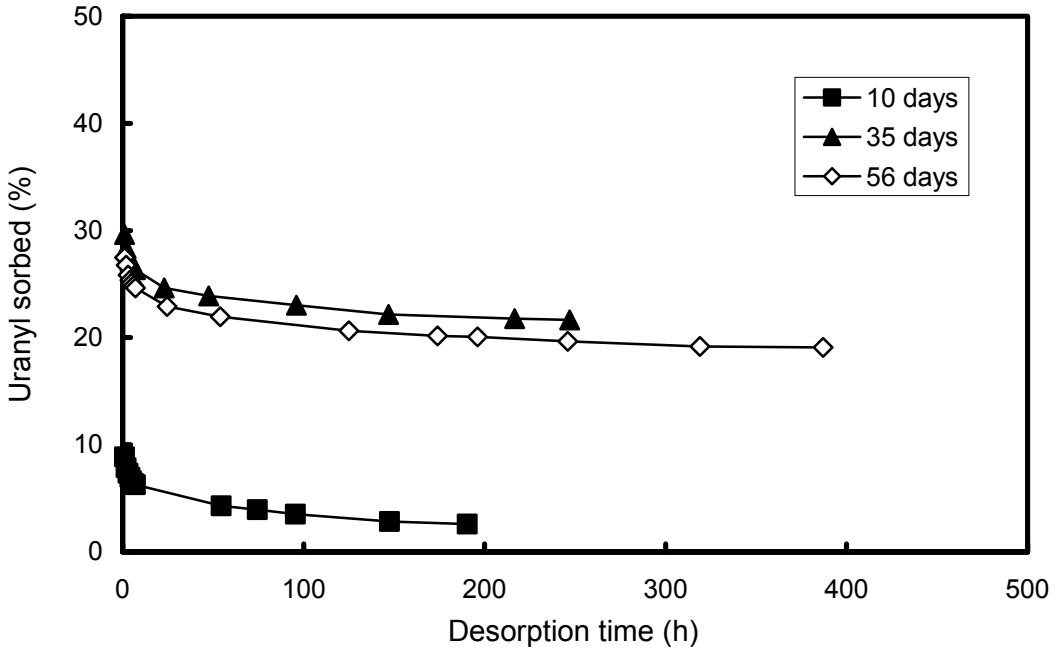

Figure 3-6. Uranyl desorption from synthetic porous goethite materials for uranyl-goethite contact times of 10, 35, and 56 days. Slow-release phase may result from the preferential metal adsorption and precipitation within nanometer-scale pores, whereas the initial fast-release phase is related to desorption from outer surfaces of material.

The modification of surface chemistry and pore water activity by the nanopore confinement effect also has an impact on mineral dissolution and precipitation kinetics. It was observed that diatomaceous materials display unique nonlinear dissolution kinetics (Van Cappellen and Qiu, 1997): in the vicinity of the equilibrium point, the dissolution rates are nearly linear. With increasing distance from equilibrium, there is a pronounced transition in the functional dependence on the relative degree of understaturation. Beyond the transition, the dissolution rates rises much faster with increasing degree of solution undersaturation. On our TEM observations (Figure 3-1A), this nonlinear behavior is probably due to the presence of nanopore structures in biogenic materials. The water inside the nanopores has a low activity and so is less undersaturated than the unconfined fluid; thus nanopore surfaces have less of a tendency to dissolve than unconfined outer surfaces. A similar process can be used to explain the large discrepancy between

laboratory measurements and field observations in weathering rates (e.g., Brantley, 1992), considering that nanopores in soils can account for >90% of their total surface area. The work summarized herein also sheds new light on dolomite formation. Dolomite formation is inhibited by strong Mg^{2+} hydration (de Leeuw and Parker, 2001). The decrease in water activity and the resulting reduction in Mg^{2+} hydration in nanopores can possibly enhance dolomite formation in natural systems.

3.6 References

Ahn J. H., H. Xu, and P. R. Buseck. 1997. "Transmission electron microscopy of native copper inclusions in illite," *Clays and Clay Minerals*. Vol. 45, pp. 295-297.

Axe, L. and P. Trivedi. 2002. "Intraparticle surface diffusion of metal contaminants and their attenuation in microporous Al, Fe, and Mn oxides," *Journal of Colloid and Interface Science*. Vol. 247, pp. 259-265.

Brantley, S. L. 1992. "Kinetic dissolution and precipitation – Experimental and field results," in: Y. Kharaka, Ed., *Water-Rock Interaction*. Park City: Balkema, Rotterdam. Vol. 1, pp. 3-6.

Conca, J. L. and J. Wright. 1992. "Diffusion and flow in gravel, soil, and whole rock," *Applied Hydrogeology*. Vol. 1, pp. 5-24.

Davis, J. A. and D. B. Kent. 1990. "Surface complexation modeling in aqueous geochemistry," in: M. Hochella Jr. and A. F. White, Eds., *Mineral-Water Interface Geochemistry*. Mineralogical Society of America. Vol. 23, Washington, D. C., 1990, pp. 177-260.

de Leeuw N. H. and S. C. Parker. 2001. "Surface-water interactions in the dolomite problem," *Physical Chemistry and Chemical Physics*. Vol. 3, pp. 3217-3221.

Denoyel, R. and R. J. M. Pellenq. 2002. "Simple phenomenological models for phase transitions in a confined geometry. 1: Melting and solidification in a cylindrical pore," *Langmuir*. Vol. 18, pp. 2710-2716.

Dzombak, D. A. and F. M. M. Morel. 1990. *Surface Complexation Modeling: Hydrous Ferric Oxide*. New York: Wiley-Interscience. 393p.

Feng, X., G. E. Fryxell, L. Q. Wang, A. Y. Kim, J. Liu, and K. M. Kemner. 1997. "Functionalized monolayers on ordered mesoporous supports," *Science*. Vol. 276, pp. 923-926.

Glover II, L. J., M. J. Eick, and P. V. Brady. 2002. "Desorption kinetics of cadmium^{2+} and lead^{2+} from goethite: Influence of time and organic acids," *Soil Science Society of America Journal*. Vol. 66, pp. 797-804.

Görres, J. H., M. A. Stolt, J. A. Amador, C. P. Schulthess, and P. Johnson. 2000. "Soil pore manipulations to increase bioaccessible pore volume," in: O. Sililo, Ed, *Groundwater: Past Achievement and Future Challenge*. A. A. Balkema, Rotterdam. pp. 755-756.

Hiemenz, P. C. 1986. *Principles of Colloid and Surface Chemistry*. New York: Marcel Dekker. 815p.

Hochella, M. F. 2002. "There's plenty of room at the bottom: Nanoscience in geochemistry," *Geochimica et Cosmochimica Acta*. Vol. 66, pp. 735-743.

Hummer, G., J. C. Rasaiah, and J. P. Noworyta. 2001. "Water conduction through the hydrophobic channel of a carbon nanotube," *Nature*. Vol. 414, pp. 188-190.

Jung, J., J. A. Kim, J. K. Suh, J. M. Lee, and S. K. Ryu,. 2001. "Microscopic and macroscopic approaches of Cu(II) removal by FSM-16," *Water Research*. Vol. 35, pp. 937-942.

Klabunde, K. J. 2001. *Nanoscale Materials in Chemistry*. New York: Wiley Interscience. 269 p.

Kresge, C. T., M. E. Leonowicz, W. J. Roth, J. C. Vartuli, and J. S. Beck. 1992. "Ordered mesoporous molecular-sieves synthesized by a liquid-crystal template mechanism," Nature. Vol. 359, pp. 710-712.

Lobel, K. D., J. K. West, and L. L. Hench. 1996. "Computational model for protein-mediated biomineralization of the diatiom frustule," *Marine Biology*. Vol. 126, pp. 353-360.

McLaren, R. C., C. A. Backes, A. W. Rate, and R. S. Swift. 1998. "Cadmium and cobalt desorption kinetics from soil clays: Effect of sorption period," *Soil Science Society of America Journal*. Vol. 62, pp. 332-337.

Ollver, S., A. Kuperman, N. Coombs, A. Lough, and G. A. Ozln. 1995. "Lamellar aluminophosphates with surface patterns than mimic diatom and radiolarian microskeletons," *Nature*. Vol. 378, pp. 47-50.

Shin, Y. S., M. C. Burleigh, S. Dai, C. E. Barnes, and Z. L. Xue,. 1999. "Investigation of uranyl adsorption on mesoporous titanium-based sorbents," *Radiochimica Acta*. Vol. 84, pp. 37-42.

Stumm, W. 1992. *Chemistry of the Solid-Water Interface*. New Yory: Wiley Interscience. 428 p.

Tachi, Y., T. Shibutani, H. Sato, and M. Yui. 1998. "Sorption and diffusion behavior of selenium in tuff," *Journal of Contaminant Hydrology*. Vol. 35, pp. 77-89.

Tardy, Y. and D. Nahon. 1985. "Geochemistry of laterites, stability of al-goethite, al-hematite, and Fe^{3+}-kaolinite in bauxites and ferricretes: an approach to the mechanism of concretion formation," *American Journal of Science*. Vol. 285, pp. 865-903.

Teixeira, J., J. M. Zanotti, M. C. Bellissent-Funel, and S. H. Chen. 1997. "Water in confined geometries," *Physica B*. Vol. 234, pp. 370-374.

Trivedi, P. and L. Axe. 2001. "Ni and Zn sorption to amorphous versus crystalline iron oxides: Macroscopic studies," *Journal of Colloid and Interface Science*. Vol. 244, pp. 221-229.

Van Cappellen, P. and L. Qiu. 1997. "Biogenic silica dissolution in sediments of the Southern Ocean. II. Kinetics," *Deep-Sea Research II*. Vol. 44, pp. 1129-1149.

Veblen, D. R.. 1991. "Polysomatism and polysomatic series: A review and applications," *American Mineralogist*. Vol. 76, pp. 801-826.

Wang, C. and W. Zhang. 1997. "Nanoscale metal particles for dechlorination of PCE and PCB," *Environmental Science and Technology*. Vol. 31, pp. 2154.

Wang, L., Y. Wang, M. Li, W. Zhang, F. Zhang, and T. Li. 2002a. "Biogenic nanostructured silica," *Progress in Natural Science*. Vol. 12, p. 401-406.

Wang, Y., C. Bryan, H. Xu, P. Pohl, Y. Yang, and C. J. Brinker. 2002b. "Interface chemistry of nanostructured materials: Ion adsorption on mesoporous alumina," *Journal of Colloid and Interface Science*. Vol. 254, pp. 23-30.

Xu, Y.-M., R.-S. Wang, and F. Wu. 1999. "Surface characterization and adsorption behavior of Pb(II) onto a mesoporous titanosilicate molecular sieve," *Journal of Colloid and Interface Science*. Vol. 209, pp. 380-385.

Zhao, H., K. L. Nagy, J. S. Waples, and G. F. Vance. 2000. "Surfactant-templated mesoporous silicate materials as sorbents for organic pollutants in water," *Environmental Science and Technology*. Vol. 34, pp. 4822-4827.

Zhmud, B. V., J. Sonnefeld, W. A. House. 1997. "Role of ion hydration in the charge regulation at the surface of porous silica gel," *J. Chem. Soc., Faraday Trans.* Vol. 93, 3129-3136.

Zilberbrand, M. 1997. "A nonelectric mechanism of ion exclusion in thin water films in finely dispersed media," *Journal of Colloid and Interface Science*. Vol. 192, pp. 471-474.

4. Anion Sorption on Layered Double Hydroxides: Effect of Calcination

4.1 Introduction

^{99}Tc, ^{79}Se, and ^{129}I are long-lived fission products with a half-life ranging from 2.13 x 10^5 to 1.57 x 10^7 years (Liang et al., 1996; Kunze et al., 1996; Kang et al., 1999). Under oxidizing conditions, these radionuclides are highly soluble and exist as TcO_4^-, SeO_4^{2-}, and I^-. These anionic species present a serious environmental concern, because they are negatively charged and thus are poorly sorbed on most materials under basic conditions (pH > 7) (Liang et al., 1996; Kunze et al., 1996; Kang et al., 1999; Bond et al., 1999; Monteil-Rivera et al., 2000). Currently, the Department of Energy (DOE) has 90 million gallons of high-level and low-level radioactive liquid waste stored in underground tanks (http://www.pnl.gov/tfa/emsp). Some of these tanks have known or suspected leaks. The high mobility of anionic species of ^{99}Tc, ^{79}Se, and ^{129}I radionuclides thus poses a challenging technical issue for tank closure. Similarly, non-radioactive anionic contaminants such as arsenate in drinking water are also a serious environmental concern (National Academy of Sciences, 1999). Therefore, there is an urgent need for development of anion getter materials for effective removal and immobilization of these anionic contaminants.

Only a few materials have so far been identified that can potentially immobilize anionic radionuclides. Fe^0-based or Fe(II)-containing materials could immobilize TcO_4^- and SeO_4^{2-} by reducing them to relatively insoluble, low-oxidation state compounds (Liang et al., 1996; Kumata and Vandergraaf, 1993; Cui and Eriksen, 1996; Yllera et al., 1996). In fact, Savannah River Site uses FeS to trap Tc (http://www.pnl.gov/tfa/emsp). However, the problem with reductive immobilization is that the precipitated Tc and Se can be easily re-mobilized if a reducing environment is not maintained and therefore the long-term stability of the immobilization is always questionable. A similar question also arises for I^- sorption on Fe or Cu sulfides, which become unstable under oxidizing conditions. Among candidate anion getter materials identified so far, layer double hydroxides (LDH) have shown the most promise (Kang et al., 1999; Balsley et al., 1998).

4.2 Chemistry of Layered Double Hydroxides

The layered double hydroxides, of general formula $M(II)_{1-x}M(III)_x(OH)_2Y_{x/n}$, consist of positively charged, close-packed, metal hydroxide layers, whose surplus positive charge, arising from the substitution of the trivalent cation M(III) for the divalent cation M(II), is neutralized by the exchangeable anion Y. LDH swell with large anions, but do not exfoliate, presumably because in these materials, unlike normal clays, there is hydrogen bonding between the layers and the interlayer species. Since hydrotalcite, $Mg_6Al_2(OH)_{16}CO_3.4H_2O$, is a member of this family, they are often referred to as

hydrotalcite-like compounds. The materials occur in nature but are easily and cheaply synthesized in bulk and some formulations are commercially available. Mineral specimens commonly include Mg, Mn, Fe, Co or Ni as divalent cations, along with Fe(III), Al(III), or occasionally Cr(III), and the exchangeable anion is usually chloride, carbonate, or sulfate. Synthetic analogs can incorporate Cu(II), V(III), and Ga(III) among others, while almost any anion can be incorporated, subject to restrictions on size that have not as yet been fully understood. Among the anions known to incorporate into the interlayer space of LDH are a range of negatively charged complexes of metals, and such systems have been the subject of a recent review (Rives and Ulibarri, 1999).

For a given choice of metals, there remains the question of the M(II):M(III) ratio between them, which can readily vary between 2:1 and 3:1 or even further. We expect that in general high charge densities would favor strong anion retention, but the issue is more complicated than that. Firstly, we are concerned with competition rather than with a single adsorption strength, and, secondly, we have found that the spatial requirements of anions within the LDH layer are commonly greater than might have been expected (Boclair and Braterman, unpublished), thus pointing a possible improvement in ion selectivity by controlling interlayer spacing.

One choice of metal requires special comment, and that is the case where M(II) = Fe(II); M(III) = Fe(III). Materials of this class are known as "green rusts", are easily prepared, and are well established as intermediates in the corrosion of metallic Fe under low oxygen conditions (Hansen, 1989; Refait et al., 1998; Loyaux-Lawniczak et al., 1999; Refait et al., 1999). These materials are effective traps for selenium as selenate, and react effectively with chromate, reducing it to Cr(III) as hydroxide or, possibly, as a component of modified LDH (Loyaux-Lawniczak et al., 1999). The observed formation of LDH phases, when metallic Fe is used in the reductive removal of U and Tc, results in the incorporation of these radionuclides into highly insoluble phases (Roh et al., 2000).

LDH materials are currently of particular interest as water treatment adsorbents (Villa et al., 1999), catalysts, and catalyst precursors (Chibwe et al., 1996). LDH materials are highly insoluble over a wide pH range, with details dependent on composition. Magnesium aluminum LDH are insoluble at pH > 8, while zinc aluminum LDH remains insoluble to much lower values. The low solubility, and the ability to choose relatively harmless metals, renders them effectively non-toxic (Mg:Al LDH is the actual effective ingredient in some gastric antacids). In particular, their low solubility under basic pH conditions makes these materials especially useful in the treatment and containment of alkaline liquid tank waste at DOE sites.

LDH materials show unique promise for the removal of anionic contaminants from water, with typical ion exchange capacities of ~ 3.5 meq/g. This is in part because of their high point of zero charge (pzc > 12) (Han et al., 1998), but also because surface adsorption is supplemented by interlayer exchange. LDH materials have a particularly high affinity for doubly or triply charged anions, including sulfite and sulfate (and, by implication, selenite and selenate), as well as for a wide range of metal-containing anions[11]. They have been suggested for removal of chromate, phosphate, chloride ion,

anionic surfactants, ionic dyes, and humic substances from water (Narita et al., 1992; Shin et al., 1996; Houri et al., 1999; Seida and Nakano, 2000; Pavan et al., 2000; Kameda et al., 2000; Hermosin et al., 1996; Amin and Jayson, 1996; Onka;-Engin et al., 2000). LDH materials may even be a useful adsorbent for negatively charged colloids formed by heavy metals, including actinides, under oxidizing and/or basic conditions such as may well exist in soils and barriers.

An anion Y^- can be either adsorbed on the external surface and edge of a LDH material:

$$\text{Support}^+ + \text{Y}^-(\text{aq}) \leftrightarrow \text{Support} \equiv \text{Y(ads)}\,, \qquad (4\text{-}1)$$

or incorporated into the interlayer of the material by displacement of an existing anion X^-:

$$\text{LDH.X(s)} + \text{Y}^-(\text{aq}) \leftrightarrow \text{LDH.Y(s)} + \text{X}^-(\text{aq})\,. \qquad (4\text{-}2)$$

Both interlayer exchange and surface adsorption contribute the sorption capacity of LDH materials. (In this report, the term "sorption" is used to include both processes). If LDH.X and LDH.Y were to form continuous ideal solutions, the equilibrium would resemble a partition process, to be described by a ratio of concentrations of type [X(aq)][Y(s)]/[X(s)][Y(aq)]. This is not the case with LDH, as X and Y would in general impose different spacings between the metal hydroxide layers. Thus, LDH.X and LDH.Y should be considered as two distinct solid phases, with little if any mutual solubility, and formally represented in thermodynamic treatments by an activity of unity. Therefore, there should exist a critical ratio [Y(aq)]/[X(aq)], below which the solid will be predominantly LDH.X with, perhaps, "dissolved" Y, while above this value the roles of X and Y will be reversed. Experiments show that this is indeed the case, although there is often a narrow intermediate region showing hysteresis (Schoellhron and Otto, 1986). It follows that the uptake of a species from solution by LDH should be considered as a competitive process and, as a consequence, to improve uptake of the target anion Y^-, we must also consider the ease of loss of the displaced anion X^-. For example, uptake of anions onto calcined material involves exchange of the anion for hydroxide, and while it appears to resemble an absorption process, the nominal strength of absorption will increase by an order of magnitude (in the case of selenate, two orders) for every unit fall in pH. The sorption capacity and ion selectivity of LDH generally depend on material compositions and structures, which vary in wide ranges and, to a large extent, can be purposefully engineered.

Braterman et al. have shown that the formation of LDH from solution is a process of much greater complexity than had previously been realized (Braterman et al., 1994; Boclair and Braterman, 1998; Boclair and Braterman, 1999; Boclair et al., 1999). The conventional preparative route involves addition of base to a mixture of M(II) and M(III) salts in solution. In general, this process takes place in two stages; initial precipitation of M(III) hydroxide or hydrous oxide, and subsequent formation of the LDH by heteronucleation on and subsequent re-solution of this intermediate solid. In some cases,

this leads to porous materials as a result of in situ reaction of aluminum hydroxide precursor, but such a result method clearly depends on a happy confluence of reaction parameters. However, a formation of an intermediate solid can be avoided by using sodium aluminate solution as a precursor. The discovery of this direct route removes a major obstacle to morphological control.

4.3 Methodology

Two Mg-Al LDH materials were purchased from Alcoa Industrial Chemicals; one is activated by calcination and another is not. Both materials have a Mg/Al molar ratio of 2.4. The average particle size of the materials ranges from 5 to 8 μm. The surface area measured by N_2 BET is 40 m^2/g for the non-activated sample and 46 m^2/g for the activated one. Transmission Electron Microscopy (TEM) observations at the University of New Mexico and XRD analyses at SNL-Carlsbad have shown that the activated sample is less crystalline than the non-activated one (Figures 4-1 and 4-2). XRD analyses also indicate the presence of a detectable amount of periclase in the activated sample (Figure 4-2).

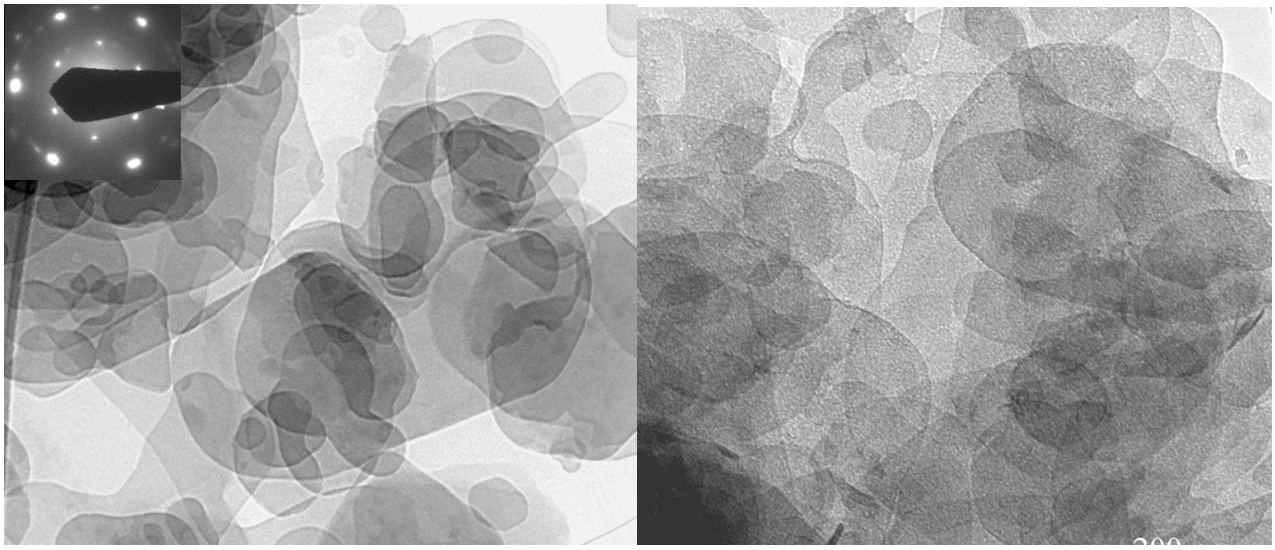

A B

Figure 4-1. Bright-field TEM images of layered double hydroxides with a molar Mg/Al ratio of 2.4. The images show different sizes of LDH plates. A - Non-activated sample. Inserted on upper-left corner is a selected-area electron diffraction pattern from one hydrotalcite plate. B – Sample activated by calcination. The activated sample has rough plate surfaces, indicating its relatively low crystallinity.

Four anions were selected for sorption experiments: PO_4^{3-}, AsO_4^{3-}, SeO_4^{2-}, and ReO_4^-. Re was used as a chemical analog to Tc. All the experiments were performed at 25 ^oC using batch methods. All the test tubes were polycarbonate, and the measurements of blank samples indicated that sorption on the surfaces of test tubes was negligible. Three sets of sorption experiments were performed. In the first set of experiments, 20 mL of solution containing either 10 or 100 mg/L of an anion of interest was added to 0.2 g of LDH. The obtained solid-liquid suspension was stirred continuously for 16 – 20 hours. The liquid was then sampled, filtered with a 0.2 μm syringe filter, and then analyzed for the target anion, using an Inductively Coupled Plasma Optical Emission Spectrometer (ICP-OES). The second set of experiments was used to determine sorption isotherms of Se and Re on the activated LDH material under ionic strengths of 0.01, 0.1, and 1.0 M NaCl. Each sample was equilibrated for 16 – 20 hours. In the third set of experiments, the kinetics of Se and Re sorption on both the activated and non-activated LDH materials was determined in a 0.01 M NaCl solution. 1.3 g of LDH was added to 130 mL of a solution spiked with 20 mg/L anion for non-activated LDH samples or 100 mg/L for activated LDH samples. The concentration of anion remaining in the solution was monitored. To study the effect of possible mineral hydration on anion sorption, dry LDH powders were added to half the samples, while LDH that had been pre-wetted for 24 hours added to the other half. In all the experiments, no pH buffer was added, and the final pH was achieved by the equilibrium of LDH with the solution.

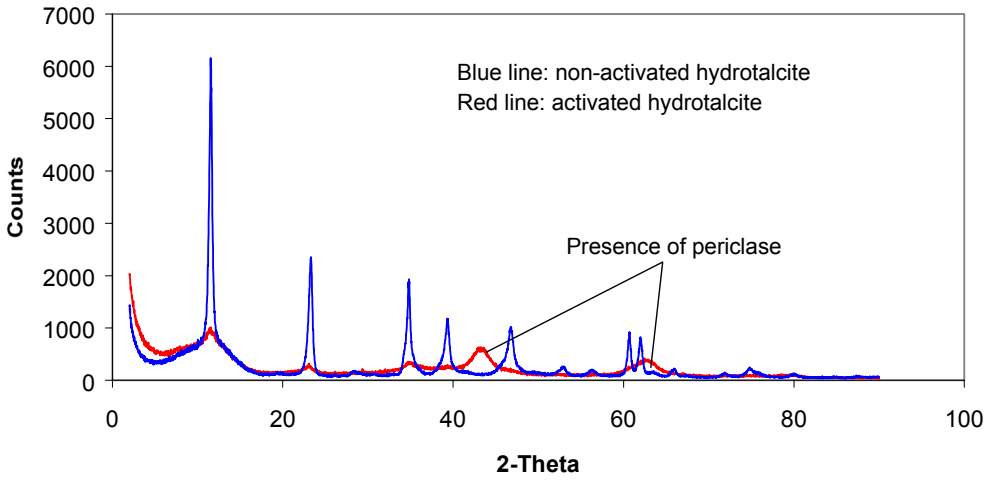

Figure 4-2. X-ray powder diffraction patterns of non-activated and activated hydrotalcite samples. The activated sample is less crystalline than the non-activated one and it contains a detectable amount of periclase, which usually disappears after the sample is immersed in solutions. No other solid phases such as spinel are detected.

4.4 Results

Sorption coefficients: activated vs. non-activated materials: The measured sorption coefficients (K_d) of anionic species of P, Re, As, and Se on both activated and non-activated LDH in deionized water are listed in Table 4-1. The activated material has a much higher anion sorption coefficient than the non-activated one. Since both materials have the same Mg/Al molar ratio of 2.4, the experimental results thus show that calcination alone can increase anion sorption capacity by up to 3 orders of magnitude. Although a mechanistic understanding of such effect yet needs to be obtained, the BET measurements show that the increase in sorption coefficients for the activated material is apparently not related to surface area changes. We expect that an optimal calcination temperature and time period may exist such that anion sorption capability of a LDH can be maximized. It should be pointed out that no special care was taken in the experiments to prevent CO_2 contamination, except that the samples were sealed during equilibration. The experimental results thus seem to indicate that anion sorption may be sensitive to the carbonate ions pre-existing in the LDH interlayer but perhaps not to those in the solution. This needs to be further confirmed by experiments.

Two chemical processes – mineral dissolution and interlayer ion exchange – could possibly control the final pH in the solution in the sorption experiments. If the control were dominated by an interlayer ion exchange, the pH would increase with the initial concentration of anion in the solution, since a high concentration of anion would cause more interlayer hydroxides to be replaced by the anion of interest. This seems not the case for the experiments with the activated LDH, in which the final pH practically remained the same for the solutions spiked with either 10 or 100 mg/L of anions (Table 4-1). Therefore, the final pH in the experiments was likely to be controlled by mineral dissolution. Through calcination and re-hydration, hydroxides are expected to become a major anion to compensate the surplus positive charge caused by the substitution of Al for Mg in LDH. The release of these hydroxides during mineral dissolution gave rise to high pH values observed in the experiments with the activated LDH. Interestingly, because of the resulting high pH, the solubility of the activated LDH was low, relative to the non-activated material. The Mg concentration in the solution decreased from ~ 35 to ~ 0.01 mg/L as the solid materials in the experiments were switched from the activated to the non-activated LDH. Notice that very high adsorption coefficients of the activated material were achieved at high pH. To the extent that uptake is due to anion exchange rather than to simple adsorption, this implies even more effective uptake at less extreme pH.

Table 4-1. Anion sorption coefficients of Mg:Al LDH measured in deionized water

	Initial concentration of anion			
	10 mg/L		100 mg/L	
	Kd (mL/g)	Final pH	Kd (mL/g)	Final pH
Activated Mg-Al LDH				
P	> 103597*	11.1	> 544863*	10.7
Re	399	11.1	325	11.1
As	> 54209*	11.3	> 609787*	11.5
Se	268531	11.3	3795	11.5
Non-activated Mg-Al LDH				
P	3061	9.5	1051	8.4
Re	4	9.6	0.2	9.4
As	4465	9.7	182	9.5
Se	139	9.7	49	9.6

*Minimum values since the anion concentrations in solutions were below detection limits.

Sorption isotherms and effect of ionic strength: Sorption isotherms of Re and Se on the activated LDH were determined under various ionic strengths (Figure 4-3). It is shown in Figure 4-3 that the sorption data roughly follow the Freundlich isotherm, indicating the existence of various sorption sites with different sorption capabilities in LDH materials (Stumm, 1992, p. 95). This is consistent with the conceptual model of LDH summarized above, in which two general types of sorption sites are expected to exist: the external surface sites and the interlayer sites.

As expected, relative to the interlayer sites, the external surface sites are more sensitive to changes in the structure of an electric double layer on the surface. As shown in Figure 3, the ionic strength of solution can have a significant effect on Se sorption on LDH, and this effect becomes even more significant for low anion concentrations in the solution. A similar observation can be made for other anions (Table 4-1). Furthermore, the sorption efficient (K_d) of Se decreases with the amount of anion adsorbed (Figure 4-4). At low sorption coverage, the sorption is very sensitive to ionic strength changes, indicating an increased contribution of the external surface sites to sorption. From all these data, the following sorption picture seems to emerge: At a low concentration, an anion tends to sorb on the external surface sites first. As the anion concentration or the ionic strength increases, more anions are forced into the interlayer sites of LDH, and consequently the sorption becomes dominated by the interlayer ion exchange. The plateau of the sorption isotherm curves in Figure 4-4 may represents a major interlayer ion exchange. The high K_d values at a low anion concentration in dilute solutions are attributed to the external surface sites. If this is the case, the performance of LDH for the purification of water slightly contaminated with toxic anions could be significantly improved by increasing the number of the external surface sites through nano-scale material engineering.

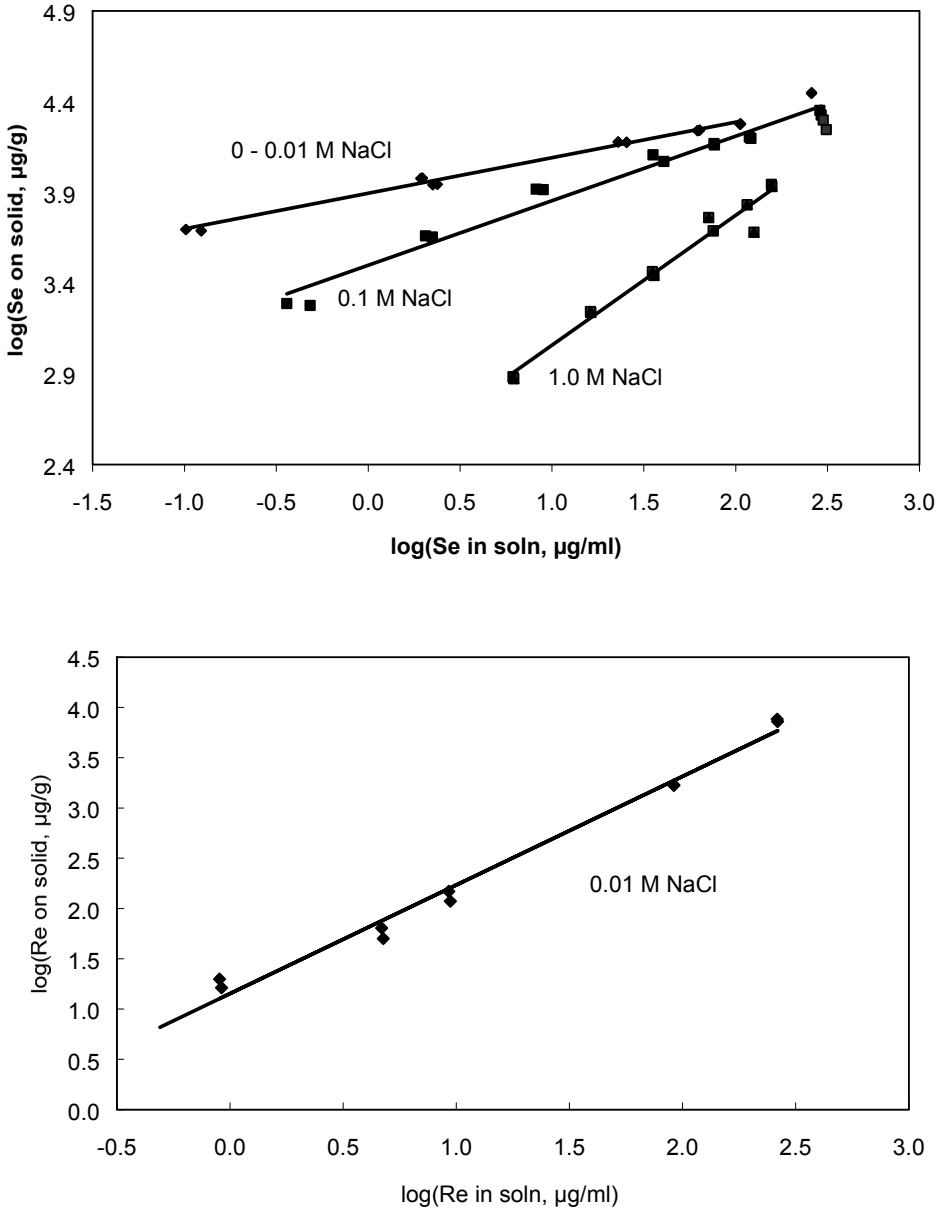

Figure 4-3. Sorption isotherms for Se and Re on activated LDH materials. The data roughly follow the Freundlich isotherm, indicating the existence of various sorption sites with different sorption capabilities in LDH materials. It is shown that the ionic strength can have a significant effect on anion sorption, especially at low anion concentrations.

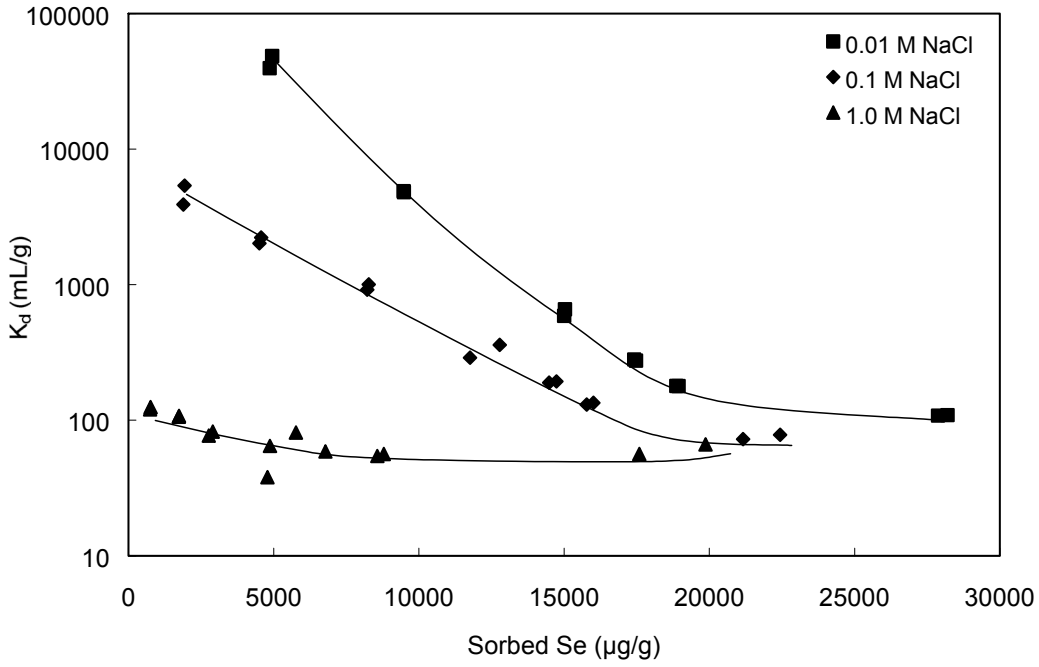

Figure 4-4. Sorption coefficient (K_d) as a function of the amount of Se sorbed. At low anion concentrations and ionic strengths, the anion sorption may be mainly contributed by the external surface sites, which are more sensitive than the interlayer sites to ionic strength changes. The plateau of the sorption isotherm curves may represents a major interlayer ion exchange.

Kinetics of anion sorption: Two parallel sets of kinetic experiments for Se and Re sorption on LDH were performed. One was added with dry activated LDH, and another with activated LDH pre-wetted for 24 hours. The percentage of Se sorbed and the related sorption coefficient (K_d) are plotted as a function of time in Figure 4-5. It is shown that the dry and pre-wetted materials have a different sorption kinetic behavior. An incubation time was required for the dry material to achieve the same K_d value as the pre-wetted material. Similar experiments were also conducted for the non-activated LDH, but no significant difference in sorption kinetics was observed between the dry and the pre-wetted materials.

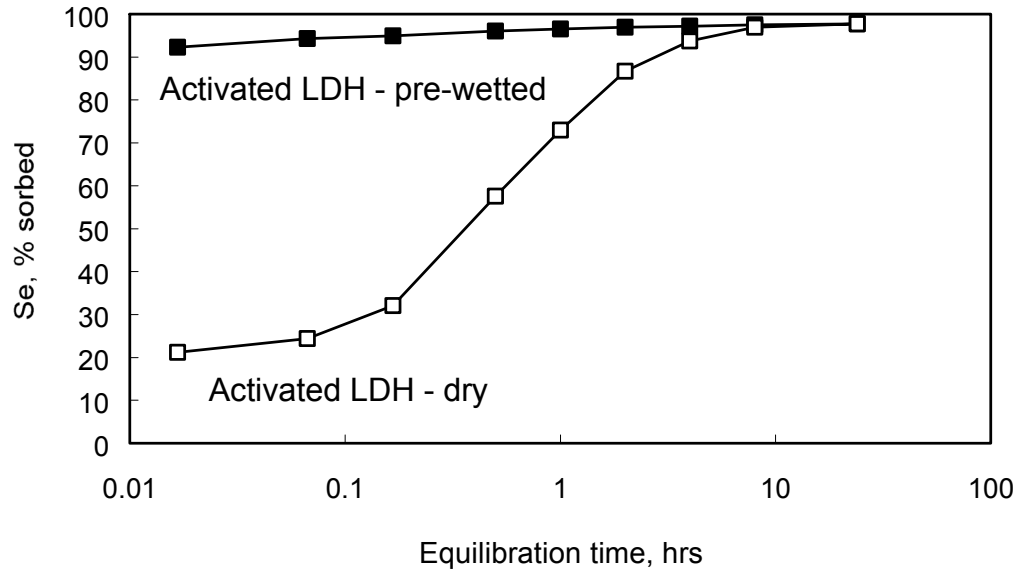

A

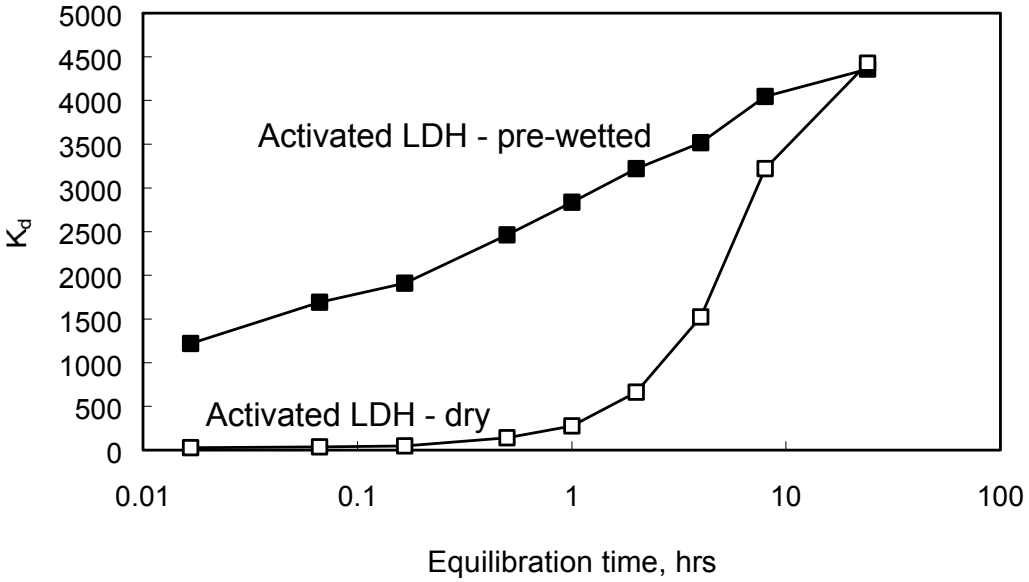

B

Figure 4-5. Percentage of Se sorbed and K_d as a function of time. Two parallel kinetic experiments were conducted. One was added with dry activated LDH, and another with activated LDH pre-wetted for 24 hours. The shift of the sorption curve for the dry LDH is attributed to the structural reconstruction of the activated material. The sorption curves for Re, which are not reported here, display the same kinetic features as those for Se.

LDH materials are known for the so-called memory effect, which allows reconstruction under mild conditions of the original structure by contact with solutions with various anions (Vaccari, 1998). We attribute the observed difference in sorption kinetics to the structural reconstruction of the activated LDH materials in solutions. To confirm this, we use an XRD analysis to monitor the structural changes of the activated LDH during hydration. It was observed that the periclase mineral phase initially present in the activated LDH disappeared over 24 hours and meanwhile a well crystalline LDH structure was restored. This observation together with the sorption data indicates a clear correlation between the increase in sorption coefficient and the structural reconstruction of the activated LDH during hydration. This also rules out the possibility of the high sorption coefficients of the activated LDH being caused by the presence of periclase, which we previously suspected.

4.5 Conclusions

Layered double hydroxides have shown the most promise for the removal of anionic contaminants. This report summarizes that experimental results that have been obtained since the inception of the LDRD project in 11/2000 on the anion sorption on two conventional LDH materials – activated and non-activated Mg-Al LDH. The major achievements are summarized as follows:

- Both activated and non-activated Mg-Al LDH materials have a Mg/Al molar ratio of 2.4 and a surface area 40 - 46 m^2/g. TEM and XRD analyses have shown that the activated material is less crystalline than the non-activated one and it contains a detectable amount of periclase, which generally disappears after material re-hydration.
- The anion sorption coefficients (K_d) have been measured for both activated and non-activated Mg-Al LDH materials. The activated material has a much higher anion sorption coefficient than the non-activated one, indicating that calcination can significantly improve anion sorption capacity of LDH. An optimal calcination temperature and time period are expected to exist such that the anion sorption capability can be maximized. Anion sorption on LDH seems sensitive to the pre-existing interlayer carbonate ions but not to those in the solution.
- Sorption isotherms for Re and Se on activated LDH materials have been determined under various ionic strengths. The obtained data roughly follow the Freundlich isotherm, indicating the existence of various sorption sites with different sorption capabilities. The ionic strength of a solution can have a significant effect on the anion sorption. Anions tend to first sorb on the external surface sites. As the anion concentration or the ionic strength increases, more anions are forced into the interlayer of LDH, and consequently the sorption becomes dominated by an interlayer ion exchange. The experimental data have indicated that the external surface sites have a very high affinity for anions, especially divalent and trivalent anions.
- In the kinetic experiments, the activated LDH material was added to solution either as a dry powder or as a pre-wetted suspension. The dry and pre-wetted materials have a different sorption kinetic behavior. An incubation time is required for the dry material to achieve the same K_d value as the pre-wetted material. This difference in sorption

kinetics is attributed to the structural reconstruction of the activated LDH material in solution. An XRD analysis indicates a clear correlation between the increase in sorption coefficient and the structural reconstruction of the activated material.

4.6 References

Amin, S and G. G. Jayson. 1996. "Humic substance uptake by hydrotalcites and PILCs," *Water Research.* Vol. 30, no.2, pp.299-306.

Balsley, S. D., P. V. Brady, J. L. Krumhansl and H. L. Anderson.1998. "Anion scavengers for low-level radioactive waste repository backfills," *Journal of Soil Contamination.* Vol.7, no.2, pp.125-141.

Boclair, J. W and P. S. Braterman. 1998. "One-step formation and characterization of Zn(II)-Cr(III) layered double hydroxides, $Zn_2Cr(OH)_{6X}$ (X = Cl, $1/2SO_4$)," *Chemistry of Materials.* Vol.10, no.8, pp.2050-&.

Boclair, J. W and P. S. Braterman. 1999. "Layered double hydroxide stability. 1. Relative stabilities of layered double hydroxides and their simple counterparts," *Chemistry of Materials.* Vol.11, no.2, pp.298-302.

Boclair, J. W., P. S. Braterman, J. P. Jiang, S. W. Lou and F. Yarberry. 1999. "Layered double hydroxide stability. 2. Formation of Cr(III)-containing layered double hydroxides directly from solution," *Chemistry of Materials.* Vol.11, no.2, pp.303-307.

Bond, A. H., F. W. K. Chang, A. H. Thakkar, J. M. Williamson, M. J. Gula, J. T. Harvey, S. T. Griffin, R. D. Rogers and E.P. Horwitz. 1999. "Design, synthesis, and uptake performance of ABEC resins for the removal of pertechnetate from alkaline radioactive wastes," *Industrial & Engineering Chemistry Research*. Vol.38, no.4, pp.1676-1682

Braterman, P. S., C. Q. Tan, and J. X. Zhao. 1994. "Orientational effects in the infrared-spectrum of the double-layer material, magnesium aluminum hydroxide ferrocyanide," *Materials Research Bulletin*. Vol.29, no.12, pp.1217-1221.

Chibwe, M., L. Ukrainczyk, S. A. Boyd and T. J. Pinnavaia. 1996. "Catalytic properties of biomimetic metallomacrocycles intercalated in layered double hydroxides and smectite clay: The importance of edge-site access," *Journal of Molecular Catalysis A – Chemical.* Vol. 113, no.1-2, pp.249-256.

Cui, D. Q and T. E. Eriksen.1996. "Reduction of pertechnetate in solution by heterogeneous electron transfer from Fe(II)-containing geological material," *Environmental Science and Technology.* Vol. 30, no.7, pp.2263-2269.

deLlano, A. Y., G. Bidoglio, A. Avogadro, P. N. Gibson, and P. R. Romero. 1996. "Redox reactions and transport of selenium through fractured granite," *Journal of Contaminant Hydrology.* Vol.21, no.1-4, pp.129-139.

Han, S. H., W. G. Hou, C. G. Zhang, D. J. Sun, X. R. Huang and G. T. Wang. 1998. "Structure and the point of zero charge of magnesium aluminum hydroxide," *Journal of the Chemical Society – Faraday*. Vol. 94, no. 7, pp. 915-918.

Hansen, H. C. B. 1989. "Composition, stabilization, and light-absorption of Fe(II)-Fe(III) hydroxy-carbonate (green rust)," *Clay Minerals.* Vol.24, no.4, pp.663-669.

Hermosin, M. C., I. Pavlovic, M. A. Ulibarri, J. Cornejo. 1996. "Hydrotalcite as sorbent for trinitrophenol - sorption capacity and mechanism," *Water Research.*Vol. 30, no.1, pp.171-177

Houri, B., A. Legrouri, A. Barroug, C. Forano and J. P. Besse. 1999. "Removal of chromate ions from water by anionic clays," *Journal de Chimie Physique et de Physico-Chimie Biologique;* Vol.96, no.3, pp.455-463.

Kameda, T., Y. Miyano, T. Yoshioka, M. Uchida and A. Okuwaki. 2000. "New treatment methods for waste water containing chloride ion using magnesium-aluminum oxide," *Chemistry Letters.* no.10, pp.1136-1137.

Kang M. J., K. S. Chun, S. W. Rhee, and Y. Do 1999. "Comparison of sorption behavior of I- and TcO4- on Mg/Al layered double hydroxide," *Radiochimica Acta*. Vol. 85, no.1-2, pp. 57-63.

Kumata, M and T. T. Vandergraaf. 1993. "Technetium behavior under deep geological conditions," *Radioactive Waste Management and the Nuclear Fuel Cycle.* Vol.17, no.2, pp.107-117.

Kunze, S., V. Neck, K. Gompper. And T. Fanghanel. 1996. "Studies on the immobilization of technetium under near field geochemical conditions," *Radiochimica Acta.*Vol.74, pp.159-163.

Liang, L. Y., B. H Gu and X. P. Yin. 1996. "Removal of technetium-99 from contaminated groundwater with sorbents and reductive materials," *Separation Technology.* Vol..6, no.2, pp.111-122.

Loyaux-Lawniczak, S., P. Refait, P. Lecomte, J. J. Ehrhardt and J. M. R. Genin. 1999. "The reduction of chromate ions by Fe(II) layered hydroxides," *Hydrology and Earth System Sciences.* Vol.3, no.4, pp.593-599.

Monteil-Rivera, F., M. Fedoroff, J. Jeanjean, L. Minel, M. G. Barthes and J. Dumonceau. 2000. "Sorption of selenite (SeO32-) on hydroxyapatite: An exchange process," *Journal of Colloid and Interface Science.* Vol.221, no.2, pp.291-300

Narita, E., T. Yamagishi, and T. Tonai. 1992. "Adsorption property of ionic dyes by heat-treated layered double hydroxide-cristobalite rock composite-materials," *Nippon Kagaku Kaishi* ; no.3, pp.291-296.

National Academy of Sciences. 1999. *Arsenic in Drinking Water*. National Academy Press, Washington, D.C.

Onkal-Engin, G., R. Wibulswas. and D. A. White. 2000. "Humic acid uptake from aqueous media using hydrotalcites and modified montmorillonite," *Ennvironmental Technology.* Vol. 21, no.2, pp.167-175.

Pavan, PC; Crepaldi, EL; Valim, JB 2000. "Sorption of anionic surfactants on layered double hydroxides," *Journal of colloid and Interface Science*. Vol. 229, no.2, pp.346-352.

Refait, P., C. Bon, L. Simon, G. Bourrie, F. Trolard, J. Bessiere and J. M. R. Genin. 1999. "Chemical composition and Gibbs standard free energy of formation of Fe(II)-Fe(III) hydroxysulphate green rust and Fe(II) hydroxide," *Clay Minerals.* Vol.34, no.3, pp.499-510.

Refait, P. H., M. Abdelmoula and J. M. R. Genin. 1998. "Mechanisms of formation and structure of green rust one in aqueous corrosion of iron in the presence of chloride ions," *Corrosion Science*. Vol. 40, no.9, pp.1547-1560.

Rives, V and M. A. Ulibarri. 1999. “Layered double hydroxides (LDH) intercalated with metal coordination compounds and oxometalates,” *Coordination Chemistry Review.* Vol.181, pp.61-120

Roh, Y., S. Y. Lee, M. P. Elless, and J. E. Foss. 2000. “Incorporation of radioactive contaminants into pyroaurite-like phases by electrochemical synthesis,” *Clays and Clay Minerals.* Vol. 48, no.2, pp.266-271.

Schollhorn, R and B. Otto. 1986. “Cooperative anion-exchange mechanism of layered transition-metal hydroxide systems,” *Journal of the Chemical Society-Chemical Communications.* no.15, pp.1222-1223.

Seida, Y and Y. Nakano. 2000. “Removal of humic substances by layered double hydroxide containing iron,” *Water Research*. Vol. 34, no.5, pp.1487-1494.

Shin, H. S., M. J. Kim, S. Y. Nam and H. C. Moon. 1996. “Phosphorus removal by hydrotalcite-like compounds (HTLcs),” *Water Science and Technology*. Vol. 34, no.1-2, pp.161-168.

Stumm, W. 1992. *Chemistry of the Solid-Water Interface*. John Wiley & Son. 428 pp.

Vaccari, A. 1998. “Preparation and catalytic properties of cationic and anionic clays,” *Catalysis Today.* Vol.41, no.1-3, p.53-71.

Villa, M.V., M. J. Sanchez-Martin, and M. Sanchez-Camazano 1999. “Hydrotalcites and organo-hydrotalcites as sorbents for removing pesticides from water,” *Journal of Environmental Science and Health Part B-Pesticides Food Contaminants and Agricultural Wastes*. Vol. 34, no.3, pp.509-525.

5. Anion Sorption on Layered Double Hydroxides: Effect of Structural Reconstruction

5.1 Introduction

Contaminants that occur in anionic forms are commonly highly mobile in surface and subsurface environments, because they are negatively charged and are poorly sorbed by most soil and sediment components under neutral or basic conditions (pH > 7) (Liang et al., 1996; Kunze et al., 1996; Kang et al., 1996; Bond et al., 1999; Monteil-Rivera et al., 2000). Anionic contaminants include ^{99}Tc, ^{79}Se, and ^{129}I, long-lived fission products (half-lives ranging from $2.13 \cdot 10^5$ to $1.57 \cdot 10^7$ years) released during reprocessing of nuclear fuel for weapons production. Under oxidizing conditions, these radionuclides are highly soluble and exist as TcO_4^-, SeO_4^{2-}, and I^-. Currently, the Department of Energy (DOE) has 90 million gallons of high-level and low-level liquid waste generated by weapons production activities. This material is stored in underground tanks, some of which have known or suspected leaks. The high mobility of ^{99}Tc, ^{79}Se, and ^{129}I anionic species poses a technical challenge for tank closure. A nonradioactive anionic contaminant of concern is arsenate, AsO_4^{3-}, which exceeds the new EPA drinking water standard of 10 ppb in the municipal water supplies for many cities in the western U.S.

Layered double hydroxide (LDH) materials have shown great promise as anion getters. LHDs consist of positively charged, close-packed, metal hydroxide layers, whose surplus positive charge, arising from the substitution of a trivalent cation M(III) for a divalent cation M(II), is neutralized by an interlayer anion or anionic complex. LDH materials have the general formula (Kovanda et al., 1999; You et al., 2001a; You et al., 2001b; Rives and Ulibarri, 1999):

$$[M^{II}_{1-x}M^{III}_{x}(OH)_2]^{x+} A_{x/n} \cdot y\, H_2O \qquad (5\text{-}1)$$

where M^{II} = divalent cation (generally Mg^{2+}, Ca^{2+}, or a divalent transition metal); M^{III} = trivalent cation (commonly Al^{3+} or a trivalent transition metal), present in a mole fraction of x; and A = exchangeable interlayer anion (Cl^-, CO_3^{2-}, SO_4^{2-}) of charge n. Since hydrotalcite, $Mg_6Al_2(OH)_{16}CO_3.4H_2O$, is a member of this family, they are often referred to as hydrotalcite-like compounds.

LDH materials have high anion exchange capacities, with typical ion exchange capacities of ~ 3.5 meq/g (You et al., 2001a). Both interlayer exchange and surface adsorption contribute to the sorption capacity of LDH — the point of zero charge (PZC) is 12-12.5 (Han et al., 1998). LDH materials have a particularly high affinity for doubly or triply charged anions, including sulfite and sulfate (and, by implication, selenite and selenate), as well as for a wide range of metal-containing anions (Rives and Ulibarri, 1999). They have been suggested for removal of chromate, phosphate, chloride ion, anionic surfactants, ionic dyes, and humic substances from water (Narita et al., 1992; Shin et al., 1996; Houri et al., 1999; Seida and Nakano, 2000; Pavan et al., 2000; Kameda et al., 2000; Hermosin et al., 1996; Amin and Jayson, 1996; Onkal-Engin et al., 2000).

Calcination of LDH commonly increases measured sorption of anionic species (Kovanda et al., 1999; You et al., 2001b). The enhanced reactivity of the calcined material has been postulated to be due to the removal of strongly bound carbonate ions from the interlayer sites during heating and the subsequent replacement by readily-exchanged hydroxyl groups during rehydration (Kovanda et al., 1999). We examined the effects of calcination and rehydration of Mg/Al LDH (Mg/Al molar ratio = 2.4:1), and measured the kinetics of sorption of ReO_4^- (as an analog for TcO_4^-), SeO_4^{2-}, and AsO_4^{3-} onto calcined LDH.

5.2 Materials and Methods

Carbonated magnesium-aluminum LDH (Mg/Al = 2.4) was obtained from ALCOA Industrial Chemicals. The average particle size of the material is 5 to 8 μm, and the surface area, measured by N_2 BET, is ~ 40 m^2/g. To investigate the effects of calcination, aliquots of the uncalcined material were calcined at temperatures of 100º–800ºC for 4 hours, and then analyzed by X-ray diffraction using a Bruker D-8 Advance diffractometer equipped with a Kevex solid-state detector, and a Cu Ka X-ray tube (40 KV and 30 mA). Samples were analyzed for carbon content using a UIC, Incorporated carbon coulometer with a high-temperature furnace front-end. When calcined LDH is exposed to humid air, it readsorbs water and CO_2, and its efficiency as an anion getter decreases. Thus, for these experiments, only freshly calcined LDH was used, and the material was stored in tightly sealed containers until use.

Sorption isotherms for selenate, perrhenate, and arsenate onto freshly calcined LDH (500ºC) were determined using batch methods. For Se and Re, Oak Ridge-type screw-cap centrifuge tubes were used, with 0.2 g calcined LDH and 20 ml of degassed 0.01 M, 0.1 M, or 1.0 M NaCl. Following 24 hours equilibration in an N_2-purged glove box, the samples were spiked with the target anion, in initial concentrations ranging from 0.1-300 μg/ml for Re, and 10-400 μg/ml for Se. Samples were mixed continuously for 16-20 hours, and the liquid was sampled, filtered through a 0.2μm syringe filter, and analyzed for the target anion by Inductively-Coupled Plasma Optical Emission Spectrometry (ICP-OES).

Sorption K_ds are extremely high for arsenate, so a sequential spiking approach was used to determine the sorption isotherm. In this method, 0.8 g of calcined LDH was placed in 160 ml of 0.01 M NaCl and pre-equilibrated for 24 hours, and then 32 mg As was added as arsenate, to yield an initial concentration of 200 μg/ml As. After equilibrating for 24 hours, 10 ml was extracted and filtered (0.2 μm) for analysis, and 10 ml electrolyte, containing an additional 32 mg As as arsenate was added. This was repeated five times.

Sorption kinetics experiments were run as batch systems, using 1.3 g of freshly calcined LDH material (500 ºC) in 130 ml of 0.01 M NaCl. Experiments were carried out in two different formats. In one, the powdered material was pre-wetted for 24 hours, and the pH was adjusted to ~8.0 prior to adding the Re, Se, or As. In the second, the dry

powder was added to electrolyte already containing the anion of interest—no pH adjustment was possible. Initial spike concentrations were 20 µg/ml for Re and Se. An initial concentration of 100µg/ml was used for As because of the high affinity of LDH for arsenate. The containers were placed on an orbital mixing platform and agitated continuously over the course of the experiment. Samples were collected periodically over the next 24-48 hours, filtered through 0.2 µm filters, and analyzed for the anion of interest by ICP-OES (Perkin-Elmer Optima 3300DV). To minimize the effect of carbonate competition, degassed electrolyte was used and samples were agitated in a nitrogen-purged glove box.

5.3 Results and Discussion

Effect of calcining temperature: X-ray diffraction analysis of the calcined LDH (Figure 5-1) shows that heating to 200º C for 4 hours has little effect on LDH. Heating to 300ºC results in loss of surface water and structural water in the interlayers, and structural decomposition of the LDH (Constantino and Pinnavaia, 1995). Interlayer carbonate in not lost. Heating to 400ºC results in dehydroxylation and decarbonation, and periclase (MgO) diffraction peaks are present in the X-ray pattern. LDH calcined at less than 300ºC rapidly rehydrates and structurally reconstitutes when exposed to water or even to humid air (Constantino and Pinnavaia, 1995). LDH calcined at 400ºC or higher rapidly absorbs water and CO_2 from the air, but does not structurally reform until it is immersed in water. Upon immersion, the material rehydrates slowly over the space of one-two days—periclase disappears from the XRD pattern, and LDH X-ray peaks appear and sharpen with time.

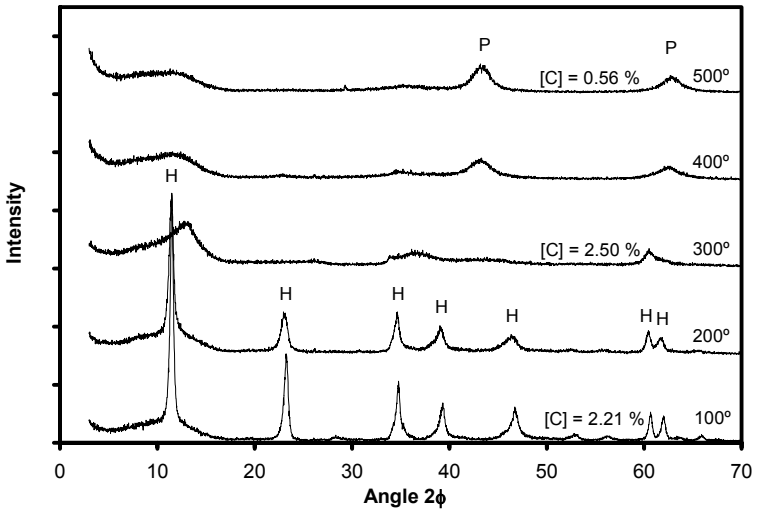

Figure 5-1. X-ray diffraction patterns for Mg-Al LDH calcined at temperatures from 100ºC to 500ºC. H denotes diffraction peaks for hydrotalcite, and P, diffraction peaks for periclase.

Sorption isotherms: Selenate, perrhenate, and arsenate all display Freundlich-type sorption behavior (Figure 5-2) onto calcined LDH, indicating the existence of various sorption sites with different sorption energies (Stumm, 1992, p. 95). The observed sorption behavior may be due to the high surface area of this material, as both external surface sites and interlayer sites will contribute significantly to sorption. Selenate sorption varies strongly with ionic strength, especially at low surface anion loadings; it is not clear whether this is due to Cl^- competition with selenate for the interlayer sites, or competition with surface-bound (outer sphere) selenate.

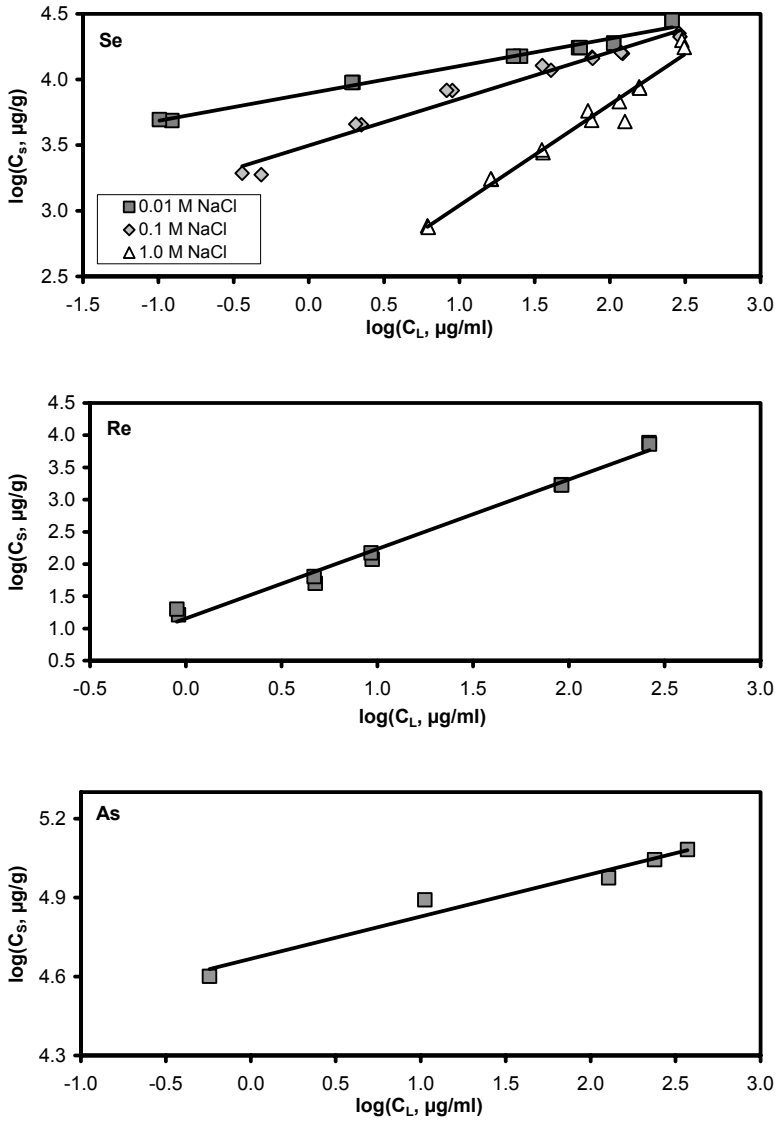

Figure 5-2. Freundlich sorption isotherms for selenate, perrhenate, and arsenate on freshly calcined Mg-Al LDH (500ºC). Selenate isotherms were measured in 0.01 M, 0.1 M, and 1.0 M NaCl; perrhenate and arsenate isotherms were measured only in 0.01 M NaCl.

Kinetics of sorption onto calcined LDH: We investigated As, Se, and Re sorption onto calcined LDH as a function of the initial state of the material (dry, or pre-wetted) and as a function of contaminant contact time. Results are shown in Figure 5-3. Sorption results varied for different anionic complexes. For selenate and perrhenate, sorption was initially quite low on the dry material, but increased over the next 24 hours. Sorption onto the pre-wetted material was initially much higher, and rose slowly. An incubation time of about 24 hours was required for the dry material to achieve the same K_d value as the pre-wetted material. This suggests that sorption is increasing as the material hydrates and the LDH structure is reconstructed, and is consistent with the interpretation that sorption is higher on LDH than on the products of calcination. Thus, anionic forms Se and Re are not highly sorbed by the phases present in the calcined material, but are incorporated as interlayer anions in the LDH structure upon hydration and reconstruction. For arsenate, however, sorption was initially higher on the dry material, and K_ds for both pre-wetted and dry material decreased with time. This behavior suggests that arsenate, unlike selenate and perrhenate, is more strongly sorbed onto the phases formed by calcination, and that it is partially released during hydration. The pre-wetted material shows similar behavior because, after 24 hours, it has only partially rehydrated to form LDH.

5.4 Conclusions

Layered double hydroxides show considerable promise for the removal of anionic contaminants. Calcination of the material increases sorption affinity for most anionic compounds, including selenate and perrhenate, through removal of strongly bound carbonate from the interlayer sites. Sorption increases as the calcined material rehydrates and restructures into LDH; a wetting interval is necessary to reach full sorption capacity. However, for some anionic compounds such as arsenate, sorption appears to be occurring onto phases formed during calcination, and decreases somewhat as the material rehydrates. Sorption of all three anionic complexes onto calcined Mg-Al LDH (Mg/Al = 2.4) follows a Freundlich isotherm. Thus, anion sorption K_ds onto calcined LDH are both anion-specific and strongly dependent on the initial state of the substrate (dry or rehydrated), and consideration must be given to this when developing applications for LDH materials.

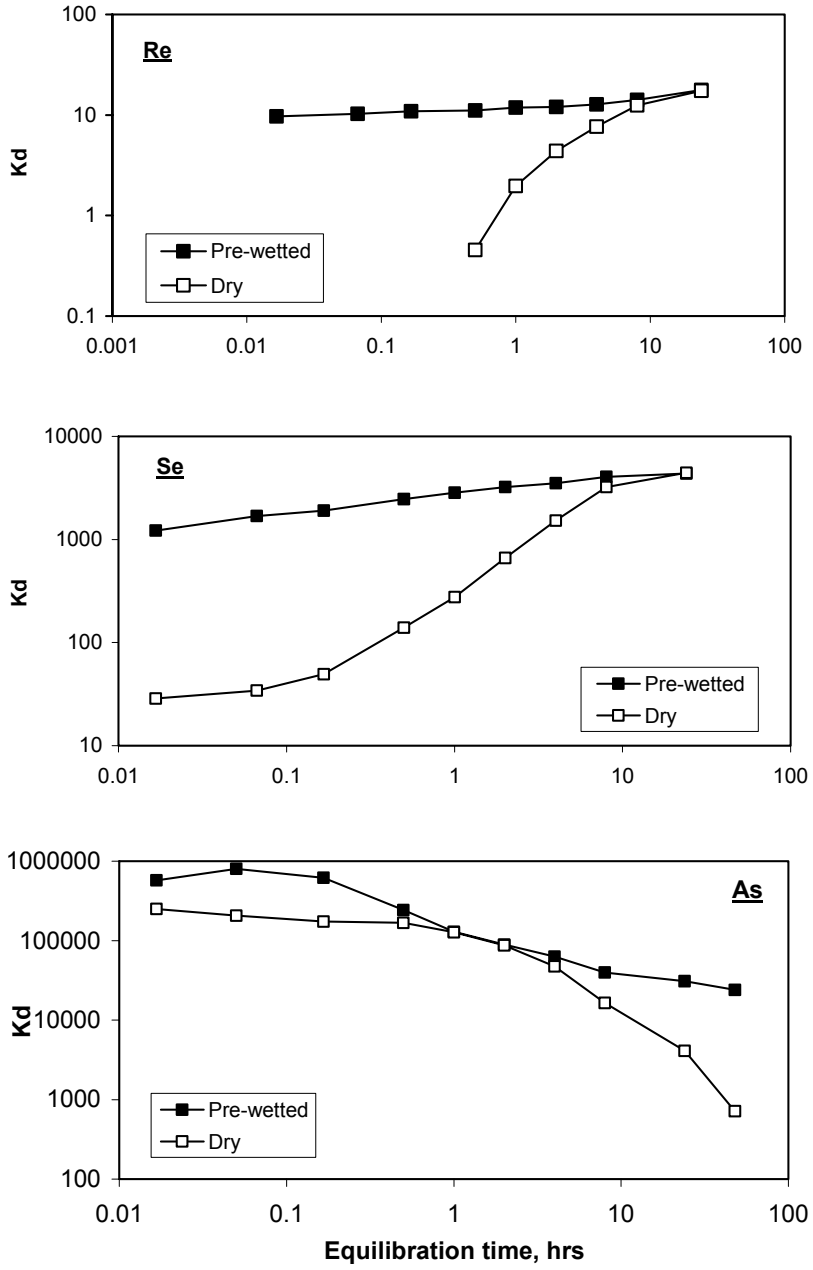

Figure 5-3. Sorption of selenate, perrhenate, and arsenate onto initially dry and pre-wetted calcined LDH. Selenate and perrhenate sorb more rapidly onto the pre-wetted solid, and sorption increases with time, as hydration continues. Arsenate, however, is more rapidly sorbed onto the initially dry material, and partially desorbs as hydration occurs.

5.5 References

Amin, S and G. G. Jayson. 1996. "Humic substance uptake by hydrotalcites and PILCs," *Water Research*. Vol. 30, no. 2, pp.299-306.

Bond, A. H., F. W. K. Chang, A. H. Thakkar, J. M. Williamson, M. J. Gula, J.T. Harvey, S. T. Griffin, R. D. Rogers and E. P.Horwitz. 1999. "Design, synthesis, and uptake performance of ABEC resins for the removal of pertechnetate from alkaline radioactive wastes," *Industrial & Engineering Chemistry Research*. Vol. 38, no.4, pp.1676-1682.

Constantino, V. R.L and T. J. Pinnavaia. 1995. "Basic properties of $Mg^{2+}_{1-x}Al^{3+}_{x}$ layered double hydroxides intercalated by carbonate, hydroxide chloride and sulfate anions," *Inorganic Chemistry* v. 34, no. 4, p. 883-892.

Han, S. H., W. G. Hou, C. G. Zhang, D. J. Sun, X. R. Huang and G. T. Wang. 1998. "Structure and the point of zero charge of magnesium aluminum hydroxide," *Journal of the Chemical Society – Faraday*. Vol. 94, no. 7, pp. 915-918.

Hermosin, M. C., I. Pavlovic, M. A. Ulibarri and J. CORNEJO. 1996. "Hydrotalcite as sorbent for trinitrophenol - sorption capacity and mechanism," *Water Research.* Vol.30, no.1, pp.171-177.

Houri, B., A. Legrouri, A. Barroug, C. Foranoand J. P.Besse. 1999. "Removal of chromate ions from water by anionic clays," *Journal de Chimie Physique et de Physico-Chimie Biologique;* Vol. 96, no. 3, p. 455-463.

Kameda, T., Y. Miyano, T. Yoshioka, M. Uchida and A. Okuwaki. 2000. "New treatment methods for waste water containing chloride ion using magnesium-aluminum oxide," *Chemistry Letters*. Vol. 5; no. 10, pp.1136-1137.

Kang M. J., K. S. Chun, S. W. Rhee and Y. Do. 1999. "Comparison of sorption behavior of I- and TcO4- on Mg/Al layered double hydroxide," *Radiochimica Acta*. Vol. 85, no.1-2, pp. 57-63.

Kovanda, F; Kovacsova, E; and D. Kolousek. 1999. "Removal of anions from solution by calcined hydrotalcite and regeneration of used sorbent in repeated calcination-rehydration-anion exchange processes," *Collection of Czechoslovak Chemical Communications*. Vol. 64, no. 9, pp.1517-1528.

Kunze, S., V. Neck, K. Gompper and T. Fanghanel. 1996. "Studies on the immobilization of technetium under near field geochemical conditions" *Radiochimica Acta*. Vol. 74, pp.159-163.

Liang, L. Y., B. H. Gu and X. P. Yin 1996. "Removal of technetium-99 from contaminated groundwater with sorbents and reductive materials," *Separations Technology*. Vol. 6, no. 2, pp.111-122.

Monteil-Rivera, F., M. Fedoroff, J. Jeanjean, L. Minel, M. G. Barthes and J. Dumonceau 2000. "Sorption of selenite (SeO_3^{2-}) on hydroxyapatite: An exchange process.," *Journal of Colloid and Interface Science*. Vol. 221, no. 2, pp.291-300.

Narita, E; T. Yamagishi and T. Tonai. 1992. "Adsorption property of ionic dyes by heat-treated layered double hydroxide-cristobalite rock composite-materials," *Nippon Nagaku Kaishi*. no. 3, pp.291-296.

Onkal-Engin, G., R. Wibulswas and D. A. White. 2000. "Humic acid uptake from aqueous media using hydrotalcites and modified montmorillonite," *Environmental Technoloy.* Vol. 21, no. 2, pp.167-175.

Pavan, P. C., E. L. Crepaldi and J. B. Valim. 2000. "Sorption of anionic surfactants on layered double hydroxides," *Journal of Colloid and Interface Science*. Vol. 229, no.2, pp.346-352.

Seida, Y and Y. Nakano. 2000. "Removal of humic substances by layered double hydroxide containing iron," *Water Research.* Vol. 34, no. 5, pp.1487-1494.

Shin, H. S., M. J. Kim, S.Y. Nam and H. C. Moon. 1996. "Phosphorus removal by hydrotalcite-like compounds (HTLcs)," *Water Science and Technology*; Vol.34, no.1-2, pp.161-168.

Stumm, W. 1992. *Chemistry of the Solid-Water Interface*. John Wiley & Son. 428 pp.

You, Y. W., G. F. Vance and H. T. Zhao. 2001. "Selenium adsorption on Mg-Al and Zn-Al layered double hydroxides," *Applied Clay science*. Vol. 20, no. 1-2, pp.13-25.

You, Y. W., H. T. Zhao, and G. F. Vance. 2001. "Removal of arsenite from aqueous solutions by anionic clay," *Environmental Technology.* Vol. 22, no. 12, pp.1447-1457.

6. New Hydrocarbon Chain Packing Mode and New Crystallite Growth Habit in the Self-Assembled Nanocomposite Zinc-Aluminum-Hydroxide Oleate [$Zn_2Al(OH)_6(cis\text{-}CH_3(CH_2)_7CH{=}CH(CH_2)_7COO^-)$]

6.1 Introduction

Layered double hydroxides (LDHs), also known as anionic clays, are composed of positively charged hydroxide layers similar to the brucite structure consisting of the octahedrons, with exchangeable anions and water molecules in the interlayer (Cavani et al., 1991; Rives and Ulibarri, 1999). The research on LDH materials receives much attention in the recent decade due to its wide applications in catalysis, anion absorbents, environment remediation, electron devices and polymer/clay nanocomposite materials etc. The exchanging property makes it convenient to introduce various organic anions into LDH, and thus leading to the formation of alternating hydroxide layer-organic anion layer hybrids, i.e., alternating inorganic/organic nanocomposite materials based on the LDH framework. It has been reported that many long-chain surfactant anions including alkyl carboxylates, alkyl sulfate, alkyl sulfonates are intercalated by exchange, expanding the interlayer and rendering a hydrophobic surface (Kanoh et al., 1999; Takagi et al., 1993; Carlino, 1997; Meyn et al., 1990; Braterman et al., 2003). However, some important issues, in particular the organic anion packing in the interlayer and their interactions, are still under contraversion because of the versatility in organic anion species and geometrical variety. In general, the hydrocarbon chains are closely packed either in a monolayer or in a bilayer mode at a slant angle respect with the hydroxide layer. The interlayer spacing is strongly related to the chain length and packing mode (Kanoh et al., 1999; Takagi et al., 1993; Carlino, 1997; Meyn et al., 1990; Braterman et al., 2003). We report here a new packing mode specific to cis-unsaturated tail group (exemplified here by oleate, $cis\text{-}CH_3(CH_2)_7CH{=}CH(CH_2)_7COO^-$) in LDH, in comparison with the mono- and bi-layer packing mode of its trans analogue: elaidate (elaidate: $trans\text{-}CH_3(CH_2)_7CH{=}CH(CH_2)_7COO^-$) in the similar cases.

We also report that these hybrid organic-inorganic LDH materials show novel particle morphologies and growth habits. In a conventional LDH, i.e. carbonate or chloride, the crystallites preferentially grow along the *a* and *b* axes, giving hexagonal platelets with a lateral aspect ratio (*a/c*) of 10-30 (Kanoh et al., 1999; Takagi et al., 1993; Cai et al., 1994). The materials described here, and LDH-anionic surfactant nanocomposites in general, adopt completely different morphologies. We report here on the relationship between morphology (SEM) and detailed structure (HRTEM), and discuss our results in terms of molecular self-assembly and hydrophobic forces (Xu and Braterman, 2003).

Being interested in the possible production of our materials from low cost and naturally ocurring precursors, we selected a commercial olive oil, which contains oleate (70-80%), palmitate (~11%) and linoleate (~10%) triglycerides (Kuksis, 1978), as the oleate source. We report that the one-pot preparation of oleate-like LDH, including in situ hydrolysis of olive oil in an alkaline solution, leads to formation of oleate-like LDH, as shown by XRD and FTIR.

The transformation of conventional LDHs to the mixed metal oxides is usually carried out by calcination, involving several common steps, such as dehydration, the collapse of hydroxide layers and depletion of inorganic anions, and, in some cases, redox reactions of metal ions (Braterman et al., 2003; Xu and Zeng, 1998). However, the decomposition of organic anions in surfactant LDHs is anticipated to be very different, as reported for MgCoAl-terephthalate-LDHs (Xu and Zeng, 2000). In this section, we also describe the thermolysis of our materials under air and under N_2.

6.2 Experimental Section

Materials Preparation: The precursor layered double hydroxide $Zn_2Al(OH)_6Cl{\cdot}nH_2O$ was prepared, then thoroughly washed via centrifuge and dried in vacuum over molecular sieves, as described elsewhere (Boclair and Braterman, 1999; Boclair et al., 1999). Briefly, 50 mmol $AlCl_3{\cdot}6H_2O$ (Aldrich, 99%) and 150 mmol $ZnCl_2{\cdot}6H_2O$ (Aldrich, 98%) were dissolved in 500 mL pure water (18.2 MΩ cm). After being purged with N_2 for around 30 minutes, the solution was treated with 15.7 mL 50% NaOH (300 mmol, Alfa Aesar), followed by an overnight reflux under a slow stream of N_2. Thus the metal stoichiometry is controlled by the amount of added base while excess Zn^{2+} is present in solution. The precipitate was collected and thoroughly washed with deionized water via centrifuge, and dried in vacuum over molecular sieves. This precursor was used to prepare organic LDH by the exchange method. Samples ZAO (Zn_2Al-LDH-oleate) and ZAE (Zn_2Al-LDH-elaidate) were obtained by exposing the precursor (*ca.* 4 mmol) to 100 mL of a colloidal solution containing oleate (*ca.* 6 mmol) or elaidate (*ca.* 4 mmol), and refluxing overnight. The surfactant solutions were prepared by dispersing potassium oleate paste (40% w/w in water, Aldrich) in water or elaidic acid (6.0 mmol, 98%, Avocado) in aqueous NaOH (6.0 mmol). After separation and thoroughly washing, the samples were dried in vacuum over molecular sieves. In comparison, ZAED (Zn_2Al-LDH-elaidate) was prepared in a similar way but using 150% excess elaidate, i.e. 10 mmol exchanging with 4 mmol precursor LDH. We also carried out several preparations of Zn_2Al-LDH-elaidate with 5-100% excess elaidate present. The filtrate in all cases has a pH of 10-11. Mg_2Al-LDH compounds with these two anions were also made in the similar way.

Table 6-1. Observed XRD data for samples ZAO, MAO, ZAE and ZAED.

ZAO			MAO			ZAE			ZAED [2]			Miller indices
2θ/deg	d/nm[1]	(I/I_0)(%)	2θ/deg	d/nm[1]	(I/I_0)(%)	2θ/deg	d/nm[1]	(I/I_0)(%)	2θ/deg	d/nm[1]	(I/I_0)(%)	hkl
2.47	3.58	100	2.43	3.63	100	2.85	3.10	100	1.81	4.88	100	003
4.93	1.79	21.0	4.91	1.80	20	5.73	1.54	39.3	3.61	2.45	21.2	006
7.51	1.18	5.7	7.41	1.19	8.1	8.61	1.03	12.0	5.42	1.63	39.2	009
10.1	0.876	2.0	10.2	0.87	3.6	11.49	0.770	3.4	7.24	1.22	6.3	0,0,12
						14.45	0.613	2.0	9.08	0.974	12.5	0,0,15
						17.41	0.509	2.1	10.90	0.812	1.5	0,0,18
~20	0.44	2.0	19.7	0.45	8.0	20.7	0.429	3.5	12.73	0.695	3.8	0,0,21
						23.2	0.384	2.0	14.59	0.607	1.0	0,0,24
						26.1	0.342	1.0	16.40	0.540	1.0	0,0,27
33.9	0.265	3.3	34.5	0.260	3.2	33.8	0.265	2.7	34.2	0.263	1.0	012
60.5	0.153	2.0	60.3	0.154	2.0	60.5	0.153	2.0	60.5	0.153	1.5	110
a=0.306 nm, *c*=3×3.56 nm			*a*=0.308 nm, *c*=3×3.57 nm			*a*=0.306 nm, *c*=3×3.08 nm			*a*=0.306 nm, *c*=3×4.88 nm			

Note: [1] The average interlayer spacing was estimated as $(d_{003} + 2d_{006} + ... + nd_{00(3n)})/n$.

[2] Only those data corresponding to the bi-layer phase were listed.

The one-pot method, i.e. precipitating metal ions in anion-containing basic solution and refluxing overnight, gave LDH compounds of similar composition. In particular, a commercial olive oil was used as the oleate precursor for a one-pot preparation of Mg_2Al-oleate-LDH. In a typical preparation, 2.413g mol $AlCl_3 \cdot 6H_2O$ (10 mmol, Aldrich, 99%) and 4.067g $MgCl_2 \cdot 6H_2O$ (20.0 mmol, Aldrich, 99%) were dissolved in 150 ml deionized water, and then mixed with 3.62g olive oil (MW=860-900, 4.0-4.2 mmol, i.e. 12.0-12.6 ×80% = ~10.0 mmol oleate part) and treated with 3.7 ml 50% NaOH solution (71 mmol, Alfa Aesar). This mixture was heated to reflux overnight and followed by a similar separation, washing, and drying procedure for ZAO and ZAE, giving an Mg:Al LDH product (sample name MAO).

Materials Characterization: Powder diffraction patterns were collected on a powder x-ray diffractometer (XRD, Siemens F-series) with Cu Kα (λ=0.15418 nm) radiation at a scanning rate of 1.2^o per minute from $2\theta = 2^o$ to $2\theta = 65^o$. Powdered CaF_2 was used as an internal calibrant, and the d-spacing was calculated from the several orders of basal reflections as described in Table 6-1. Infrared spectra were collected using KBr discs on a Perkin-Elmer 1760X FTIR after 40 scans within 4000-400 cm^{-1} at a resolution of 4 cm^{-1}. SEM images were taken on a JEOL T 300 microscope at a voltage of 20 kV and a filament current of around 5 mA. TEM was performed on a JEOL JEM-100 CXII electron microscope at a voltage of 100 kV and a filament current of 80-85 μA.

Zinc and aluminum content was determined by atomic absorption (Analyst 300, Perkin Elmer). Carbon and hydrogen contents were measured with CHN analyzer by MHW laboratories. Found for ZAO, 41.2% C, 6.66% H, 24.2% Zn and 5.23% Al with atomic ratios C : Zn : Al = 17.7 : 1.91 : 1 and for ZAE, 40.3% C, 7.20% H, 22.2% Zn and 5.05% Al with atomic ratio C : Zn : Al = 18.0 : 1.81 : 1; calculated for both $Zn_2Al(OH)_6(oleate) \cdot H_2O$ and $Zn_2Al(OH)_6(elaidate) \cdot H_2O$ 38.7% C, 7.33% H, 22.8% Zn and 4.84% Al with ratios 18 : 2 : 1.

The presence of free acid in ZAED was confirmed and determined by a back titration method. In general, 0.2-0.4 mmol LDH was dissolved in excess HCl solution (5.00 mmol) with gentle heating, then the excess H^+ and elaidic acid were titrated with an NaOH solution (0.100 N) by monitoring the pH to the end point of 6-7, using NaF (2-4 mmol) and $HOCH_2CH_2OH$ (4-8 mmol) as the masking agents of Al^{3+} and Zn^{2+} (Dean, 1995), respectively. The result shows that the molar ratio of free elaidic acid/ to Al was 0.50:1.

Thermogravimetric analysis (TGA, Perkin Elmer, TGA6) was carried out in both oxidizing (air) and inert (N_2) atmospheres. During the measurement, 10-15 mg of sample was heated at a rate of 10 ^oC/min with a gas flow rate of 100 ml/min respectively over a temperature range of 30-800 ^oC.

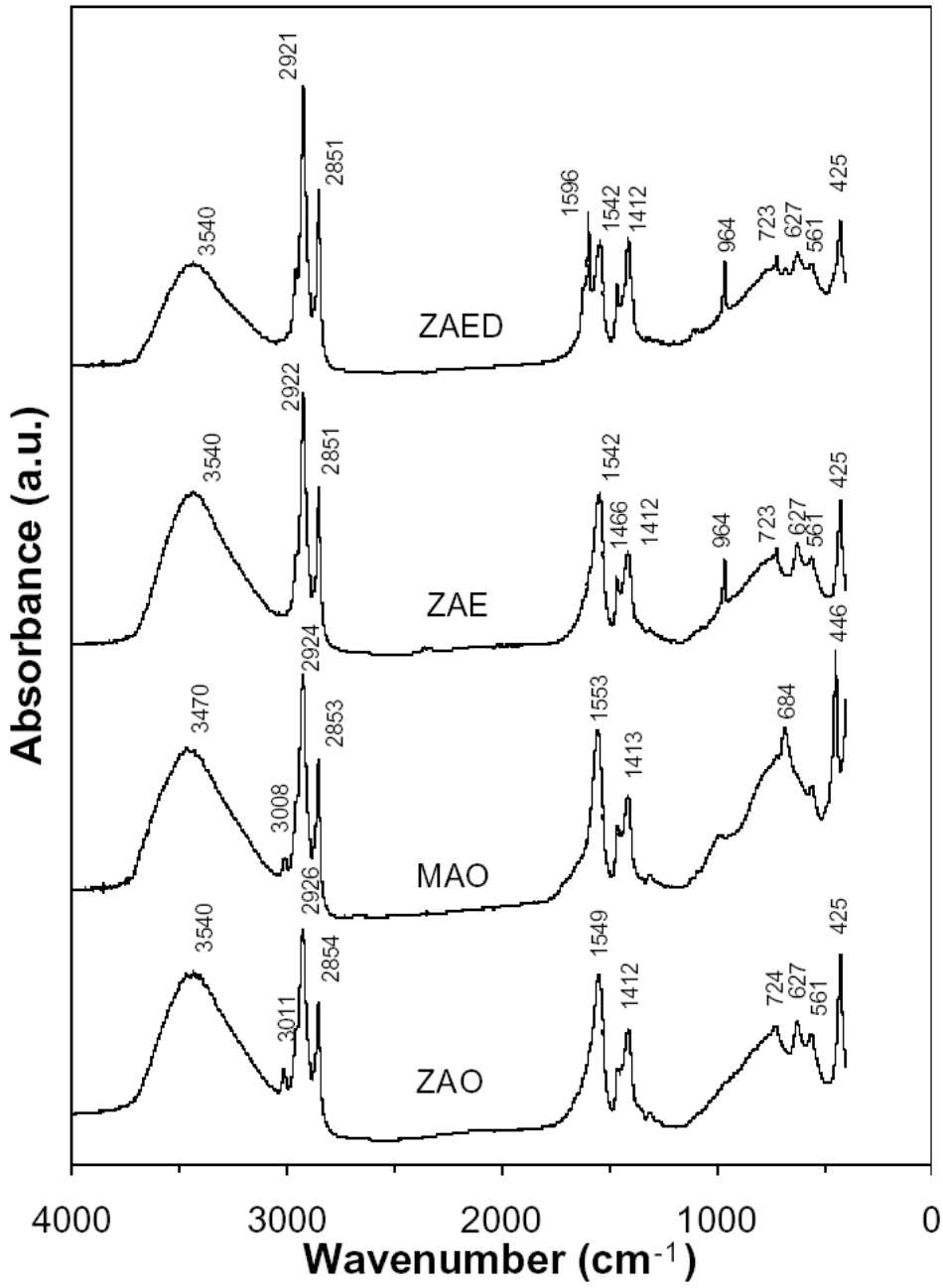

Figure 6-1. The FTIR spectra of samples ZAO, ZAE and MAO.

6.3 Results And Discussion

Structural Features: As shown in Figure 6-1, ZAO, ZAE and MAO show the common IR characteristics of long-chain carboxylate LDH compounds. These include a broad band at ~3500 cm^{-1} (ν_{OH}) (Cavani et al., 1991; Rives and Ulibarri, 1999), a group of strong peaks at 2800-3000 cm^{-1} (asymmetric and symmetric ν_{CH}) (Williams and Fleming, 1989; Simons, 1978), two strong bands at 1400-1600 cm^{-1} (asymmetric and symmetric $\nu_{C=O}$) and δ_{CH2} at 1466 cm^{-1}, as well as bands at 724 (δ_{CH}) (Williams and Fleming, 1989; Simons, 1978; Borla and Dutta, 1992), 627, 561 and 425 cm^{-1} (ν_{MO}) (Cavani et al., 1991; Rives and Ulibarri, 1999). However, there are also more distinctive features: ν_{CH} attached to a double bond in ZAO (3011 cm^{-1}) (Simons, 1978, p. 710) and MAO (3008 cm^{-1}) (Simons, 1978, p.741), and δ_{CH} (out-of-plane deformation) for elaidate in sample ZAE at 964 cm^{-1} (Simons, 1978). It is worth mentioning that the sharp peak at 446 cm^{-1} in sample MAO indicates the formation of a well-ordered 2:1 Mg:Al LDH (Xu and Zeng, 2001; Kloprogge and Frost, 1999). The characteristic peaks of asymmetric and symmetric ν_{CH} at 2800-3000 cm^{-1} are actually identical in MAO and ZAO, confirming the intercalation of the oleate hydrocarbon chain. In addition, we note an extra peak at 1596 cm^{-1} only for sample ZAED. This extra peak is attributed to the asymmetric $\nu_{C=O}$ of an undissociated carboxylic acid group (COOH) that is H-bonded in the interlayer in sample ZAED (Borja and Dutta, 1992), as also required by the back-titration data and elemental analyses reported above. The existence of free acid groups (Kloprogge and Frost, 1999) is a general phenomenon, when excess carboxylate anions are used in the exchange or preparation, even at such high pH (Xu et al., 2002).

Powder x-ray diffraction patterns in Figure 6-2 show strong basal reflections (*00l*) (Cavani et al., 1991; Rives and Ulibarri, 1999), as expected for an expanded layer structure. The 2θ angles, corresponding d-spacings and relative intensities are summarized in Table 6-1. It is calculated from the reflections that the interlayer spacing is 3.56 nm for ZAO and 3.57 nm for MAO, respectively, the identity of which further confirms that they have the same intercalated anion: oleate. There is a consistent reflection series for sample ZAE, up to the ninth reflection order, i.e., (*0,0,27*) peak, indicating an average spacing of 3.08 nm. However, the XRD patterns of sample ZAED comprise not only the series of reflections of ZAE, but also a new series of much sharper reflection peaks, as indicated by bold indexes in Figure 6-2. These new reflections correspond to an interlayer spacing of 4.88 nm. We have found in other experiments in this series that 5-10% excess elaidate can lead to the formation of this new phase. Therefore, ZAED contains two discrete LDH phases, in which the intercalated species (elaidates/elaidic acid) are presumed to pack in monolayer and bi-layer modes, as addressed in the following section.

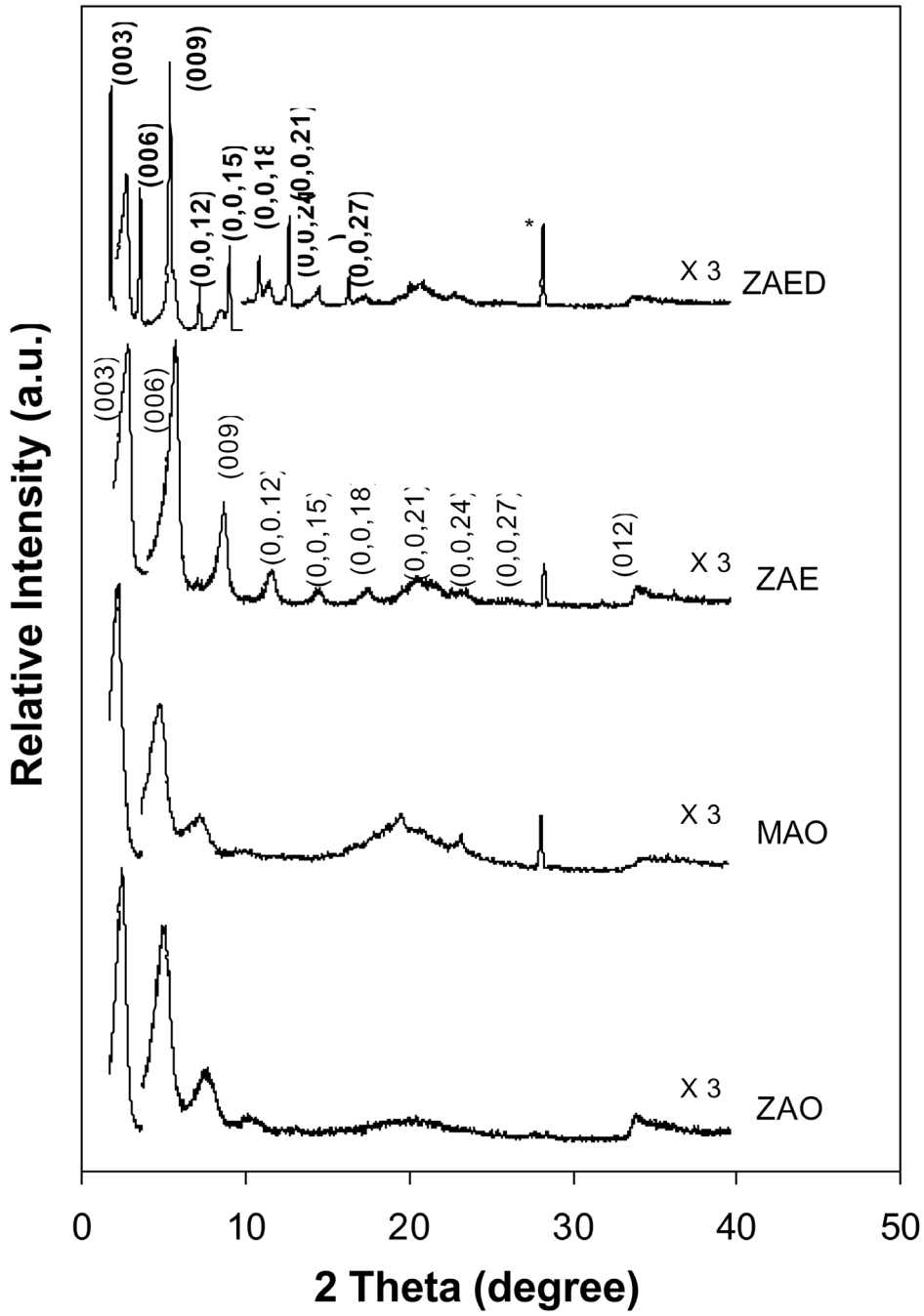

Figure 6-2. The XRD patterns of samples ZAO, ZAE and MAO. The peak marked with * is ascribed to the plane (111) of the internal calibrant CaF_2.

The nominal particle thickness in the c-axis direction was calculated from the measured widths of peaks *(00l)*, using the Debye-Scherrer equation without instrument correction (Cullity, 1978), to be 20-30 nm for samples ZAO, MAO and ZAE, and 70-80 nm for the new phase in ZAED. We also note that peak (*0,0,21*) of ZAE overlaps a broad reflection, presumably associated with the hydrocarbon chains in the interlayer (Xu and Braterman, 2003); such a broad band is also observed for all other samples in the same region.

Anion packings: If the chains of these two anions were completely extended and tilted at about 55^{o} as is usual for straight chain carboxylate LDH (Carlino, 1997; Meyn et al., 1990; Lagaly, 1976), their vertical height in LDH would be the same (1.82 nm for the hydrocarbon chain, refer to Figures 6-3a and 6-3c). Thus, such an anti-parallel packing mode implies an overall basal spacing of 2.99 nm for an extended C_{18} chain anion (Kanoh et al., 1999; Tagagi et al., 1993). This is in good agreement with the spacing found for elaidate (3.08 nm, sample ZAE) and for saturated carboxylates (Gunstone, 1967) (Figure 6-3a). Additionally, the implied tilting of the hydrocarbon chains in the interlayer at *ca.* 55^{o} is similar to the tilting habit in saturated fatty acids in their crystals (~60^{o}) (Xu and Braterman, 2003), and allows both carboxylate oxygen atoms to form hydrogen bonds to the hydroxide layers equally.

If excess elaidate/elaidic acid is used in the exchange, then a new phase (4.88 nm, in sample ZAED) is also formed, corresponding to a bilayer packing as plotted in Figure 6-3b. The interlayer spacing is predicted to be 4.82 nm, in quantitative agreement with the observed in sample ZAED. We note that elaidic acid is intercalated even at pH is up to 11 and we attribute this to the formation of H-bond of free acid groups with carboxylate group and/or hydroxide groups pending on the brucite layers (Gunstone, 1967). It is known that the asymmetric $\nu_{C=O}$ of free elaidic acid is 1715 cm^{-1} (Simons, 1978). The down-shift to 1596 cm^{-1} further supports the formation of H-bond of the acid group (COOH) in the interlayer.[18] Similar infrared features were also observed for LDHs with stearate/stearic acid intercalated (Kanoh et al., 1999; Gunstone, 1967).

However, oleate requires a packing mode different from above two cases (Figure 6-3c) because the cis geometry includes a bend in the middle of the chain which hinders the full overlapping described above. In fact, this bend allows the chains to overlap only in the region below the double bond (Figure 6-3c), sticking the chains together like Velcro. The calculated spacing (3.61 nm), for this packing mode, is quite close to that observed (3.56 or 3.57 nm). The bending geometry of oleate in the LDH interlayer is similar to the boomerang shape that oleic acid employs in its crystallization (Xu and Braterman, 2003). Though 50% excess oleate was used in the exchange, no new phase like that in ZAED is observed. The situation for MgAl-oleate-LDH is similar.

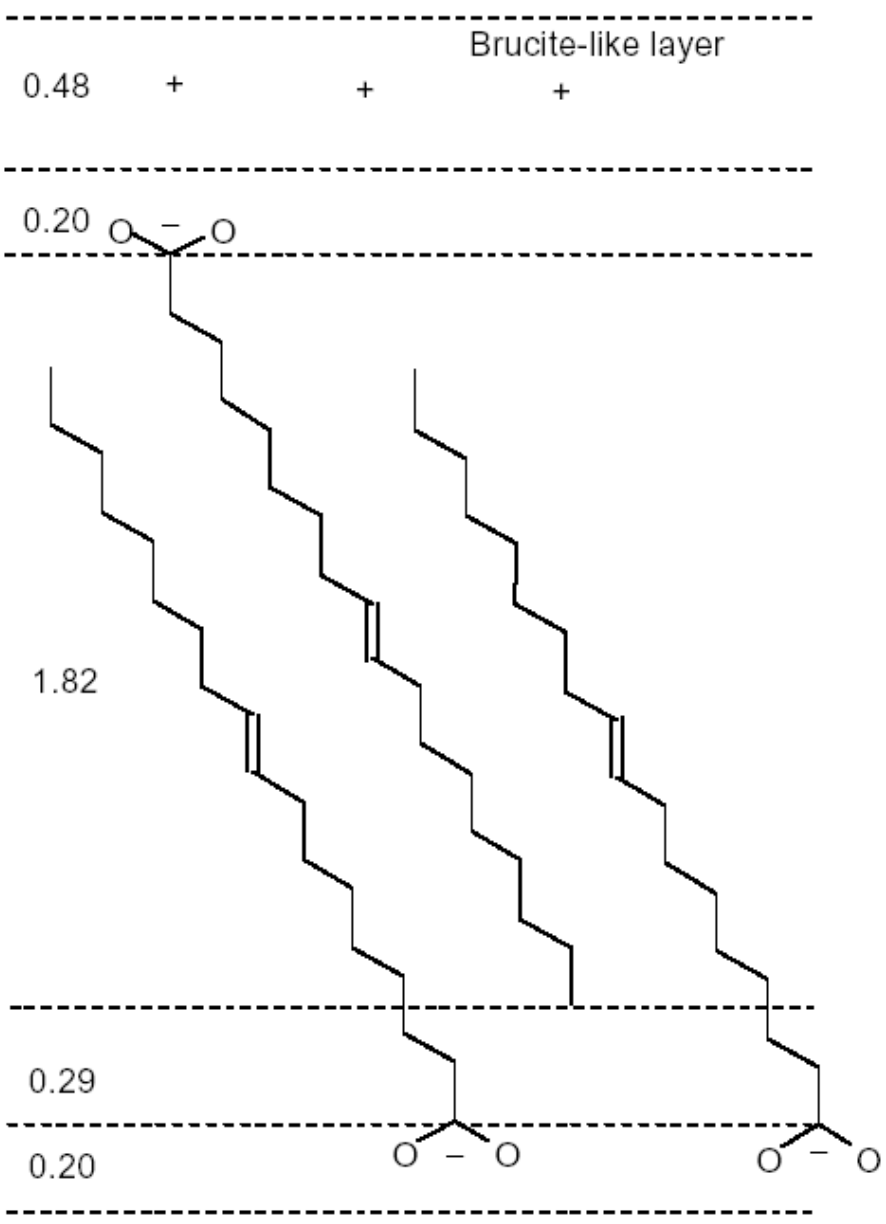

A

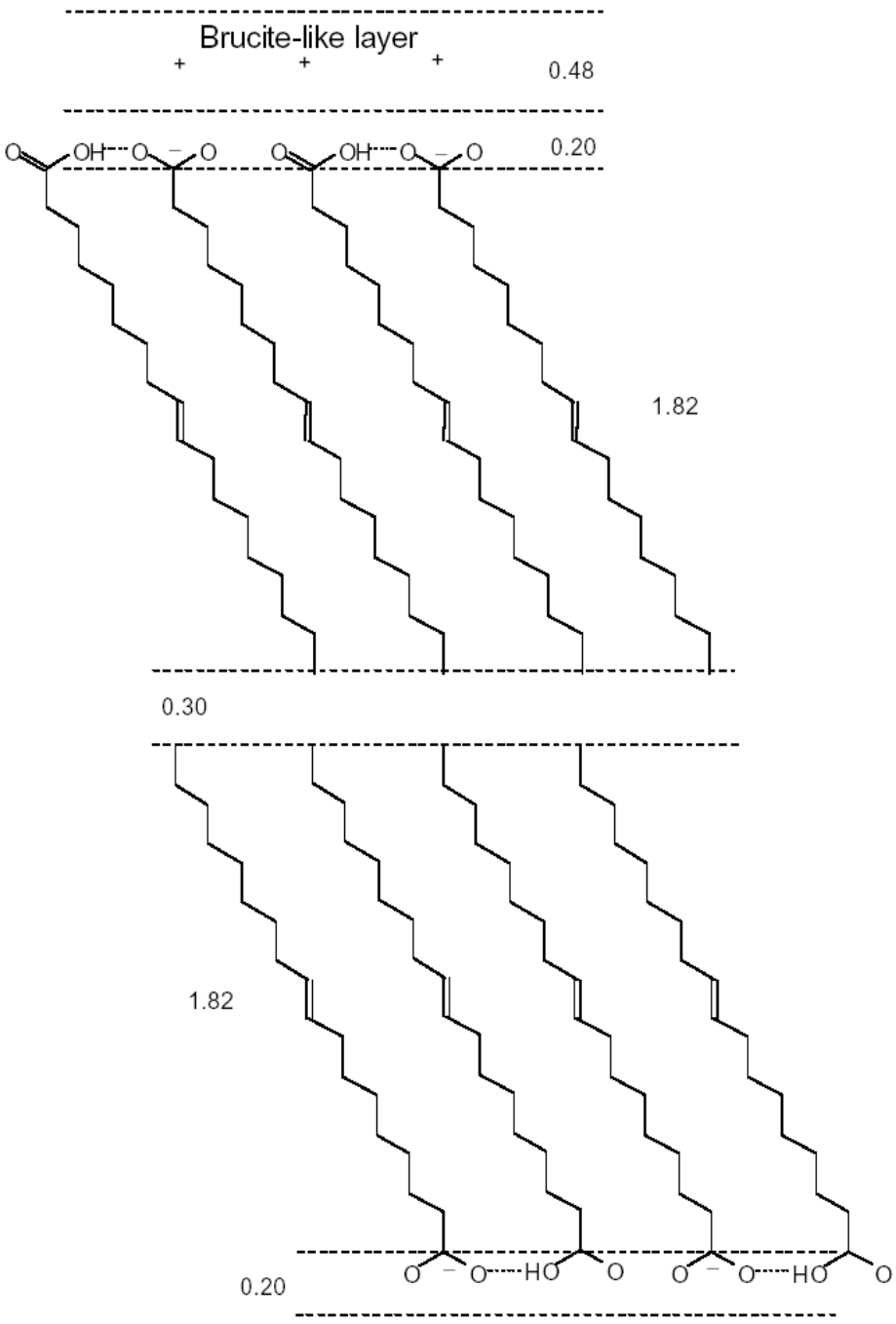

B

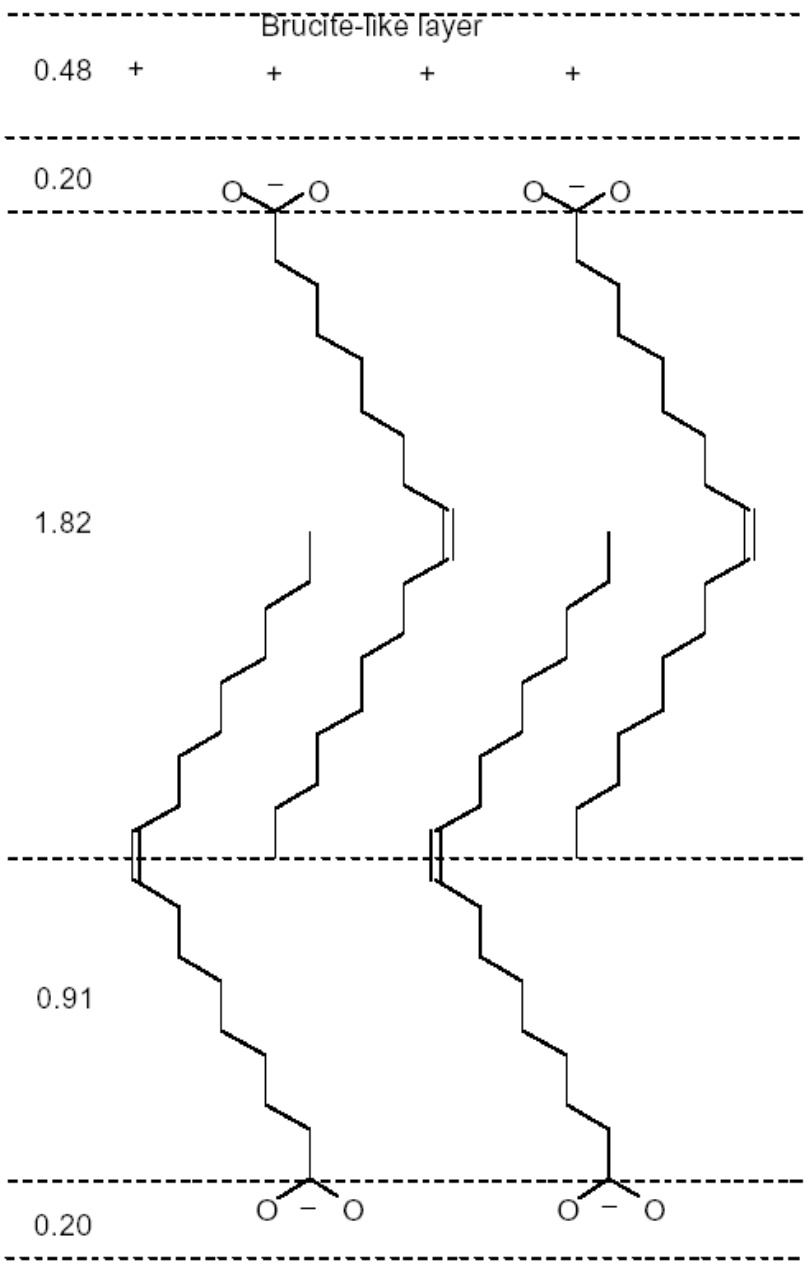

C

Figure 6-3. The proposed models for the packing of (a) elaidate and (b) oleate in the interlayer and unit in nm.

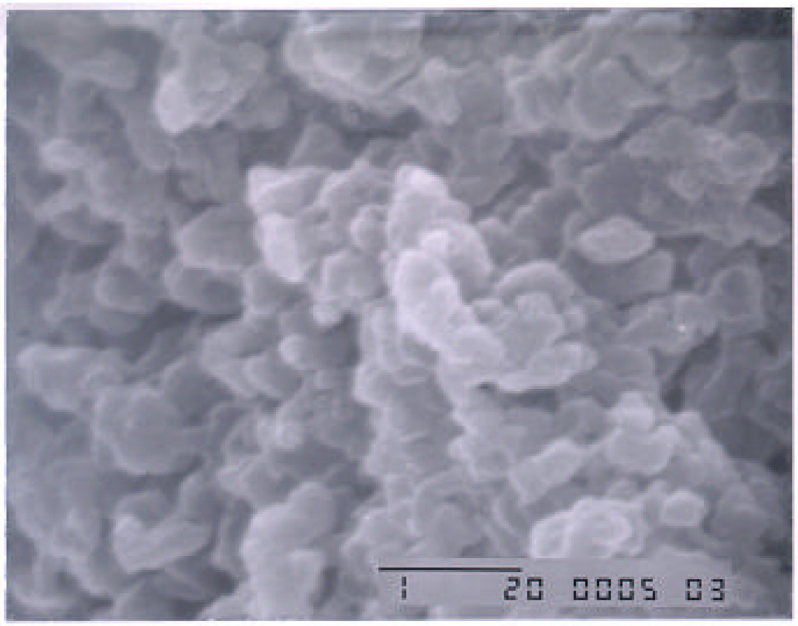

(a)

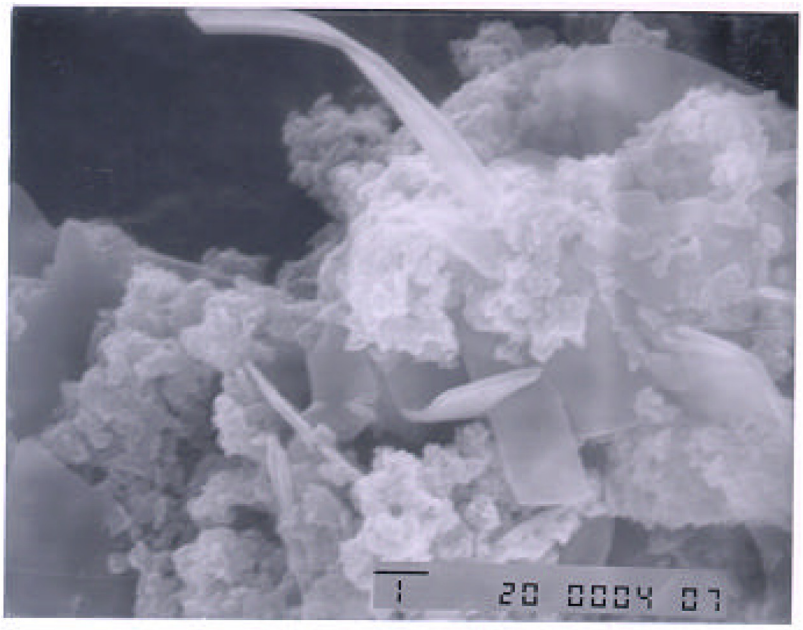

(b)

Figure 6-4. Scanning electron micrographs of (a) ZAO and (b) ZAE and scale bar 1 μm.

Morphology and growth habit: The different packing in the interlayer gives rise to different morphologies, as shown in Figure 6-4. There are homogeneous sub-micron platy sheets in ZAO (Figure 6-4a) while ZAE gives much bigger sheets or ribbons with length and width in micrometers, as shown in Figure 6-4b (Ogawa and Asai, 2000), although small irregular particles are scattered around. These features are clearly quite different from the regular hexagonal platy sheets of inorganic LDH (Kanoh et al., 1999; Takagi et al., 1993; Cai et al., 1994; Ogawa and Asai, 2000; Labajos et al., 1992).

As further shown in Figure 6-5, TEM images indicate the stacking of hydroxide or organic anion layers. The black (hydroxide layers) and white (anion layers) stripes are alternating and roughly parallel. We note that sample ZAE has larger uniform stacking regions than sample ZAO and that the average fringe distances are 3.3 nm for ZAE and 3.5 nm for ZAO, in tolerable agreement with the XRD observation. We can also directly note the layer bending and layer merging or branching as indicated in the insert of the figure.

We suggest that these features are related to a major difference between the growth habit of hybrid organo-LDH crystallites and that of inorganic LDH. It is known that crystallites of inorgano-LDHs grow along the *a* and *b* axes to form hexagonal thin sheets, which tend to lie flat with the *c* axis perpendicular to the plane of the support. Thus it is very difficult to directly observe the stacking of hydroxide layers in TEM. However, we have clearly observed the layer stacking in ZAO and ZAE. The ribbon-like sheets observed in SEM for ZAE and the corresponding alternation of black and white stripes clearly show that the crystallites have grown along the *c* axis.

We attribute this to self-assembly of surfactant-rich layers by hydrophobic interactions at the edge of the growing crystallite. The positively charge hydroxide layers bind the hydrophilic heads of the anions on the plane via electrostatic interactions, leaving their tails to form a thin, self-assembled, hydrophobic layer. This hydrophobic layer adsorbs another layer of anions with anti-parallel orientation, which provides a nucleus for the next layer, thus promoting growth along the *c* axis.

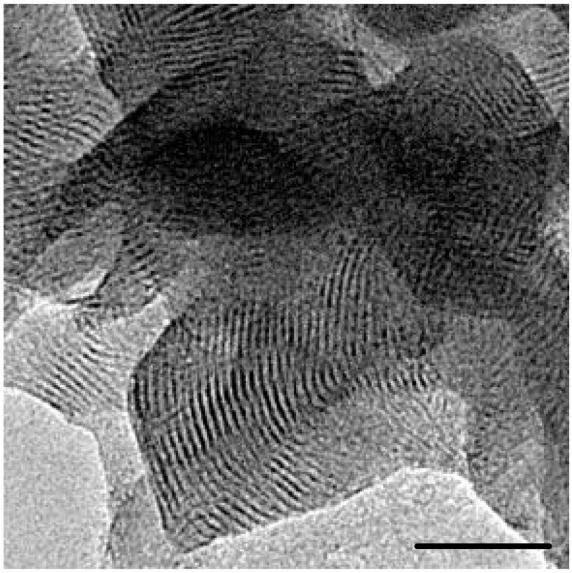

(a)

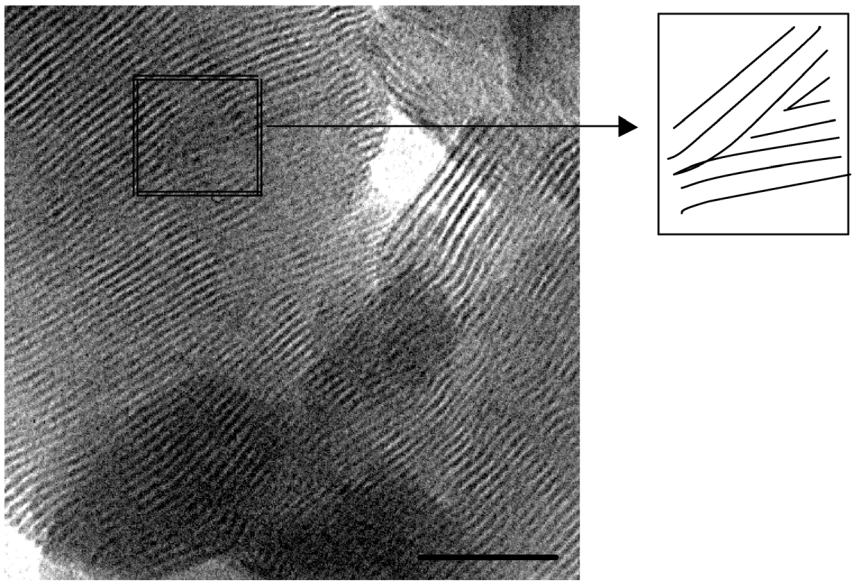

(b)

Figure 6-5. Transmission electron micrographs of (a) ZAO and (b) ZAE (x80,000) and scale bar 50 nm.

Table 6-2. Weight losses (%) and thermal events of samples ZAO and ZAE in Air and N_2

Temperature (^oC)		in Air	in N_2	Cal. [1]	Thermal events
40-175	ZAO	7.9	8.9	8.0	Dehydration
	ZAE	7.2	7.2	7.1	
175-240	ZAO	13.3	14.0	17.2 [2]	Partial dehydroxylation
	ZAE	12.0	11.4	15.9 [2]	
240-600	ZAO	64.9	58.5	--	Further dehydroxylation and decomposition of organic anions
	ZAE	66.1	61.7	--	
600-800	ZAO	65.4	63.3	63.8 [3]	Decomposition of carbonate salts and some carbon residues.
	ZAE	66.6	66.6	65.2 [3]	

Note: [1] The calculation of weight loss percentage is based on nominal formula: $Zn_{1.91}Al(OH)_{5.82}(oleate)_{0.98}\cdot 2.4H_2O$ for ZAO and $Zn_{1.81}Al(OH)_{5.62}(Elaidate)_{1.00}\cdot 2.2H_2O$ for ZAE.

[2] The weight loss calculated accounts for full dehydration and dehydroxylation.

[3] The final oxide has a nominal formula $Zn_{1.91}AlO_{3.41}$ for ZAO and $Zn_{1.81}AlO_{3.31}$ for ZAE.

Thermal decomposition behavior: The thermal decomposition processes of samples ZAO and ZAE in air and N_2 are shown in the TGA and differential TGA curves of Figure 6-6. As summarized in Table 6-2, there are four main stages of thermolysis. The first two stages are not influenced by the atmosphere in which the thermolysis takes place (Cavani et al., 1991; Rives and Ulibarri, 1999; Braterman et al., 2003). The first event is unambiguously attributed to loss of absorbed water molecules, in which the observed weight loss of 7.9-8.9% for ZAO and 7.2% for ZAE is in good agreement with that calculated 8.0% for ZAO and 7.1% for ZAE from the loss of 2.4 and 2.2 water molecules per formula unit, respectively. Note here that there are more waters due to the physical absorption that is not pre-dried prior to the TGA measurement. We tentatively assign the second step to partial dehydroxylation of the layer structure. In this stage, the weight loss is 5.1-5.4% for ZAO and 4.2-4.8% for ZAE, about half of the 9.2% and 8.8% respectively estimated for total dehydroxylation.

The major event in the third stage, involving decomposition of organic species as well as further dehydroxylation, is more complicated. In the N_2 environment (Figure 6-6A), ZAE shows one sharp weigh loss while ZAO shows two weight losses around 400^{o}C. Decomposition in air, however, begins at as low as 250-300^{o}C, and is followed by a second process at around 450 ^{o}C (Figure 6-6B). As reported (Xu and Zeng, 2000), decomposition of organic species takes place by several parallel and/or serial processes, such as dehydrogenation, thermal cracking to various hydrocarbons, decarboxylation and/or oxidation to CO_2, and graphitization.

In an inert environment more hydrocarbons are generated through thermal cracking and less CO_2 is formed. By contrast, dehydrogenation and oxidation are major processes in air due to the sufficient oxygen supply, taking place at low temperatures. However, it is not so clear why there is a second process appearing at around 450 ^{o}C under air. We would suggest that the early oxidation, like burning, occurs mainly on the particle surface and forms oxide film on the surface. This oxide film may hinder the diffusion of oxygen and delay the oxidation of inner organic species.

We suggest, on the basis of the weight loss and an earlier report (Tsuji et al., 1993), that stage four consists of carbonate decomposition and, in air, burning of carbon residues. The final weight losses at 800 ^{o}C in both cases are in quantitative agreement with the calculation from nominal chemical formulae (Table 6-2) assuming metal oxides are the only products.

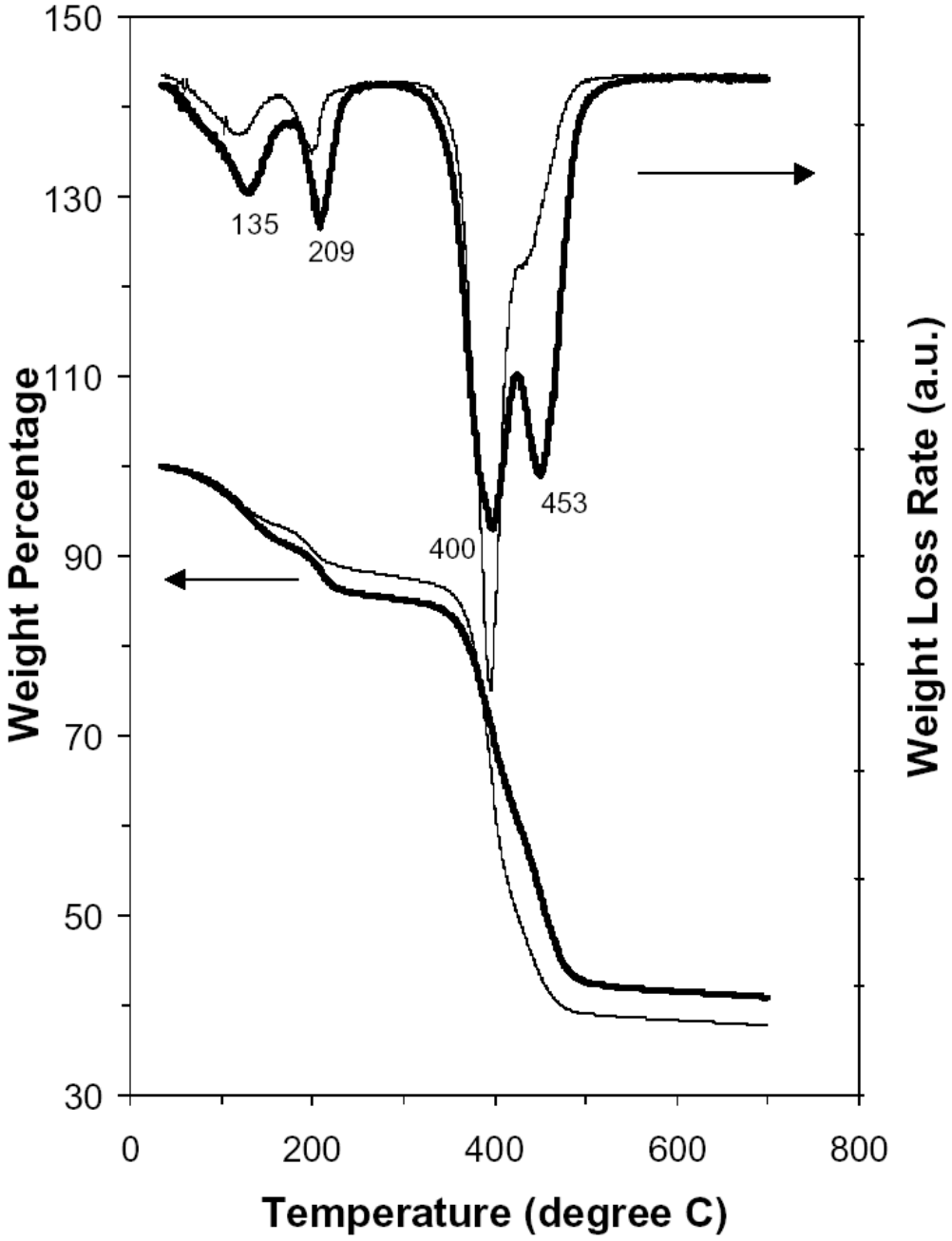
150
130
110
90
70
50
30
Weight Percentage
Weight Loss Rate (a.u.)
135
209
400
453
0
200
400
600
800
Temperature (degree C)

A

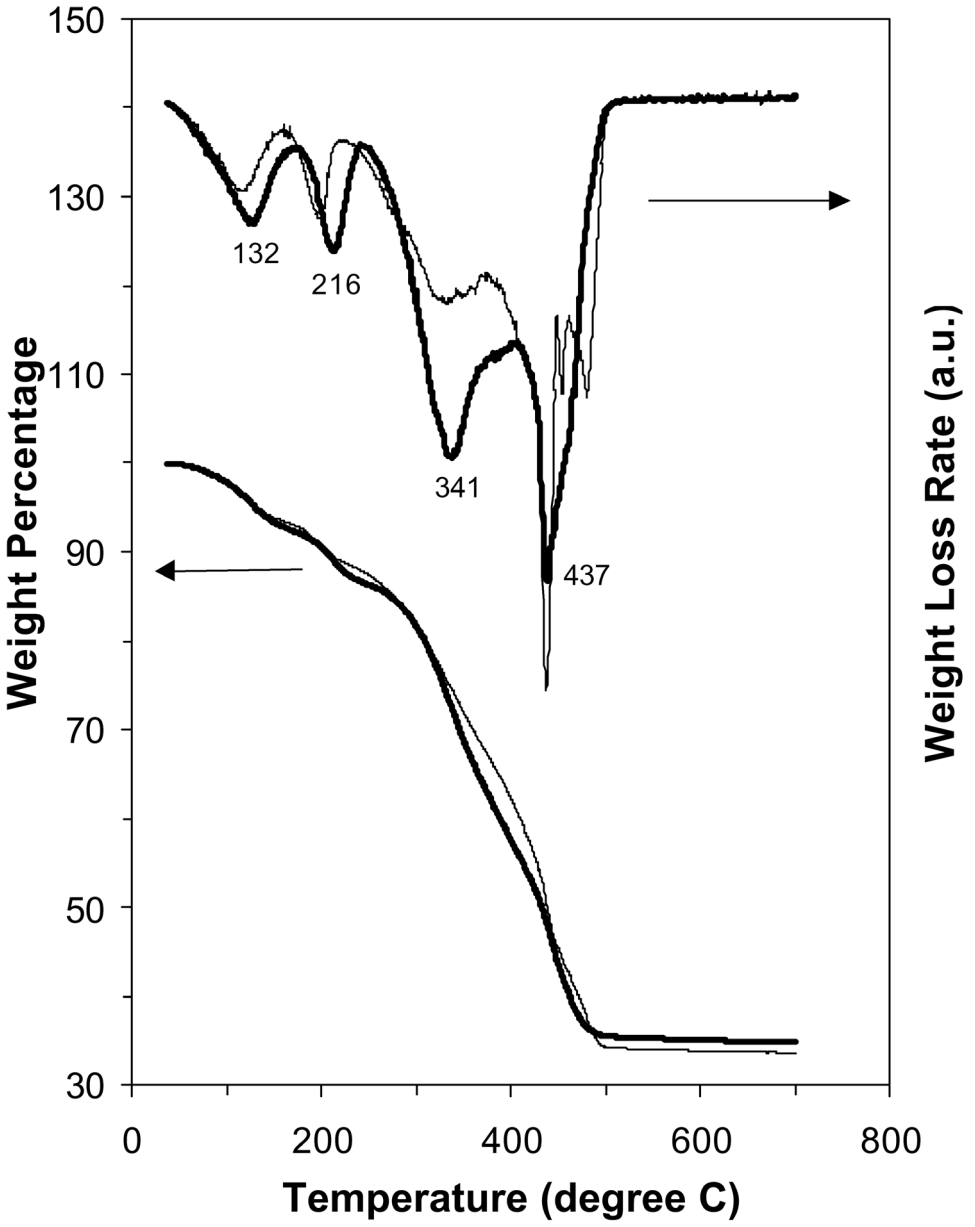

B

Figure 6-6. TGA and differential TGA curves of samples ZAO and ZAE in N_2 (A) and in air (B) environment. The bold curves belong to sample ZAO whose differential TGA peaks are marked.

6.4 Conclusions

In conclusion, when two cis-trans isomers (oleate and elaidate anions) are intercalated into Zn_2Al- and Mg_2Al-LDH interlayer, they show different packing modes and morphologies. Like saturated straight chain organic anions, elaidate packs either in an anti-parallel (monolayar) or bi-layer mode based on the surfactant amount used. For oleate, however, its boomerang shape imposes hook-like partial overlap, which prevents the chains from packing in the above modes but allows a Velcro-like partial overlap.

For both anions, the growth habit is completely different from that found for inorganic LDH, being dominated by a c-axis preferable growth. There are, however, detailed differences between the two anions due to their geometrical restriction. Bigger platy ribbon-like sheets (flat, bent or twisted in rectangle) are the typical morphology of LDH elaidate while smaller irregularly-shaped platy sheets are the morphological feature of LDH oleate. In addition, the complete overlapping of hydrocarbon chains in LDH elaidate results in much better crystallinity than that in LDH oleate, as shown by the more extended orderly regions evident in the TEM images of LDH elaidate.

The thermolysis investigation of typical organic/inorganic hybrids reveals four major decomposition steps either in air or nitrogen, the third step, i.e. the decomposition of organic species, being different in the two atmospheres.

6.5 References

Boclair, J. W .and P. S. Braterman. 1999. "Layered double hydroxide stability. 1. Relative stabilities of layered double hydroxides and their simple counterparts**,"** **C***hemistry of Materials*. Vol.11, no. 2, pp. 298-302

Boclair, J. W., P. S. Braterman, J. P. Jiang, S. W. Lou and F. Yarberry. 1999. "Layered double hydroxide stability. 2. Formation of Cr(III)-containing layered double hydroxides directly from solution," C*hemistry of Materials*. Vol. 11, no. 2, pp.303-307.

Borja, M. and P. K. Dutta. 1992. "Fatty-acids in layered metal-hydroxides - membrane-like structure and dynamics," *Journal of Physical Chemistry*. Vol. 96, no.13, pp.5434-5444.

Braterman, P. S.; Z. P. Xu and F. Yarberry, 2003. "Chemistry of Layered Double Hydroxides," in *Handbook of Layered Materials*. In Press. Marcel Dekker, Inc.

Cai, H., A. C. Hillier, K. R. Franklin, C. C. Nunn and M. D. Ward. 1994. **"**Nanoscale imaging of molecular adsorption," *Science*. Vol. 266, no. 5190, pp.1551-1555.

Cavani, F., O. Clause, F. Trifiro, and A. Vaccari. 1991. "Anionic clays with hydrotalcite-like structure as precursors of hydrogenation catalysts," A*dvances in Catalyst Design*. pp. 186-190.

Culity, B. D. 1978. *Elements of X-ray Diffraction*, 2nd. Addison-Wesley. Massachusetts. p. 278.

Dean, J. A. 1995. *Analytical Chemistry Handbook*. McGraw-Hill Inc. New York. pp. 2.12-2.13.

Gunstone, F. D. 1967. *An Introduction of the Chemistry and Biochemistry of Fatty Acid and Their Glycerides*, 2nd ed. Chapman and Hall Ltd., London. P 70-74.

Kanoh, T., T. Shichi and K. Takagi. 1999. "Mono- and bilayer equilibria of stearate self-assembly formed in hydrotalcite interlayers by changing the intercalation temperature," C*hemistry Letters*. No.2, pp.117-118..

Kloprogge, J. T and R. L. Frost. 1999. "Fourier transform infrared and Raman spectroscopic study of the local structure of Mg-, Ni-, and Co-hydrotalcites," *Journal of Solid State Chemistry*. Vol.146, no.2, pp.506-515.

Kuksis, A. 1978. *Fatty Acids and Glycerides*. Plenum Press, New York. p 225 & p. 359.

Labajos, F. M., V. Rives and M. A. Ulibarri. 1992. "Effect of hydrothermal and thermal treatments on the physicochemical properties of Mg-Al hydrotalcite-like materials," *Journal of materials science*. Vol. 27, no. 6, pp.1546-1552.

Lagaly, G. 1976. "Kink-block and gauche-block structures of bimolecular films," *Angewandte Chemie-International Edition in English*. Vol. 15, no. 10, pp.575-586

Meyn, M., K. Beneke and G. Lagaly. 1990. "Anion-exchange reactions of layered double hydroxides," *Inorganic Chemistry*. Vol. 29, no. 26, pp.5201-5207.

Ogawa, M. S and Asai. 2000. **"**Hydrothermal synthesis of layered double hydroxide-deoxycholate intercalation compounds," C*hemistry of Materials*. Vol.12, no.11, pp.3253-

Rives, V and M. A. Ulibarri. 1999**. "**Layered double hydroxides (LDH) intercalated with metal coordination compounds and oxometalates," *Coordination Chemistry Reviews.* Vol. 181, pp.61-120.

Simons, W. W. 1978. *The Sadtler Handbook of Infrared Spectra*. Sadtler Research Laboratories, Inc. Pennsylvania. P. 26, p. 710 and p. 741.

Takagi, K., T. Shichi, H. Usami and Y. Sawaki. 1993. "Controlled photocycloaddition of unsaturated carboxylates intercalated in hydrotalcite clay interlayers," *Journal of the American Chemical Society*. Vol. 115, no.10, pp.4339-4344.

Tsuji, M., G. Mao, T. Yoshida and Y. Tamaura, 1993. "Hydrotalcites with an extended Al^{3+}-substitution - synthesis, simultaneous tg-dta-ms study, and their CO_2 adsorption behaviors," *Journal of Materials Research*. Vol. 8, no. 5, pp.1137-1142.

Williams, D. H and I. Fleming. 1989. *Spectroscopic Methods in Organic Chemistry*, 4th ed.; McGraw-Hill Inc. New York.

Xu, Z. P and P. S. Braterman. 2003. "Multiple phases and self-assembly in layered double hydroxides," in Encyclopedia of Nanoscience and Nanotechnology. In press. Marcel Dekker, Inc.

Xu, Z. P and H. C. Zeng. 1998. "Thermal revolution of cobalt hydroxides: a comparative study of their various structural phases," *Journal of Materials Chemistry.* Vol. 8, no.11, pp.2499-2506.

Xu, Z. P and H. C. Zeng. 2000. "Decomposition processes of organic-anion-pillared clays $Co_aMg_bAl(OH)_c(TA)_d \bullet nH(2)O$," *Journal of Physical Chemistry B*. Vol. 104, no. 44, pp.10206-10214.

Xu, Z. P and H. C. Zeng. 2001. “Abrupt structural transformation in hydrotalcite-like compounds $Mg_{1-x}Al_x(OH)(2)(NO3)x.nH_2O$ as a continuous function of nitrate anions,” *Journal of Physical Chemistry B.* Vol. 105, no. 9, pp.1743-1749.

Xu, Z. P and P. S. Braterman. 2003. “High affinity of dodecylbenzene sulfonate for layered double hydroxide and resulting morphological changes,” *Journal of Materials Chemistry*. Vol. 13, no. 2, pp.268-273.

Xu, Z. P., P. S. Braterman and N. Seifollah. 2002. “Self-assembly and multiple phases in ZnAl-Stearate Layered Double Hydroxides,” *Abstracts of Papers of the American Chemical Society*. Vol. 224, pt.1, pp.U430-U430.

7. General Conclusions

This report summarizes the results obtained from a Laboratory Directed Research & Development (LDRD) project entitled "Investigation of Potential Applications of Self-Assembled Nanostructured Materials in Nuclear Waste Management". The major results are summarized below:

- Acid-base titration experiments were performed on both mesoporous alumina and alumina particles under various ionic strengths. Under the same chemical conditions, the surface charge per mass on mesoporous alumina was as much as 45 times higher than that on alumina particles. This difference cannot be fully explained by the surface area difference between the two materials. The titration data have demonstrated that the nano-scale confinement has a significant effect, most likely via the overlap of the electric double layer (EDL), on ion sorption onto mesopore surfaces. This effect cannot be adequately modeled by existing surface complexation models, which were developed mostly for an unconfined solid-water interface.
- As the pore size is reduced to a few nanometers, the difference between surface acidity constants *(*$\Delta pK = pK_2 - pK_1$) decreases, giving rise to a higher surface charge density on a nanopore surface than that on an unconfined mineral-water interface. The change in surface acidity constants results in a shift of ion sorption edges and enhances ion sorption on nanopore surfaces. Also, the water activity in a nanopore is greatly reduced, thus increasing the tendency for inner sphere complexation and mineral precipitation. All these effects combine to preferentially enrich trace elements in nanopores. This enrichment mechanism has a significant implication to many fundamental geochemical issues such as the irreversibility of ion sorption/desorption and the bioavailability of subsurface contaminants. The discovery of this mechanism provides a scientific basis for engineering high-performance ion adsorbents for nuclear waste management.
- Layered double hydroxides (LDH) have shown a great promise for removing anionic contaminants. The anion sorption coefficients (K_d) have been measured for both activated and non-activated Mg-Al LDH materials. The activated material has a much higher anion sorption coefficient than the non-activated one, indicating that calcination can significantly improve anion sorption capacity of LDH. Sorption isotherms for Re and Se on the activated LDH material roughly follow the Freundlich isotherm, indicating the existence of various sorption sites with different sorption capabilities. Anions tend to first sorb on the external surface sites. As the anion concentration or the ionic strength increases, more anions are forced into the interlayer of LDH, and consequently the sorption becomes dominated by an interlayer ion exchange. The experimental data have indicated that the external surface sites have a very high affinity for anions, especially divalent and trivalent anion.
- To study sorption kinetics, calcined Mg-Al LDH was added to the solution both as a pre-wetted slurry (allowing 24 hours for rehydration), and as a dry powder. Sorption results varied for different anionic complexes. For selenate and perrhenate, an incubation time was required for the dry material to achieve the same K_d value as the pre-wetted material. For arsenate, however, both wetted and dry materials initially

had high K_ds, which decreased with time. These behaviors are attributed to the structural reconstruction of the calcined LDH material in solution. Se and Re are not highly sorbed by the phases present in the calcined material, but are incorporated as interlayer anions in the LDH structure upon hydration and reconstruction, while As may be sorbing onto the dehydration products, and being partially released during rehydration.

- A self-assembled layered double hydroxide-surfactant hybrid nanomaterial was developed. A novel packing mode specific to the cis-unsaturated hydrocarbon chain in this material was proposed. The kink imposed by the cis-double bond in oleate leads to partial overlap between chains on adjacent layers. Incorporation of surfactant into the growing crystallite leads to a reversal of the usual LDH growth habit, and results in crystallite shapes featuring ribbon-like sheets, therefore increasing external surface sites for anion sorption. The thermal decomposition behavior of as-prepared organic/inorganic nanocomposites in air and N_2 was determined. The thermal decomposition of the LDH-surfactant nanomaterial in N_2 leads to the formation of a highly dispersed nanocomposite material of metal oxides and activated-carbon-like compound, which is expected to exhibit a high sorption affinity for both anions and cations.

8. Acknowledgments

Sandia is multi-program laboratory operated by Sandia Corporation, a Lockheed Martin Co., for the United States Department of Energy's (DOE) National Nuclear Security Administration under Contract DE-AC04-94AL85000. This research is supported by the DOE through a Laboratory Directed Research and Development (LDRD) project and partly by Yucca Mountain Project (YMP) Science & Technology (S&T) Program.

Federal Agencies

Margaret Chu, Director
Office of Civilian Radioactive Waste Management
1000 Independence Avenue
Room 5A-085
Washington, D. C. 20585

Laboratories

David J. Wesolowski
Senior Research Scientist
Oak Ridge National Laboratory
Chemical and Analytical Science Division
P. O. Box 2008
Oak Ridge, TN 37831-6110

Jonathan P. Icenhower
Research Scientist
Pacific Northwest National Laboratory
Applied Geology & Geochemistry Group
P. O. Box 999
902 Battelle Boulevard
Richland, WA 99352

Shas V. Mattigod
Senior Research Scientist
Pacific Northwest National Laboratory
Applied Geology & Geochemistry Group
P. O. Box 999
902 Battelle Boulevard
Richland, WA 99352

Frank S. Felicione
Technical Staff
Argonne National Laboratory-West
Waste Programs
Technology Development Division
Idaho Falls, Idaho 83403-2528

James L. Conca
Los Alamos National Labortory
115 Main Street
Carlsbad, NM 88220

Universities

Huifang Xu
Department of Earth and Planetary Sciences
University of New Mexico
Albuquerque, NM 87131-1116

Paul S. Braterman
Department of Chemistry
University of North Texas
Denton, TX 76203-5-70

Weixian Zhang
Department of Civil and Environmental Engineering
Lehigh University
13 East Packer Avenue
Bethlehem, PA 18015-3176

Cristian P. Schulthess
Dept. of Plant Science, U-4067
The University of Connecticut
1376 Storrs Road
Storrs, CT 06269-4067

Enrique Merino
Department of Geology
Indiana University
1005 E. Tenth Street
Bloomington, IN 47405

Michael F. Hochella, Jr.
Department of Geological Sciences
Virginia Polytechnic Institute and State University
4044 Derring Hall
Blacksburg, VA 24061-0420

Susan L. Brantley
Department of Geological Sciences
Penn State University
239 Deike Building
University Park, PA 16802

Libraries

Thomas Branigan Memorial Library
200 Picacho Avenue
Las Cruces, NM 88001

Government Publications Department
Zimmerman Library
University of New Mexico
Albuquerque, NM 87131

New Mexico Tech
Martin Speere Memorial Library
801 Leroy Place
Socorro, NM 87801

Internal Addresses

MS	Org.	
0724	6000	Robert J. Eagan
0771	6800	Dennis L. Berry
0720	6804	Phillip I. Pohl
1395	6820	Paul E. Shoemaker
1395	6820	Frank D. Hansen
1395	6821	David S. Kessel
1395	6821	David Lord
1395	6821	Joshua Stein
1395	6822	Mark Rogali
1395	6822	Richard Beauheim
1395	6822	Laurence H. Brush
1395	6822	Huizhen Gao
1395	6822	Randall Roberts
0779	6849	Hong-Nian Jow
0779	6849	Robert C. Moore
0779	6849	Lori Doston
0779	6849	Joseph A. Jones
1399	6850	S. Andrew Orrell
0778	6851	Peter Swift
0778	6851	Carlos F. Jove-Colon
0778	6851	Robert J. Mackinnon
0778	6851	Bill Arnold
0778	6851	Mary-Alena Martell
0776	6852	M. Kathryn Knowles
0776	6852	Teklu Hadgu

0776	6852	Stephanie P. Kuzio
0776	6852	Al Reed
0776	6852	Yifeng Wang (10 copies)
1399	6855	Cliff Howard
1399	6855	Charles Bryan
1399	6855	Russell L. Jarek
1399	6853	Mel Marietta
0887	1800	Wendy R. Cieslak
0323	1011	Henry R. Westrich
0750	6118	Tom Hinkebein
0750	6118	James Krumhansl
0750	6118	Patrick Brady
0750	6118	Louise Criscenti
0750	6118	Malcolm Siegel
0750	6118	Randall T. Cygan
0735	6115	Ray Finley
0735	6115	Clifford K. Ho
0735	6115	Susan Altman
0918	7030	Susan Y. Pickering

1	MS 9018	Central Technical Files, 8945-1
2	MS 0899	Technical Library, 9616
3	MS 0323	LDRD Office (3 copies)